May 2019

Size Effects in Periodic Lattice Structured Cellular Materials

Marcus J. Yoder
Clemson University, marcusyoder@gmail.com

SIZE EFFECTS IN PERIODIC LATTICE STRUCTURED CELLULAR MATERIALS

A Dissertation
Presented to
the Graduate School of
Clemson University

In Partial Fulfillment
of the Requirements for the Degree
Doctor of Philosophy
Mechanical Engineering

---

by
Marcus Yoder
May 2019

Accepted by:
Dr. Lonny Thompson, Committee Chair
Dr. Joshua Summers, Committee Co-Chair
Dr. Gang Li
Dr. Georges Fadel
Dr. Nicole Coutris

Abstract

When the material properties of cellular materials are tested, small samples may have different apparent material properties than large samples. This difference is known as a size effect. This work examines size effects in periodic thin walled cellular materials using a discrete beam element lattice model.

Chapter 2 uses this lattice model to characterize size effects for a variety of lattice topologies and boundary conditions. It also compares those size effects to results coming from a nominally equivalent micropolar model. Micropolar elasticity extends classical elasticity to incorporate size dependent behaviors and can therefore capture size effects in a continuum model. The micropolar model used here typically under predicts the size effects seen in the lattice model by an order of magnitude. The lattice size effects are examined for patterns and the size effect patterns found can be explained by the shape of the free edges, and by the specifics of how material is distributed within the material domain. These are causes for size effects that are not captured in the micropolar model.

Chapter 3 examines two hypotheses taken from the literature. The literature has attributed stiffening size effects to the local beam bending behavior of lattice materials; there is an additional stiffness connected to the rotation of the beam nodes at lattice vertices, that causes a stiffening size effect. This work decomposes the strain energy of the beams in the lattice into energy from axial stretching and beam bending, and shows that size effects are connected to bending strain energy in certain situations.

Other literature has shown a softening size effect in stochastic foams caused by damaged or incomplete cells on the free surfaces. This work uses a continuum like strain map of

the lattice model to show that these edge softening effects can appear in periodic cellular materials when the surface cells are neither damaged nor incomplete. This effect is only observed for certain lattice topologies and is quantified and connected to a global size effect. In conjunction with the beam bending size effect, this edge effect is able to explain the origin of size effects for a variety of lattice topologies and boundary conditions.

Chapter 4 examines the ability of micropolar elasticity to predict size effects in periodic cellular materials in both bending and shear. It shows that a set of micropolar material properties that predict size effects accurately in bending, is inaccurate for shear. A different set of properties does well for shear, but poorly for bending. This suggests that, for periodic cellular materials, size effects in shear and bending arise from different mechanisms.

Chapter 4 presents a novel mechanism causing size effects in periodic cellular materials in bending, called a material distribution effect. In bending, material far from the neutral axis contributes more to stiffness than material close to the neutral axis. A sample with only a few unit cells can have a relatively large amount of its material close to the neutral axis, or far away, depending on topology and choice of unit cell. A sample with many cells must have its material spread more evenly. This can cause either a stiffening or softening size effect. This work derives formulas to predict the magnitude and direction of these size effects, and shows that these formulas are able to predict size effects for a variety of different cellular materials in different types of bending boundary conditions.

These chapters provide an explanation of the origin of size effects in periodic cellular materials for a variety of boundary conditions and lattice topologies.

Dedication

I have been able to persevere and complete this dissertation because of the support and friendship of the people around me. My wife, Diana, has been exceptionally patient and supportive. The friendship, feedback, and comradery of my CEDAR lab mates has been a constant source of encouragement.

Teaching ME2220 labs has provided a source of meaning and purpose that kept me mentally balanced when my research was particularly frustrating. My fellow TAs have also provided constant support. I would like to particularly thank my longtime coworkers, Ivan Mata, Steven Fredericks, Rucha Natu, Kyle Yeomans, Matthew Sheppard and Richard Snyder for their help making the sophomore labs excellent and a rewarding place to teach. Our supervisor Dr. Todd Schweisenger has been instrumental in building a positive and rewarding atmosphere to work in. Teaching labs has given my time at Clemson richness, meaning, and a little extra friendship.

I would like to thank my advisor and committee. Dr. Thompson has provided valuable scientific and theoretical assistance when I was struggling. Dr. Summers has helped me navigate grad school and smoothed out hurdles and obstacles. Dr. Coutris provided theoretical insight into micropolar elasticity. Dr. Fadel offered me a chance to work with his creative inquiry team, doing related research. That experience was a rewarding one.

Table of Contents

Page

Table of Contents (Continued)

Page

Table of Contents (Continued)

Page

List of Figures

Page

List of Figures (Continued)

Page

List of Figures (Continued)

Page

List of Figures (Continued)

Page

List of Tables

Page

1. Introduction

1.1 Background and Motivation

Cellular materials are a class of lightweight materials composed of a repeating pattern of solid material and empty space. They include materials such as wood, bone, foams, and honeycombs. Cellular materials can be categorized as periodic cellular materials, such as honeycomb lattices, which have a strictly repeating pattern, and stochastic cellular materials which have a random component to their structure. Cellular materials can also be characterized by their relative mass density, their density compared to the density of the material they are made from. This work focuses on periodic cellular materials with thin cell walls and a low relative density, known as periodic lattice structured cellular materials.

The effective material properties of cellular materials is not independent of the specimen size; for example, if multiple specimens are cut from a block of metallic foam and compression tested, a small specimen will have a lower apparent Young's modulus than a large specimen. The dependence of tested material properties on specimen size happens when the individual cells are an appreciable fraction of the overall size of the specimen; the number of repeated cells is important rather than the absolute size of a material specimen.

Figure 1 shows 2 different sizes of virtual tension specimens of a cellular material with a hexagonal lattice. Despite the fact that the cells have the same cell geometry and size, the two samples will have different apparent Young's moduli, because the cell size is different relative to the overall size.

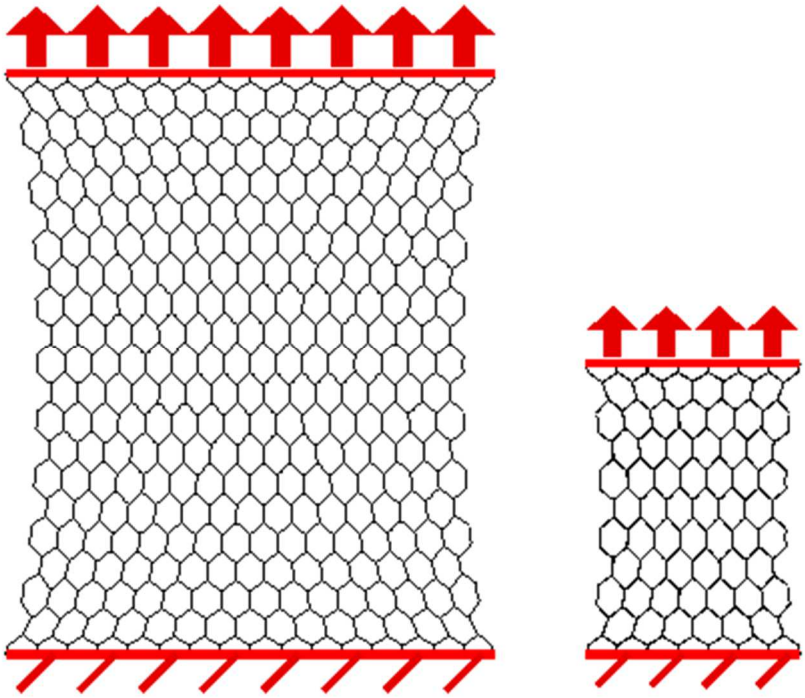

Figure 1: A large and small virtual sample of a hexagonal lattice

When the moduli are stiffer with fewer cells, this is known as a stiffening size effect. When the moduli are softer, it is a softening size effect. Although this work focuses on size effects that affect the stiffness of cellular materials, other quantities can also depend on cell size. For example, the stress (Nakamura & Lakes, 1988) and strain (Tekoğlu, 2007) concentrations around a hole depend on the size of the hole relative to the size of a unit cell. The strength of a cellular material can also depend on the sample size relative to the cell size (Tekoğlu, Gibson, Pardoen, & Onck, 2011). This work characterizes stiffness size effects in periodic cellular materials, and seeks to explain the mechanisms that cause them.

It is common to model cellular materials as a continuum; the cellular structure is represented as a continuous material that has material properties that nominally match the effective mechanical behavior of the cellular material. Because classical (Cauchy) elasticity has no mechanism for modeling any size dependent information, micropolar elasticity was

developed to allow a continuum model to capture size effects. Micropolar elasticity is an extension of classical elasticity that introduces micro-rotation as a free variable in addition to the displacement that is the free variable in classical elasticity. Chapter 2 contains some additional background on micropolar elasticity, including the foundational equations and a finite element implementation. This work tests the ability of micropolar elasticity to model size effects in periodic cellular materials.

1.2 Summary

The chapters of this work were originally published as stand-alone journal papers. Therefore, each chapter has a stand-alone literature review of relevant works cited. Chapter 2 uses a beam element finite element model of periodic cellular materials to characterize stiffness size effects for a variety of lattice types and boundary conditions. It then compares these size effects to size effects in a micropolar model. The micropolar model is constructed to match the lattice model, and uses material properties taken from the literature that were derived for the lattice types used in the lattice model. The lattice model showed both stiffening and softening size effects depending on the boundary condition, and lattice topology. The micropolar model predicts exclusively stiffening size effects that are usually much smaller than the size effects shown in the lattice model. Chapter 2 also presents a few hypotheses about the causes of size effects that are then explored in detail in Chapters 3 and 4.

Chapter 3 investigates two potential causes of size effects. When cell walls are modeled as beam elements, the nodes of these beams have independent displacement and rotation degrees of freedom. The beam elements have a resistance to axial stretching and a mathematically separate resistance to transverse displacement and rotation. It is hypothesized

that the resistance to transverse displacement and rotation cause a stiffening size effect. This is called a local rotation size effect and is quantified by decomposing the total strain energy into energy due to beam stretching and beam bending. The results show that this effect exists, but is small in the stretching and bending boundary conditions. In shear it can be the dominant cause of size effects.

Chapter 3 also investigates an observation from Chapter 2, that cells near the free edges of lattice structures seem to contribute less to stiffness than cells on the interior. In order to investigate this a novel method is presented for mapping the effective strain in each unit cell of the lattice. Then the material properties originally used in the micropolar model in Chapter 2 are used along with the micropolar constitutive law to calculate an expected strain energy for each cell. For certain lattice topologies and boundary conditions, the expected energy near the free edges is greater than the actual energy. This indicates that these cells have a softer constitutive relationship than interior cells. This data is combined with data about local rotation size effects and it explains size effects in shear and for the cases which have edge softening.

Chapter 4 examines size effects in bending. One of the hypotheses put forward in Chapter 2 was that lattices with fewer cells can have more of their material concentrated in one place. As the lattice refines, material moves around and must be spread more evenly. In a bending boundary condition, material contributes more to stiffness the farther it is from the centerline. Chapter 4 shows that redistribution of material as the lattice refines can cause either a stiffening or softening size effect. A formula is derived to make predictions of this size effect, based on a non-dimensional quantity describing the effective bending resistance of a single unit cell. It is also shown that this cause of size effects is absent in shear and is inconsistent with micropolar elasticity.

Together these chapters characterize and explain size effects in a variety of boundary conditions and a variety of lattice topologies.

2. A Comparison to Micropolar Elasticity

2.1 Introduction

2.1.1 General Background

Modeling the elastic behavior of cellular materials defined by materials composed of repeating or random unit cell structures, poses challenges that are not seen in solid homogenous materials. The apparent elastic moduli of cellular materials can depend on the size of the sample being tested (Andrews, Gioux, Onck, & Gibson, 2001a, 2001b; Gibson & Ashby, 1999), due to edge effects. Additionally, cellular materials have been shown to behave differently near a stress concentrator than a classical material. The non-homogenous nature of the material can redirect stress, and lowers the stress concentration factor of a flaw or hole (Lakes, Nakamura, Behiri, & Bonfield, 1990). Cellular materials with larger unit cells compared to the hole size have a more reduced stress concentration factor. The dependence of material properties and behavior based on the unit cell size compared to material sample size is known as a size effect.

Many authors (Alderson et al., 2010; Gibson & Ashby, 1999; Zheng et al., 2014) have attempted to model cellular materials as homogenous elastic solids. This practice is known as continuum modeling. These authors find an effective Young's modulus and Poisson's ratio, such that the behavior of an elastic solid will match the behavior of the cellular material. Although these effective material properties have been used successfully for design, they cannot effectively capture size effects. Classical elasticity theory has no way to describe the cellular nature of a material, and no mechanism to describe size effects (Eringen, 1999).

Micropolar elasticity is an extension of classical elasticity that adds an extra microrotation field variable, in addition to displacement (Eringen, 1999). In the same way that derivatives of displacement define strain, derivatives of micro-rotation define curvature. It should be noted that the addition of micro-rotation removes the classical elastic requirement that shear stresses are symmetric. The micropolar constitutive law includes the same normal stresses found in classical elasticity, but allows for nonsymmetric shear stresses, and a couple-stress based on curvature. The anti-symmetric component of shear stress, and the relationship between curvature and couple stress requires two new isotropic material properties, commonly denoted κ and γ respectively. *Table 1* and 2 give the general equations of micropolar elasticity and notation used. In Tables 1 and 2 a comma denotes a derivative, and repeated indices imply summation over spatial dimensions. Terms highlighted in red are new to micropolar elasticity. It is noted that the shear strain is nonsymmetric and couples the displacement gradient and micropolar rotation variable. These additional equations and material properties give micropolar elasticity the ability to model size effects (Eringen, 1999).

Table 1: Equations of micropolar elasticity compared to classical elasticity.

	Classical Elasticity	Micropolar Elasticity
Constitutive Law	$\sigma_{ij} = A_{ijkl}\varepsilon_{kl}$	$\sigma_{ij} = A_{ijkl}\varepsilon_{kl}$ and $m_{ij} = C_{ijkl}k_{kl}$
Strain Definition	$\varepsilon_{ij} = \frac{u_{i,j} + u_{j,i}}{2}$	$\varepsilon_{ij} = u_{j,i} - e_{kij}\phi_k$ and $k_{ij} = \phi_{j,i}$
Equilibrium Equations	$\sigma_{ji,j} = 0$ and $\sigma_{ij} - \sigma_{ji} = 0$	$\sigma_{ji,j} = 0$ and $m_{ji,j} + e_{ijk}\sigma_{jk} = 0$

Table 2: Notation

Symbol	Name	Symbol	Name	Symbol	Name
σ_{ij}	Force stress	A_{ijkl}	Material Properties	e_{kij}	Levi-Civita tensor
ε_{ij}	Strains	C_{ijkl}	Material Properties	k_{ij}	Curvature tensor
m_{ij}	Couple stress	u_i	Displacement components	ϕ_j	Micropolar rotation components

2.1.2 Experimental Results Demonstrating Size Effects

Cellular materials can be described as periodic or stochastic. Periodic cellular materials, such as honeycombs or equilateral triangle lattices, have a repeating ordered structure. Stochastic cellular materials, such as metal or polymer foams, have a random structure. Cellular materials can also be divided into bending dominated and stretching dominated topologies (Gibson & Ashby, 1999). The bending and stretching classes of cellular material have markedly different patterns of behavior (Gibson & Ashby, 1999). Triangular lattices and closed cell foams are stretching dominated. Honeycombs and open cell foams are bending dominated. Low density stretching dominated cellular materials tend to be stiffer than bending dominated materials of the same density and parent material (Zheng et al., 2014).

Because of the difficulties in modeling the stochastic nature of foam geometry, honeycombs have sometimes been used as a model of open cell foams. Although these simplified models are only approximate, they are thought to share many of the same size effects. This paper examines size effects in periodic lattice structures. The patterns seen in stochastic foams may provide some insight into size effects in periodic lattices, and vice versa.

Experimental tests of the effective stiffness properties of cellular materials typically use samples where the global sample size is many times the local unit cell size (Gibson & Ashby, 1999); The apparent material properties derived from these tests are known as the bulk

properties. When samples with few unit cells are tested, different properties are often found. The apparent dependence of material properties on sample size is known as a size effect. Size effects are most pronounced when the sample size is the smallest. For the same size unit cells, as the sample size decreases, the volume fraction of material distributed near boundaries increases. As the sample size increases, the apparent properties asymptotically increase to the bulk values.

For example, (Andrews et al., 2001b) measured the stiffness of foam samples using a compression tester. They calculated effective Young's modulus as stiffness divided by cross sectional area, and found that small samples had a lower effective Young's modulus than large samples. This is a softening size effect; small samples are softer than large ones. The reverse behavior is a stiffening size effect. Although Andrews et al. also examined the effects of sample size on strength, this paper focuses on size effects on the linear elastic behavior of materials. Size effects on strength are not examined.

Table 3 summarizes selected papers that study size effects in cellular materials. The simple listings of topology and boundary condition conceal the details of the methods used. For example, (Brezny & Green, 1990) studied size effects in three point bending, while the papers by Lakes' group (Anderson & Lakes, 1994; Lakes, 1991b; Rueger & Lakes, 2016) study pure bending. Nevertheless, these simple listings show consistent patterns of size effects; compression shows a softening effect; bending, torsion and shear show stiffening effects.

Several papers show a softening effect in bending that is contrary to the pattern just discussed. (Anderson & Lakes, 1994) look at the effects of open or damaged cells on the surface of the material and examine the effect on size effects. These open cells contribute to the volume of the material without contributing to the stiffness. This creates a softening effect that can more than cancel out the stiffening size effect. Because global bending puts the highest stress and strain on the surface of the material, the effect is more dramatic than for other boundary conditions. (Tekoğlu, 2007) uses simulations to show a softening size effect in bending. His illustrations of his 2d foam structures show many incomplete cells near the surface of the material. (Brezny & Green, 1990) do an experimental study but they do not describe the careful specimen treatment that (Anderson & Lakes, 1994) say is needed to prevent surface damage. The methods used in this paper take care to minimize incomplete cells near the surface.

The patterns examined in

Table 3 examine only the direction of a size effect as either softening or stiffening, not its scale. (Rueger & Lakes, 2016) compared the scale of size effects between open and closed cell foams. The open cell foams they examined, show a larger size effect than the closed cell foams they examined.

Table 3: Selected papers studying size effects.

Topology	Boundary Condition	Effect	Reference
2d foam	bending	softer	(Tekoğlu, 2007)
open cell foam	bending	softer	(Brezny & Green, 1990)
open cell foam	bending	stiffer	(Lakes, 1991b)
open cell foam	bending	stiffer	(Rueger & Lakes, 2016)
closed cell foam	bending	stiffer	(Anderson & Lakes, 1994)
model material	bending	stiffer	(Beveridge, Wheel, & Nash, 2012)
model material	circular bending	stiffer	(Waseem, Beveridge, Wheel, & Nash, 2013)
closed cell foam	compression	softer	(Bastawros, Bart-Smith, & Evans, 2000)
closed cell foam	compression	softer	(Andrews et al., 2001a)
closed cell foam	compression	softer	(Jeon & Asahina, 2005)
open cell foam	compression	softer	(Andrews et al., 2001a)
2d foam	compression	softer	(Tekoğlu, 2007)
2d foam	shear	stiffer	(Tekoğlu, 2007)
Honeycomb	shear	stiffer	(Tekoğlu, 2007)
Honeycomb	shear	stiffer	(Diebels & Steeb, 2002)
closed cell foam	torsion	stiffer	(Lakes, 1983)
open cell foam	torsion	stiffer	(Anderson & Lakes, 1994)

Most of the authors examine size effects in light of micropolar elasticity theory. The additional material properties introduced in micropolar elasticity introduce additional stiffness, which becomes most apparent at small sample sizes. This has been put forth as a reason for size effects (Diebels & Steeb, 2003; Dunn & Wheel, 2016; Lakes, 1991b). The observed softening size effects in compression contradict this theory. As discussed previously, (Anderson & Lakes, 1994) experimentally show that incomplete surface cells and surface cells damaged in machining can cause a softening effect. (Tekoğlu et al., 2011) partially address this contradiction by positing that cells near the free edges of the material contribute less to stiffness than cells far from the edges. This paper will attempt to explore this contradiction and better explain its causes.

2.1.3 Material Property Models

Many of the authors in

Table 3 explain the observed size effects using micropolar elasticity, and some researchers characterize the micropolar elastic properties of their materials from experiments such as pure bending or pure torsion. Other authors, not examined in

Table 3, use analytical formulas to derive theoretical micropolar material properties for periodic lattice materials. (Bažant & Christensen, 1972) found theoretical material properties for a square lattice assuming a Taylor expansion for the displacement and rotation of a lattice unit cell and an equivalent micropolar continuum. The material properties are defined as the ones that make the strain energy of the continuum match the lattice for arbitrary strains. (Perano, 1983) followed the general method by Bazant and Christensen and extended the method for an equilateral triangular mesh. In the paper by Perano, the concept of indistinguishable node points was introduced and stated that this method can only be used when all node points in a lattice have the same connectivity to their neighbors. Square and triangular lattices follow this rule. Hexagonal honeycombs do not. Both (Pradel & Sab, 1998) and (Stronge & Wang X.L., 1999) independently derived the same material properties for hexagonal honeycombs. Their methods enforce joint equilibrium equations in a structural thin-walled frame analysis of the unit cell.

(Kumar & McDowell, 2004) extend the Taylor series method and show that it can be used on any lattice with indistinguishable node points. They apply the method to square, equilateral triangle, mixed square and triangle, and diamond lattice structures. Using a first-order Taylor series, the material property formulas derived for squares and equilateral triangles match the formulas presented by (Bažant & Christensen, 1972) and (Perano, 1983) respectively. The methods used in this work use these well-established and stable material properties and will be discussed further in Section 2.2.1. Other material property formulas were derived by Kumar and McDowell and others, using a second-order Taylor series. Because there are questions related to the consistency and stability of these results, they are not used in this work.

(Dos Reis & Ganghoffer, 2012) present another method for determining the micropolar material properties for any unit cell. This method is used to reproduce selected material

properties originally presented by (Kumar & McDowell, 2004). (Y. Chen, Liu, Hu, Sun, & Zheng, 2014; Yi Chen, Liu, & Hu, 2014; Spadoni & Ruzzene, 2012) extended the first-order Taylor series method to apply to chiral lattices. Because chiral lattices are invariant to 180 degree rotations, but do not have any planes of symmetry, they have a more complicated constitutive relationship (Lakes & Benedict, 1982).

Although these material property derivations use various methods, they all model the micropolar behavior starting from the beam nature of the thin-walled lattice material. The additional micropolar properties arise because a lattice structured material has a rotation degree of freedom in addition to displacement. The lattice's resistance to changes in rotation is used to derive the continuum's resistance to curvature and asymmetric stresses.

2.1.4 Selected Verification Studies

Many authors have validated their findings by comparing micropolar continuum and lattice simulations. (Perano, 1983) and (Tekoğlu, 2007) made validation of micropolar theory itself a focus of their work. Except for (Tekoğlu, 2007), these validations were not intended to examine size effects and they are structured in a way that does not allow size effects to be examined.

(Perano, 1983) compared a fairly broad array of micropolar and lattice simulations, and validated that results were similar with a large number of cells relative to the global material domain size. This work focused on developing and verifying various aspects of micropolar theory, with a particular focus on the application of the finite element method to micropolar elasticity. It did not examine the ability of micropolar theory to model size effects.

(Tekoğlu, 2007) studied how micropolar elasticity can model size effects in stochastic foams. He derived material properties by fitting the material constants of the micropolar model to the results of the lattice model. This allowed the micropolar model to accurately fit the size effects for particular loading conditions, but did not provide any verification of the derived material property formulas derived by other authors discussed in the previous section.

(Kumar & McDowell, 2004) focused on deriving material properties from lattice geometry. Micropolar continuum simulations using these material properties were compared to the equivalent lattice simulations to validate their results. The validation simulations compared continuum and lattice displacements and rotations in a half space.

(Dos Reis & Ganghoffer, 2012) presented a method for deriving the material properties for any periodic lattice structure. They verify their method to derive the global bending stiffness of a beam made of a hierarchical lattice material, and comparing that result to the same result derived using a discrete beam element finite element model.

All of the authors discussed above compare lattice simulations to micropolar simulations in an effort to validate their work. Typically, they compare lattice models with many unit cells to micropolar models with material properties defined by the unit cell size and geometry. In these cases, as expected, the difference between the micropolar and classical elastic models is very small. The material properties specific to micropolar elasticity have only a small influence on the results compared to classical theory. This type of verification shows that the classical elastic material properties are correct in the limit of small cell size relative to global domain size, but does little to verify the micropolar material properties can capture the size effects in lattice as the number of cells is reduced (increasing the cell size).

This paper will compare lattice simulations to equivalent micropolar simulations using the linear elastic derived material property formulas. These simulations will examine size effects directly by reducing the local cell size and compare the size effects predicted by the micropolar and lattice models. An objective of this work is to answer the research question: do the material properties derived using analytical formulas based on a repeated unit cell allow micropolar elasticity to accurately capture size effects?

2.2 Comparison Tool

The core method of this work is a comparison code that runs a trio of planar finite element simulations. The first simulation is a static discrete lattice simulation using beam elements. The second is a micropolar continuum model using theoretical material properties with the same overall size, shape, boundary conditions as the discrete lattice simulation. The third simulation is a classical elastic model. Figure 2 shows an example of the displacement results for a typical discrete lattice beam model and corresponding micropolar continuum model. The classical elastic results are not shown because they appear nearly identical to the micropolar simulation. The grid shown in the micropolar model is the finite element boundaries used in the continuum model.

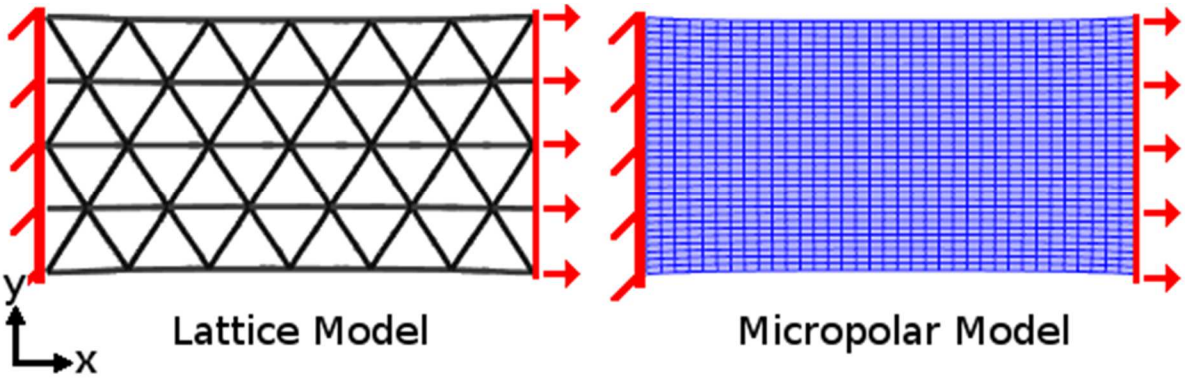

Figure 2: Results of a solved lattice and corresponding micropolar simulations and coordinate axes.

The lattice simulation uses standard thin-wall frame elements based on Euler-Bernoulli beam theory (Fish & Belytschko, 2007). The lattice model automatically tiles unit cells into a rectangular space and solves the assembled finite element equations. Beam elements that are half-in and half-out on the domain boundaries, have half the bending and stretching stiffness of interior beam elements to better match the stiffness results for the micropolar continuum material model with the same boundaries. Because Euler-Bernoulli beam elements are exact under these conditions, only one element per edge between lattice vertices is required.

The micropolar simulation uses the finite element method to approximate the solution to the equations of micropolar elasticity given in Table 1. Although the micropolar equations being solved are generalized from classic elasticity, the finite element analysis (FEA) process follows similar implementation procedures as classically elastic plane. Further details on the finite element formulation for micropolar theory are given in (Zhang, Wang, & Liu, 2005). The finite element procedures for micropolar elasticity closely parallel the procedures for classical elasticity. The micropolar FEA uses a grid of rectangular elements with 35 elements in each direction. The element formulation uses a quadratic interpolation for both displacement and micro-rotation variables and is described in (Zhang et al., 2005). The choice to use 35 elements is based on a convergence study, described in Appendix A2, which shows that this number is sufficient for numerically converged solutions.

In all three models, the total strain energy is calculated using,

$$W = 1/2\ \vec{u}^T [K] \vec{u} \qquad 1$$

where $\vec{u}$ is the generalized displacement and rotation vector, and [K] is the assembled stiffness matrix for the mesh of connected finite elements. For displacement controlled boundary

conditions used in this paper, total strain energy is proportional to stiffness against that loading condition.

As discussed earlier, the theoretical material properties for the lattice structures studied are calculated from formulas taken from the literature (Kumar & McDowell, 2004; Stronge & Wang X.L., 1999). These formulas assume all out-of-plane components in both the lattice beam model and micropolar continuum model are zero. The property formulas use the geometry of the unit cell and the cell wall thickness to define the constitutive matrix D used to relate strain to stress components, including relations between couple stress and curvature. Since all out-of-plane tensor components are assumed zero, the model includes only in-plane tensor components. The materials used in this work are centro-symmetric, and therefore have a symmetric constitutive matrix (Lakes & Benedict, 1982). The triangular, hexagonal, and mixed triangle lattices are in plane isotropic. The square and diamond lattices are in plane orthotropic. As discussed earlier, only the stable first-order properties are used resulting in a positive-definite matrix D. The structure of the constitutive law is given by

$$\begin{bmatrix} \sigma_{xx} \\ \sigma_{yy} \\ \sigma_{xy} \\ \sigma_{yx} \\ m_{xz} \\ m_{yz} \end{bmatrix} = \begin{bmatrix} D_{11} & D_{12} & 0 & 0 & 0 & 0 \\ D_{12} & D_{22} & 0 & 0 & 0 & 0 \\ 0 & 0 & D_{33} & D_{34} & 0 & 0 \\ 0 & 0 & D_{34} & D_{44} & 0 & 0 \\ 0 & 0 & 0 & 0 & D_{55} & 0 \\ 0 & 0 & 0 & 0 & 0 & D_{66} \end{bmatrix} \begin{bmatrix} u_{x,x} \\ u_{y,y} \\ u_{y,x} - \phi_z \\ u_{x,y} + \phi_z \\ \phi_{z,x} \\ \phi_{z,y} \end{bmatrix} \quad 2$$

The classical elastic FEA code uses the same element density, displacement interpolation, and boundary conditions as the micropolar elastic FEA. The micro-rotation degree-of-freedom, ϕ_z, and curvatures are suppressed. The stress tensor is symmetric such that the shear stress $\sigma_{xy} = \sigma_{yx}$. The shear strain is defined by the usual symmetric part of the displacement gradient. The material properties related to normal stresses and strains, D_{11}, D_{12},

and D_{22}, are the same as the micropolar model. Following (Eringen, 1999) the classical shear stiffness, D_{33C}, is calculated from the average of the shear coupling moduli,

$$D_{33C} = (D_{33} + D_{34})/2 \qquad 3$$

All three finite element models were coded using Matlab in order to automatically process a large number of simulation cases with different number of unit cells and boundary conditions.

2.2.1 Lattice Topologies and Material Property Formulas

The lattice topologies shown in Figure 3 were used in this study because there are well-established formulas for material properties published for these lattices from several different authors (Kumar & McDowell, 2004; Stronge & Wang X.L., 1999). In this work, an algebraic error found in (Kumar & McDowell, 2004) that affects the material property formulas for mixed triangle and diamond lattices has been corrected, see Appendix A3. A Matlab code using symbolic variables that reworks the formulas and corrects the error is given in the Supplementary materials.

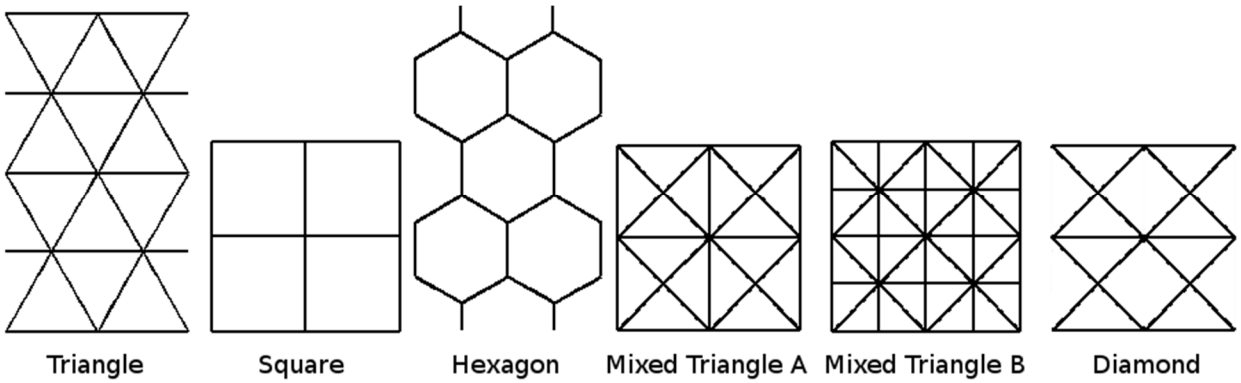

Figure 3: Two unit cells by two unit cells of each lattice topology.

Table 4: Material properties for each topology.

	Triangle	Square	Hexagon	Mixed Tri. A	Mixed Tri. B	Diamond
Relative Density	34.6%	20%	11.5%	38.9%	20.1%	29.3%
D_{11}/E_s	0.13034	0.1000	0.02944	0.13946	0.15441	0.13135
D_{22}/E_s	0.13034	0.1000	0.02944	0.13946	0.15441	0.05478
D_{12}/E_s	0.04287	0	0.02830	0.05482	0.03987	0.05351
D_{33}/E_s	0.04460	1.000e-3	8.603e-4	0.06107	0.04208	0.05541
D_{44}/E_s	0.04460	1.000e-3	8.603e-4	0.06107	0.04208	0.05478
D_{34}/E_s	0.04287	0	2.829e-4	0.05482	0.03987	0.05351
$D_{55}/(t^2E_s)$	0.05774	0.03333	4.811e-3	0.05365	0.07587	0.07219
$D_{66}/(t^2E_s)$	0.05774	0.03333	4.811e-3	0.05365	0.07587	0.03609

Table 4 presents the micropolar material properties of the different lattice topologies normalized by the Young's modulus of the parent material, E_s. The simulation tool assumes that all of the beam ligaments in a lattice have the same thickness. The ligaments in triangle, square, and hexagonal lattices are all the same length, and have a length to thickness ratio of 10. Mixed triangle and diamond lattices have two different ligament lengths. In these lattices, the average length to thickness ratio is 10. Because ligament aspect ratio is held constant, the material properties relating stresses to strains, D_{11} through D_{44}, do not depend on ligament length/unit cell size. The material properties relating curvatures to couple stresses, D_{55} and D_{66}, are dependent on ligament thickness, which is itself dependent on ligament length/unit cell size.

As discussed earlier, Kumar (Kumar & McDowell, 2004) presents two sets of formulas, one with a 1st-order Taylor series resulting in a positive definite constitutive matrix, and one with a 2nd-order Taylor series resulting in a non-positive definite constitutive matrix. The non-positive definite matrix violates stability limits presented in (Eringen, 1999). This work uses the

1st-order material property formulas for positive definite material properties, since they are stable and straight-forward to derive.

In (Kumar & McDowell, 2004), the concept of indistinguishable node points is discussed, first introduced by Perano (Perano, 1983). The paper states that the method can only be applied to lattices with indistinguishable node points, and yet applies the method to lattices without indistinguishable node points, specifically mixed triangle and diamond lattices. The symbolic code in the supplementary materials (see appendix A4) can either reproduce this method or modify these topologies to be indistinguishable. The topologies with distinguishable node points will be used in this paper.

It is worth noting that there are available micropolar material properties for chiral (Yi Chen et al., 2014; Spadoni & Ruzzene, 2012) and circular cell (Chung & Waas, 2009) lattices. Examination of these topologies is left to future work.

The details of how a unit cell is cut off (truncated) at the boundaries affects the behavior of the lattice, particularly when there are few unit cells, see for example Tekoglu (Tekoğlu, 2007) and Andrews et al (Andrews et al., 2001a). Every simulation in this work uses an integer number of unit cells; fractional cells are not used. Both papers, (Andrews et al., 2001a; Tekoğlu, 2007), find that this should produce a consistent size effect. A detailed examination of the effects of unit cell choice is left for future work.

2.2.2 Primary Set of Boundary Conditions

A number of primary boundary conditions are considered to study size effects and are used for the majority of the investigations. Local rotation and half-space boundary conditions will be described later in Sections 0 and 2.3.7 respectively. Figure 4 illustrates half of the primary

set of boundary conditions applied to the lattice model. The boundary conditions are applied in the same way for the lattice and micropolar models; if a DOF on a face is fixed, free, or prescribed in the lattice model it has the same condition in the micropolar model. The classical model has no rotation boundary DOF, but the translation DOFs are treated the same between the micropolar and classical models.

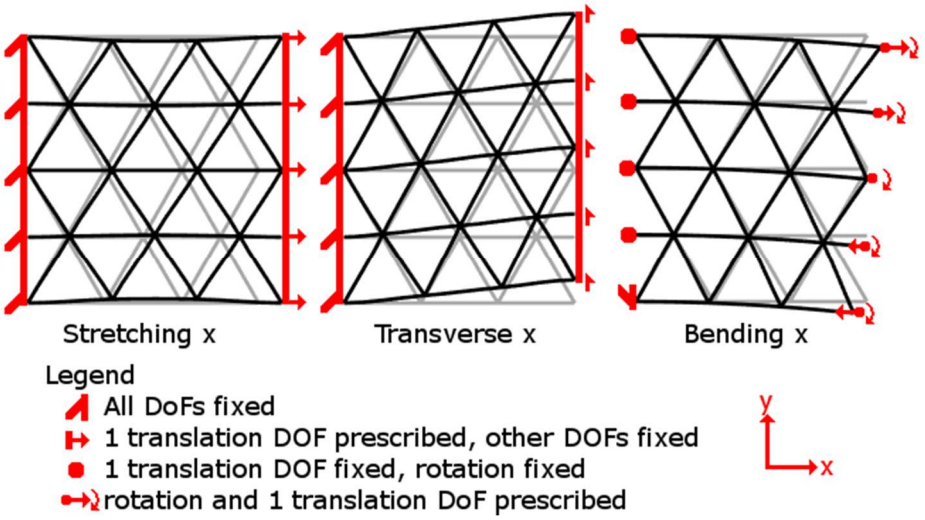

Figure 4: Primary boundary conditions for the X direction.

The three boundary conditions shown in Figure 4 have certain DOFs fixed or prescribed on the +x and –x faces, and the DOFs on the +y and –y faces are free. In these boundary conditions, the x direction is the axial direction and the y direction is the transverse. There are three additional boundary conditions defined by a 90 degree rotation: The DOFs on the +y and –y faces are fixed or prescribed, the DOFs on the x faces are free, y is the axial direction, and x is the transverse direction. All of the boundary conditions are named for their axial dimension. The results of the simulations will be discussed in terms of the macro-aspect ratio which is defined as the ratio of the axial dimension to the transverse dimension. Figure 5 shows an example of Transverse X and Transverse Y boundary conditions with a high and low aspect ratio.

In this work a boundary condition topology pair (BCT pair) is defined as a combination of a boundary condition and topology. Individual studies will hold a BCT pair constant while other variables such as the number of repeating cells are changed. This paper uses 26 distinct primary BCT pairs, spanning every non-redundant combination of topology and boundary condition described in Section 2.2.

The stretching and transverse boundary conditions simulate rigid plates being attached to opposite faces of the lattice and one of those plates undergoing a prescribed translation. In the bending x boundary condition the x DOFs are fixed or prescribed and the y DOFs are free in order to allow Poisson's effect in the y direction. For the x face, the x displacement and micro-rotation DOFs prescribed to produce a rigid body rotation of C radians are defined by

$$u_x = C\,y \quad and \quad \phi_z = C \tag{4}$$

Although the stretching boundary condition is strongly dominated by normal stresses in the axial direction, there is transverse contraction away from the fixed edges. In the continuum model, this produces relatively small shear stresses, which are responsible for small size effects.

The transverse boundary condition behaves very differently at high and low aspect ratios. At very low aspect ratios the behavior is strongly dominated by shearing stresses. At high aspect ratios, it is strongly dominated by bending (normal) stresses.

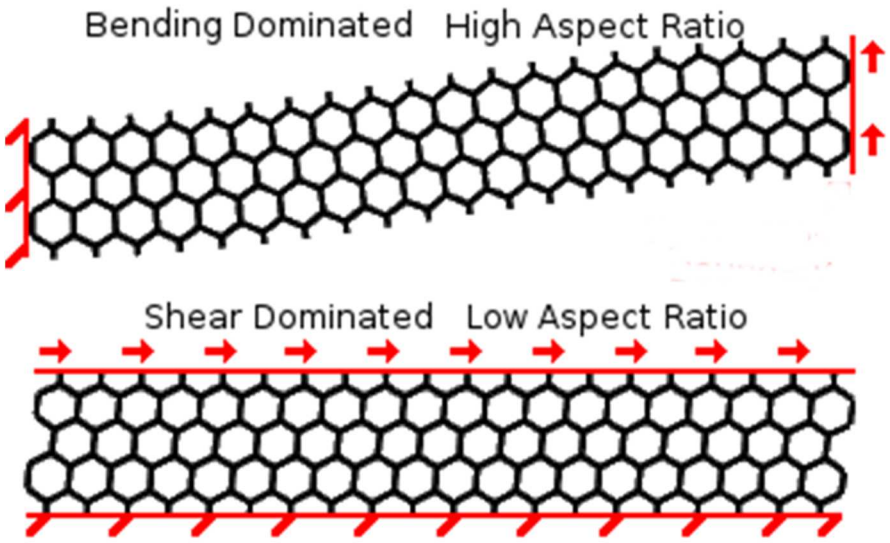

Figure 5: Transverse boundary conditions show bending at high aspect ratios and shear at low aspect ratios.

Gauthier (Gauthier, 1974) presented an analytical solution for a micropolar elastic continuum in pure bending that matches the loading conditions used in this work. Stress and strain do not depend on the axial dimension, only the transverse dimension. The non-dependence on the axial dimension has been observed in both the micropolar and lattice simulations.

2.2.3 Validation

In order to validate the Matlab FEA codes reference problems are solved and FEA results compared to references. The lattice and classical FEA codes were compared to identical simulations done in ABAQUS (Simulia, n.d.), with the non-linear geometry flag turned off for linear analysis. The results matched to 6 significant figures.

The micropolar FEA code was compared to a published analytical solution for an infinitely wide patch in shear (Diebels & Scharding, 2011b). Strains matched to 0.004% while curvatures matched to 0.01%. This validation is described in detail in the Appendix A1.

A convergence study was also done to quantify the convergence error in the micropolar FEA Matlab code. A full description of the convergence study can be found Appendix A2. The convergence study showed that using 35 quadratic finite elements in each direction for the domains used in this work produces a numerical error around 0.03%, which is considered negligible.

2.2.4 Simulation Studies

In order to investigate the ability of the micropolar elastic model to predict size effects, a series of triplets that keep BCT pair, the macro-size and macro-aspect ratio, and total mass constant, but divide the material domain into smaller and smaller unit cells. The total mass remains constant because the ratio of cell wall length to thickness is held constant with a ratio of 10 to 1. Each triplet is a lattice, micropolar, and classical simulation all solving the same problem.

The smaller dimension of the material domain was divided into between 2 and 30 unit cells. The larger dimension of the material domain was divided by a multiple number of unit cells used for the smaller dimension. This was used to create macroscopic height to width aspect ratios between 7 and 1/7. Figure 6 shows the lattice topology for a selected size study. Results are reported as ratios of stiffness, and thus are independent of the value of the macro length dimensions. Figure 7 illustrates changing aspect ratios. For the bending boundary condition, the

scale of a size effect only depends on the number of unit cells in the transverse dimension, therefore bending only uses an aspect ratio of approximately 1.

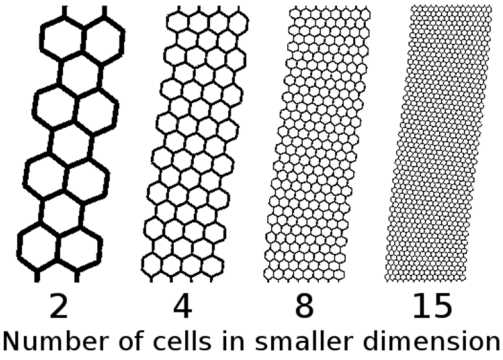

Figure 6: Example size study: Hexagons in Transverse Y loading with an aspect ratio of 3.46.

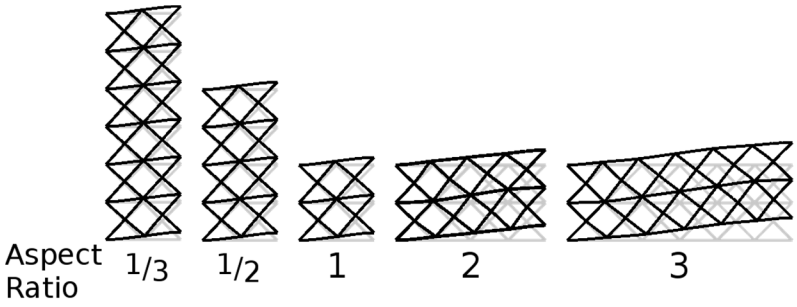

Figure 7: Selected aspect ratios for a Diamond lattice in Transverse X.

2.2.5 Data Set and Description of Supplementary Materials

In this paper, selected results from the 286 different size effect studies performed using the non-redundant combinations of 26 primary BCT pairs, and 11 aspect ratios between 7 and 1/7 are discussed. Sections 0 and 2.3.7 present results for two additional boundary conditions. The supplementary materials to this paper (see appendix A4) contain the Matlab code used to

automatically generate strain energy results and graphs for all or any subset of the BCT pairs studied in the paper. The Matlab code provided also includes a Graphical User Interface (GUI).

2.3 Results for Primary BCT Pairs

2.3.1 Examination of Individual BCT Pairs

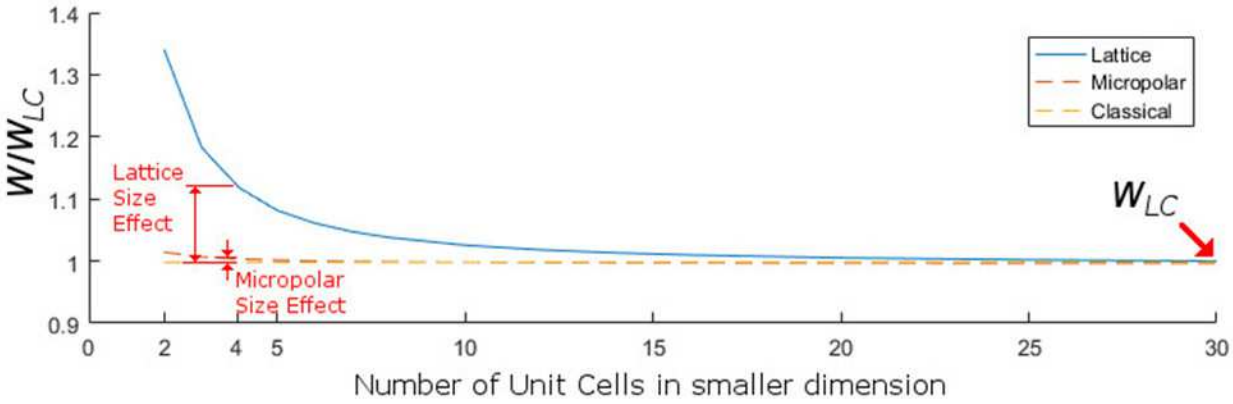

Figure 8: Size effects example for individual BCT pair:
Triangle Lattice under Transverse X boundary condition with a small aspect ratio of 0.38.

Figure 8 shows the results of a selected study for a triangle lattice under transverse load with varying number of unit cells. The total strain energy of the lattice, micropolar and classical elastic models, W_L, W_M, and W_E respectively, are taken for each individual simulation and normalized by dividing it by the lattice strain energy with 30 unit cells, W_{LC}. As expected, the strain energy of the lattice and micropolar models converges to a constant value as the number of cells increases. The difference between the strain energy with a few unit cells and many unit cells is a size effect. This size effect is largest when there are few unit cells and decays to a small fraction of its original size.

Figure 9 gives additional examples of how size effects series in different aspect ratios, boundary conditions, and lattice types have a variety of scales and can be either stiffening or

softening. Figure 9a shows a lattice softening size effect and a micropolar stiffening size effect, consistent with the findings of (Tekoglu, 2007). Figure 9c shows a size effect that is much smaller than the ones shown in a and b.

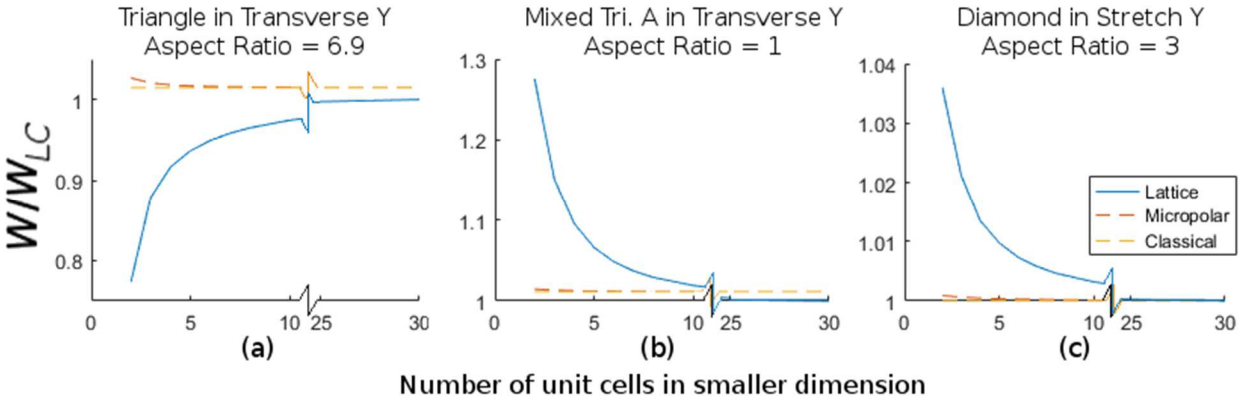

Figure 9: Additional size effect series for different lattice topologies and aspect ratios.

Figure 10 uses the same data as Figure 8 to help illustrate that even though micropolar and lattice size effects may have radically different scale, they decay at the same rate as the number of cells increases. The two sets of size effects are plotted on separate ordinate axes so that their very different scales do not hide their similar trends. When there are 10 unit cells, the size effects are roughly 1/8th of when there are two unit cells. When there are many cells, the size effects are negligible. This pattern is seen across many boundary conditions and topologies.

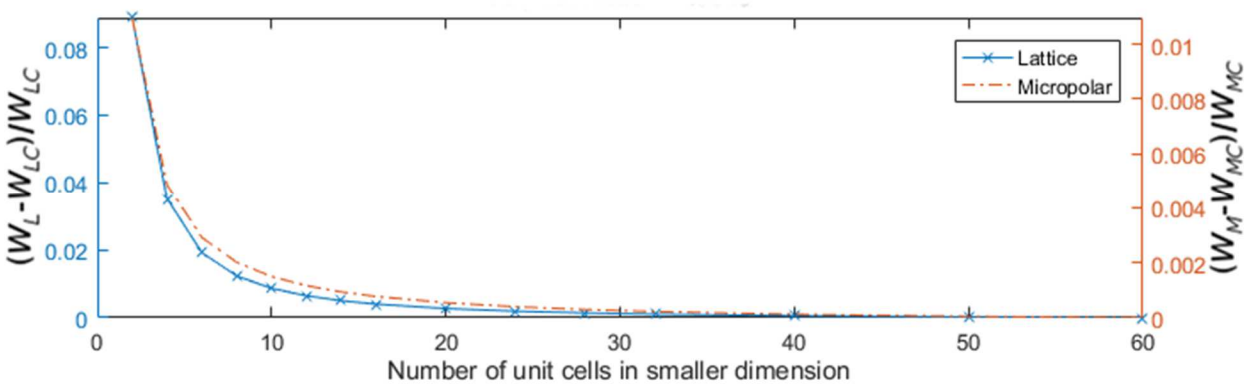

Figure 10: Size effects vs number of unit cells for triangle lattice and Transverse X load with an aspect ratio of 0.38.

Figure 8 also shows several patterns that demonstrate typical size effects of the primary boundary conditions for the different studies conducted. Most BCT pair cases studied show most of these patterns, but few of them show all of these patterns.

1. Because classical elasticity has no way to describe size effects, the global energy of the classical elastic model does not depend on the number of unit cells. All BCT pairs show this pattern.
2. The classical elastic results are close to the micropolar elastic results when there are many unit cells.
3. The global energy of the lattice and micropolar models converge to a uniform result as the number of unit cells is increased. These uniform results are usually within a few percent of each other and are often within 0.5%. The converged model errors will be examined in detail in.
4. The magnitude of the micropolar model size effect is an order of magnitude smaller than the discrete lattice model size effect.

2.3.2 Size Effects as a Function of Macro-Aspect Ratio

In order to determine when and where these patterns are observed, the studies described in the previous section were examined further by changing the macro aspect ratio. Lattice and micropolar size effects are quantified by comparing the global strain energy with four unit cells in the smaller dimension, W_{L4} *and* W_{M4}, to the global strain energies for many unit cells, W_{LC} *and* W_{MC}

$$\mathrm{SE}_L = \frac{\mathrm{W_{L4}} - \mathrm{W_{LC}}}{\mathrm{W_{LC}}}\ ,\ \mathrm{SE}_M = \frac{\mathrm{W_{M4}} - \mathrm{W_{MC}}}{\mathrm{W_{MC}}} \qquad 5$$

The choice to quantify size effects based on 4 unit cells instead of 2 or 8 unit cells is rational compromise: 4 unit cells provides enough unit cells so that the lattice structure can be said to be periodic and repetitive, but not so many that the size effects have decayed to a negligible size.

These results show that the lattice size effects are an order of magnitude larger than the micropolar size effects. This difference is highlighted by plotting the data curves for the lattice and micropolar models with two different y data scales; the left scale for the lattice, and the right for micropolar. This pattern is consistent across almost all BCT pairs studied.

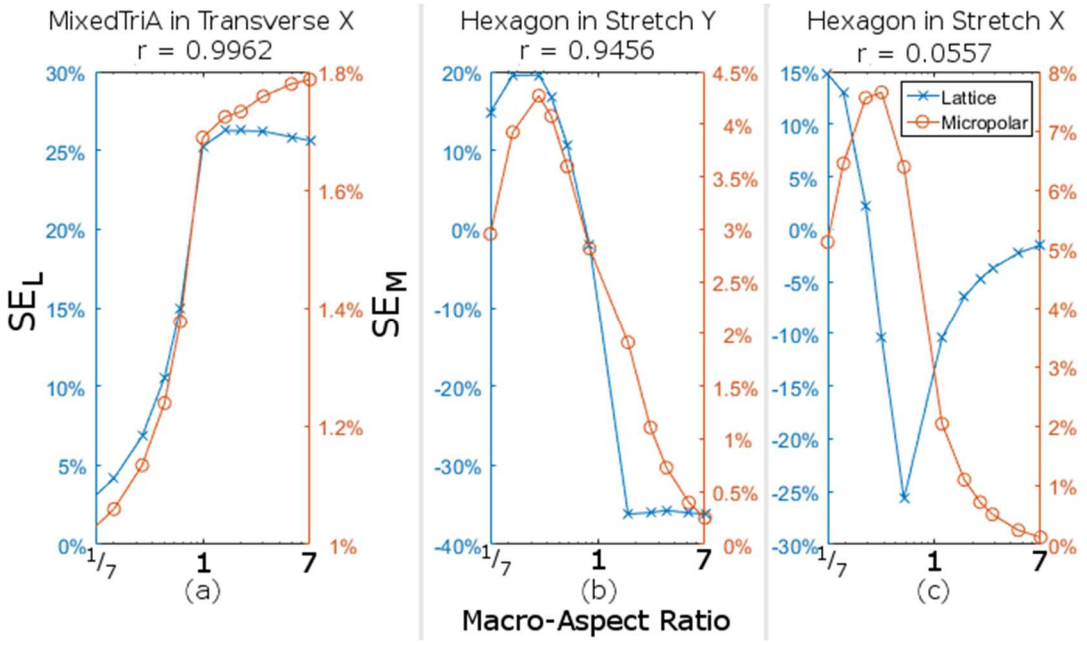

Figure 11: Size effect vs aspect ratio for three selected BCT Pairs.

Figure 11a shows a BCT pair that shows micropolar size effects strongly correlated with the lattice size effects. Correlation is calculated using the Pearson correlation coefficient, r; a value of 1 represents a perfect positive correlation (Hastie, Tibshirani, & Friedman, 2009). The size effects shown in Figures 10b and 10c have a less strong correlation, and no correlation respectively. For the 20 primary non-bending BCT pairs, 9 of the 20 have a correlation value greater than 0.9, and 4 of the 20 are negatively correlated with an r value less than -0.9.

2.3.3 Direction of Size Effects vs. Model Edge Arrangement

Table 3 summarized experimental patterns of size effects discussed in the literature. Table 5 shows the patterns of size effect by boundary condition and topology (BCT pairs) and compares these patterns documented in

Table 3 to the size effect results from the lattice model simulations studied in this work. For certain BCT pairs, the size effect is stiffening at high aspect ratios and softening at low aspect ratios or vice versa.

Model edge arrangement describes whether the transverse side edges of that lattice structure form a straight line with closed cells on the edge or are a zig-zag pattern with diagonal cell-walls on the edge. Figure 12 illustrates these two types of edge arrangement. In the case of straight edges, the edge geometry does not change as the size or number of unit cells is changed. However, for the zig-zag pattern, when the unit cell size is decreased the edge distortion from a straight line decreases as a percentage of the domain volume; Figure 13 illustrates how the zig-zag pattern becomes smaller as the unit cells become smaller.

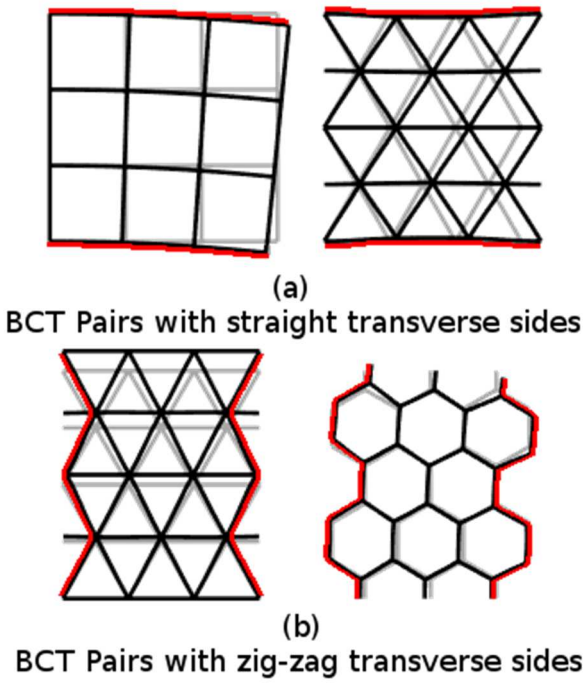

Figure 12: Straight vs zig-zag transverse sides. Transverse edges highlighted in red.

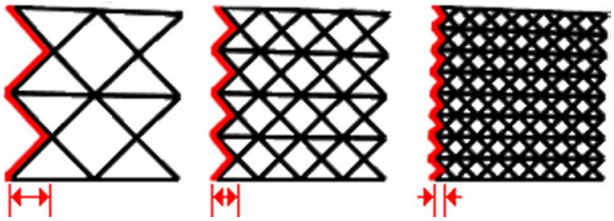

Figure 13: Size of zig-zag offset reduces with reducing unit cell size.

For the bending and compression cases, the BCT pairs with softening size effects have zig-zagging side edges. There is a single exception to this pattern; Mixed Triangle B lattices with a high aspect ratio in stretching have a softening size effect despite having straight transverse edges. The reverse of this pattern is not uniformly true; BCTs with zig-zagging edges do not all display softening size effects. This pattern is notable because it predicts size effects without any reference to micropolar theory, the rotation variables it introduces, or the resistance of lattice beams to rotation. Continuum models do not have a means to describe model edge arrangement.

Table 5: Comparison of direction of discrete lattice size effect and model edge arrangement.

Boundary Condition	Topology	Axial Dim.	Aspect Ratio	Simulated Lattice Effect	Transverse Edges zig-zag
Pure Bending	Diamond	X	All	Stiffer	No
	Mixed Triangle A	X,Y	All		No
	Mixed Triangle B	X,Y	All		No
	Square	Y	All		No
	Triangle	X	All		No
	Diamond	Y	All	Softer	Yes
	Hexagon	X,Y	All		Yes
	Triangle	Y	All		Yes
Transverse Bending Dominated	Diamond	X	High	Stiffer	No
	Mixed Triangle A	X,Y	High		No
	Mixed Triangle B	X,Y	High		No
	Square	X,Y	High		No
	Triangle	X	High		No
	Diamond	Y	High	Softer	Yes
	Hexagon	X,Y	High		Yes
	Triangle	X	High		Yes
Stretching	Diamond	X,Y	All	Stiffer	Mixed
	Hexagon	X,Y	Low		Yes
	Mixed Triangle A	X,Y	All		No
	Mixed Triangle B	X,Y	Low		No
	Triangle	X	All		No
	Triangle	Y	Low		Yes
	Hexagon	X,Y	High	Softer	Yes
	Mixed Triangle B	X,Y	High		No
	Triangle	Y	High		Yes
Shearing	All	X,Y	Low	Stiffer	Mixed

2.3.4 Model Edge Arrangement Discussed in Literature

As discussed earlier, (Anderson & Lakes, 1994) concluded that surface damage and incomplete surface cells can create a softening effect contrary to the stiffening effects seen in micropolar elasticity. (Tekoğlu, 2007) found several patterns consistent with the patterns documented in Table 5:

1. The shear boundary condition consistently produced stiffening size effects due to extra stiff layers near the fixed boundaries.

2. The compression and bending boundary conditions produce softening size effects due to softer layers near the free boundaries.

The foams examined by Tekoglu show incomplete unit cells on the free edges. These incomplete cells produce a zig-zagging pattern that is larger relative to the overall size than for a periodic structure, such as the ones used in this work. The foams show consistent softening size effects in compression and bending. By contrast the periodic structures with zig zagging edges examined in this work show mixed stiffening and softening effects. If there is a stiffening effect associated with fixed edges and a softening effect associated with free edges, those two effects cancel out and only the larger effect is observed. The smaller zig-zag layers in periodic structures may produce a smaller softening effect than a stochastic foam. For the stretching boundary condition used in this paper, this smaller softening effect is sometimes more than outweighed by a small stiffening effect caused by the restrictions on Poisson contraction. Hexagons in stretching X and Y, and triangles in stretching Y, show a stiffening effect at low aspect ratios, but not high aspect ratios, despite their zig-zag edges. At low aspect ratios, the ratio of the length of the free edges to fixed edges is low. This is consistent with the scale of the softening size effect being proportional to the free edges, and the scale of the stiffening size effect being proportional to the fixed edges.

Several of the BCTs show a trend of size effects that matches this hypothesis; Triangle lattices loaded in the Y direction, hexagons, and mixed triangle B lattices all show stiffening effects at low aspect ratios and softening effects at high aspect ratios.

(Wheel, Frame, & Riches, 2015) considered models of beams in pure bending with two different topologies. The first was made of alternating layers of two phase laminate material, where the two lamina materials had very different stiffnesses. The second was made of a solid

material with circular voids arranged in a repeating pattern. A softening size effect was seen when the laminate beam had the softer laminate material on the surface, and when the voids in the second beam intersected the transverse surface. When the voids intersect the transverse edge, it creates a zig-zag pattern. When the stiffer laminate material was on the surface, and when the voids did not intersect the surface, a stiffening size effect was observed.

Wheel et al. interpreted these stiffening size effects as being consistent with micropolar elasticity and reported their characteristic lengths. The softening size effects seen when the voids intersected the surface of second beam are consistent with the pattern of softening effects seen here; straight transverse edges are more likely to see stiffening size effects, and zig-zag edges are more likely to see softening effects.

2.3.5 Model Accuracy with a Large Number of Unit Cells

Table 6 the difference between the micropolar and lattice models when there are 30 unit cells in the smaller dimension for a fixed domain size. As shown in Figure 8, when there are many unit cells each model converges to a single result, but these results may be slightly different. The error between the micropolar and lattice models can be calculated by

$$Error = \frac{W_{LC} - W_{MC}}{W_{LC}} \qquad 6$$

In order to obtain a single representative value for each BCT pair, the absolute values of converged errors for all 11 studies for a BCT pair are averaged. Because all of the converged errors are less than 2%, the micropolar and lattice models match well for the primary BCT pairs.

Table 6: Micropolar model error for many unit cells by BCT.

	Stretch X	Stretch Y	Trans. X	Trans. Y	Bend X	Bend Y
Triangle	0.014%	0.272%	0.077%	0.554%	0.038%	0.954%
Hexagon	0.598%	1.314%	1.099%	3.468%	0.020%	3.893%
Diamond	0.070%	0.059%	0.142%	0.156%	0.127%	0.068%
Square	0%		0.302%		0.133%	
mixedTriA	1.762%		1.529%		2.216%	
mixedTriB	0.204%		0.194%		0.449%	

2.3.6 Investigation of Local Edge Rotation Boundary Conditions

For the primary boundary conditions discussed above, when there are many unit cells, lattice and micropolar models both converge to a single result. The investigations in this section show that when applying a pure local rotation degree-of-freedom boundary condition while fixing displacement components on an edge a different pattern is found. While these pure rotation boundary conditions are useful for studying the value of generalizing classical elasticity theory to micropolar theory, they do not correspond to a common boundary condition found in practical applications.

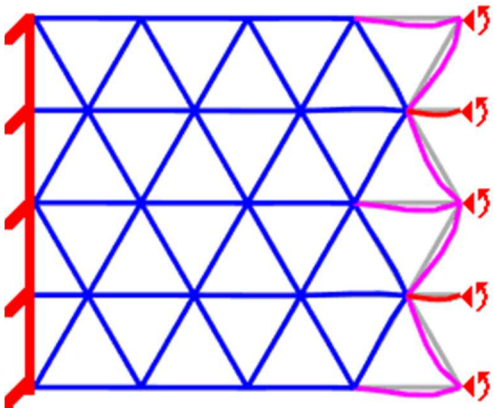

Figure 14:Illustration of the Local Rotation X boundary condition.

Figure 14 illustrates the local rotation X boundary condition. All DOFs on the left hand side are fixed. On the right hand side, the displacement DOFs are fixed and the rotation DOFs are prescribed. Because all prescribed DOFs are zero except the rotation DOFs, this boundary condition has no meaning for the classical elastic model.

The cell walls in Figure 14 are colored according to strain energy; Red is the most strain energy, and blue is close to zero strain energy. Figure 14 shows that most of the strain energy is concentrated in the unit cells adjacent to the prescribed rotation edge. If the number of cells increases, the individual cells get smaller, the stiffness of those cells decreases, and the total amount of strain energy decreases. As cell size approaches zero, global strain energy approaches zero. The entire behavior of the lattice in a local rotation boundary condition is a size effect. The global energy results of this pattern are shown in Figure 15. The green curve shows the error between the micropolar model and lattice model using the scale on the right ordinate.

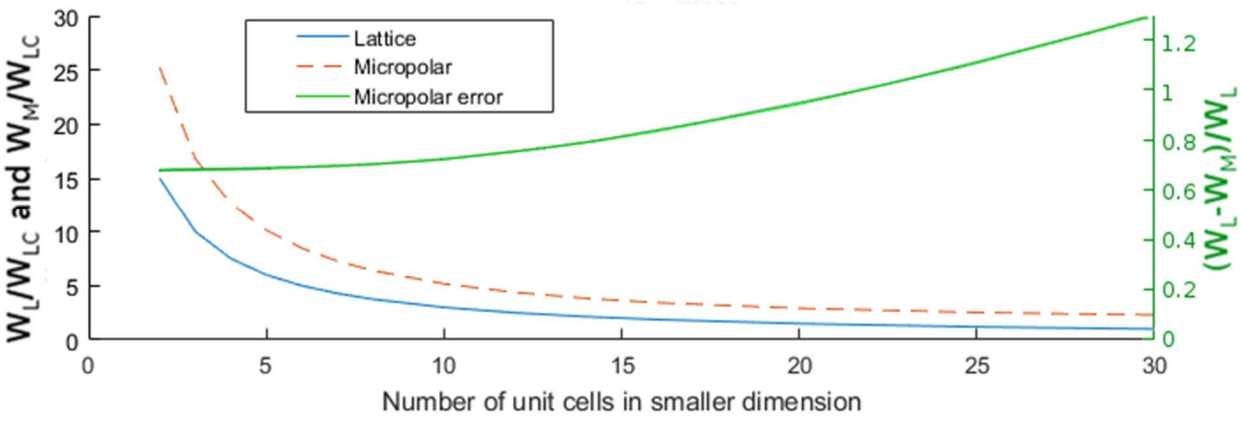

Figure 15: Size effect study for triangle lattice in Local Rotation X, with an aspect ratio of 2.3.

Results in Figure 15, show three patterns typical for size studies of local rotation boundary conditions.

1. Both models show strain energy asymptotically approaching zero, with an increasing number of unit cells.
2. For the square lattices, the micropolar model matches the lattice model to within 2%. In this particular instance, the micropolar model gives a very accurate prediction of a size effect.
3. The error in the micropolar model changes by less than an order of magnitude. There is not a consistent trend for decreasing error as the number of unit cells increases. This is in contrast to the error in the primary boundary conditions, which is high when there are many unit cells and converges to less than a few percent.

These results show that micropolar elasticity can more accurately model size effects for a local rotation boundary condition than the size effects in the primary boundary conditions studied earlier. There is still a considerable error, but is significantly smaller than the errors shown in the primary boundary conditions.

2.3.7 Investigation of Half Space Boundary Condition with Concentrated Load

The half space boundary condition with a concentrated edge load has been investigated by a number of authors. (Kumar & McDowell, 2004) compared continuum models using their material properties to lattice models, both using a finite half space boundary condition. (Warren & Byskov, 2008) and (Stronge & Wang X.L., 1999) separately developed analytical solutions for an infinite halfspace boundary condition.

Figure 16 illustrates a finite sized version of the half-space boundary condition and shows the discrete lattice and the finite element mesh used in the continuum model. The

bottom left corner has a prescribed displacement. The left side has a symmetric boundary condition, $u_x=\phi=0$. The right and top sides have all DOFs fixed. DOFs on the bottom boundary are free. Because the boundary condition contains a singularity created by a point load, it is necessary to have a very fine mesh near that corner. The cell walls in the lattice model are colored according to strain energy. The red cell walls near the corner contain most of the strain energy.

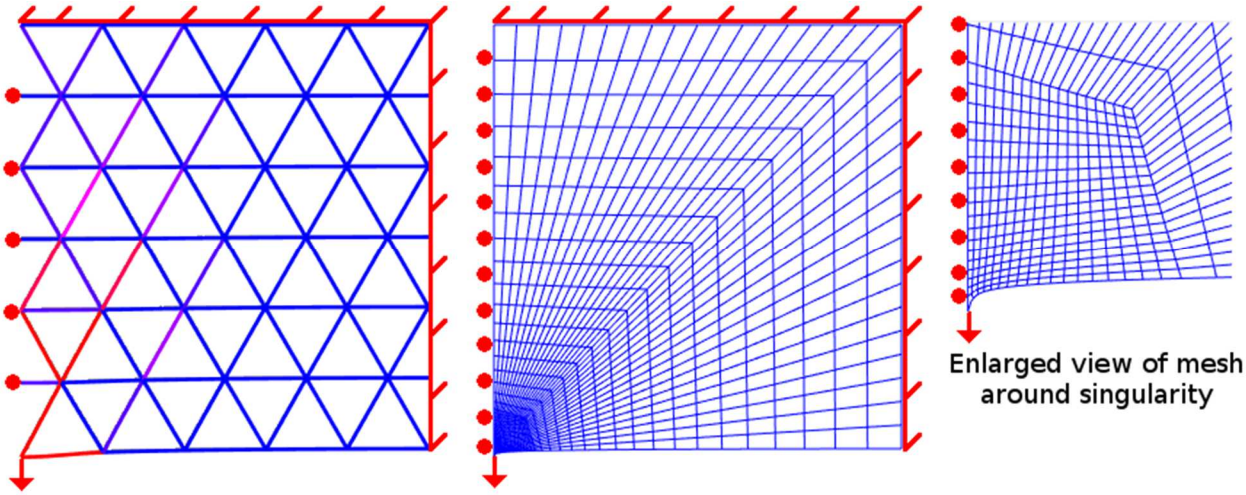

Figure 16: Half-space boundary conditions applied to lattice and continuum models.

Figure 17 shows selected size studies with patterns typical of a size study in the half-space boundary condition.

1. Both lattice and micropolar size effects are much larger than those typical for the primary BCT set. The lattice size effects range from 72% to 172%. By contrast, the lattice size effects for the primary BCT set range from 0.9% to 27%.
2. The micropolar size effects are much smaller than the lattice size effects. This is consistent with the primary BCTs.
3. The lattice model always shows stiffening size effects, never softening size effects.

4. The stiffness of the micropolar model does not match the stiffness of the lattice model, regardless of the number of unit cells. The mean convergence error for a single half space BCT (Equation 6) ranges from 24.1% to 62.7%. By contrast for the primary BCTs, convergence error ranges from 0.01% to 3.8%.

The half-space boundary condition results suggest that continuum theories do not accurately model total strain energy from concentrated point loads; The lattice model consistently shows a much higher total stiffness than the micropolar model. The primary boundary conditions studied earlier distribute the load out over an edge, instead of a single point like this half-space problem. For the point load case, the size effects measured by total strain energy shown in the discrete lattice are not accurately represented in the micropolar continuum theory, even as the number of unit cells is increased.

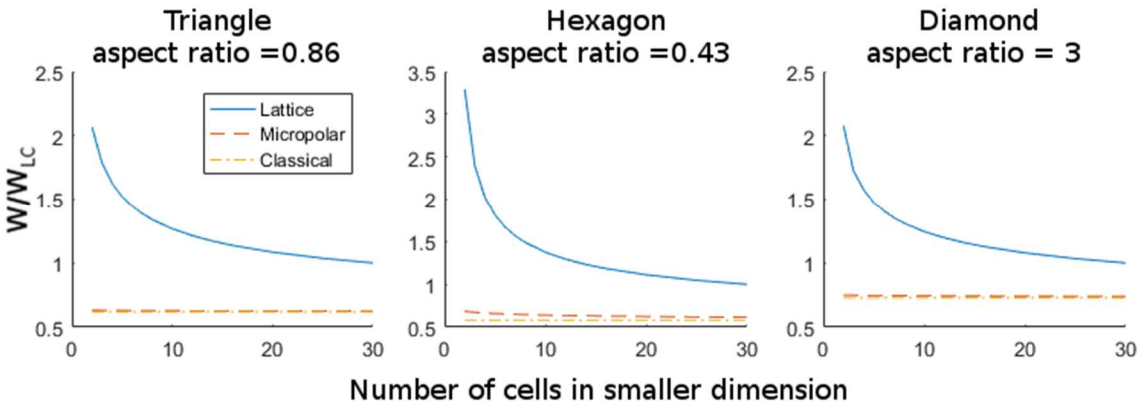

Figure 17: Typical size effect series for halfspace BC. Triangles with an aspect ratio of 0.21.

2.3.8 Effect of Material Distribution on Size Effects for Bending

This section examines a size effect due to the distribution of material on the inside of the material domain. Consider the size effect study for a square lattice in pure bending shown in

Figure 18. These simulations show a global behavior similar to a Euler-Bernoulli beam in pure bending with plane sections remaining approximately plane. As shown in the figure, the strain energy is distributed linearly from zero at the neutral axis to maximum values at the edges of the overall beam structure. Using this observation, the global stiffness of the macro-beam can be approximated by calculating the second moment of area of the individual beams and adding their contributions for a total moment of area. A similar analysis was given in (Dai & Zhang, 2009) for computing effective bending rigidity in a beam model for coupled-stress theory.

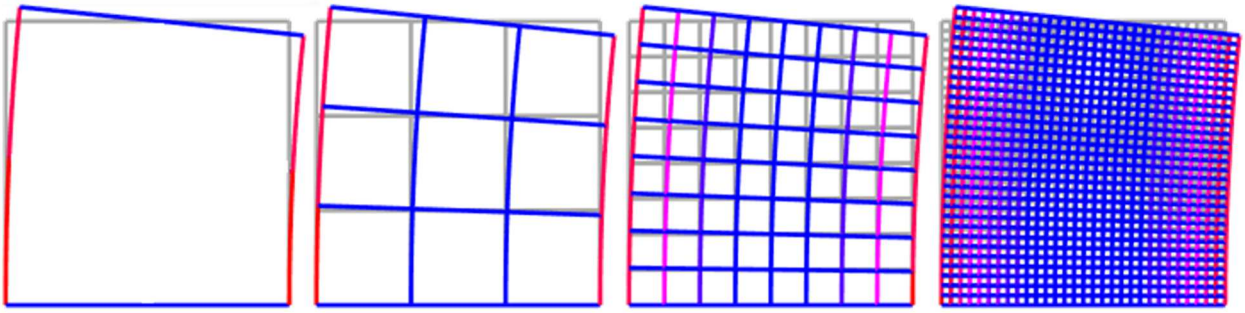

1 cell *3 cells* *8 cells* *30 cells*

Figure 18: Selected simulations for a square lattice in pure bending. The cell walls are colored according to strain energy magnitude.

Equation 7 shows how the standard formula for the second moment of area in a beam made of a solid homogenous elastic material can be specialized to a cross section of a square lattice beam. x is the horizontal dimension, z is the dimension into the page, t denotes beam thickness, and the subscript i denotes the individual beams.

$$I_z = \iint x^2 dx\, dz = \sum t_i\, x_i^2 \qquad 7$$

Equation 8 shows the strain energy for a homogeneous beam in pure bending (Budynas & Nisbett, 2006).

$$W = \frac{\theta^2 \, E_s \, I_z}{2 \, L} \qquad 8$$

Equation 8 is applied to each lattice used in the study, and Figure 19 shows the resulting energy plotted against the energy results for the actual lattice simulations. The result of Equation 8 very closely matches the results of the detailed lattice simulation. In this specific case, there is a size effect that is independent of local microrotation effects described by micropolar elasticity. This size effect happens because the second moment of area is highest when material is concentrated farther from the neutral axis, which happens when the number of cells is reduced. When there is just one cell, all of the material is as at a maximum distance from the neutral axis. As more and more cells are added, the amount of material close to the neutral axis increases.

This size effect is not present in the continuum models for homogenized material properties because the continuum models do not describe the specific arrangement of beams. In the construction of the micropolar model from a beam lattice model, the arrangement of a single unit cell is used to derive continuum material properties, and then the information about where those beams are located is discarded.

The difference between the predictions of beam theory for the lattice and the lattice FEA begins at 0.35% for the one-unit cell division, and decreases as the number of cells increase. The resolution of Figure 19 is too low to show any difference.

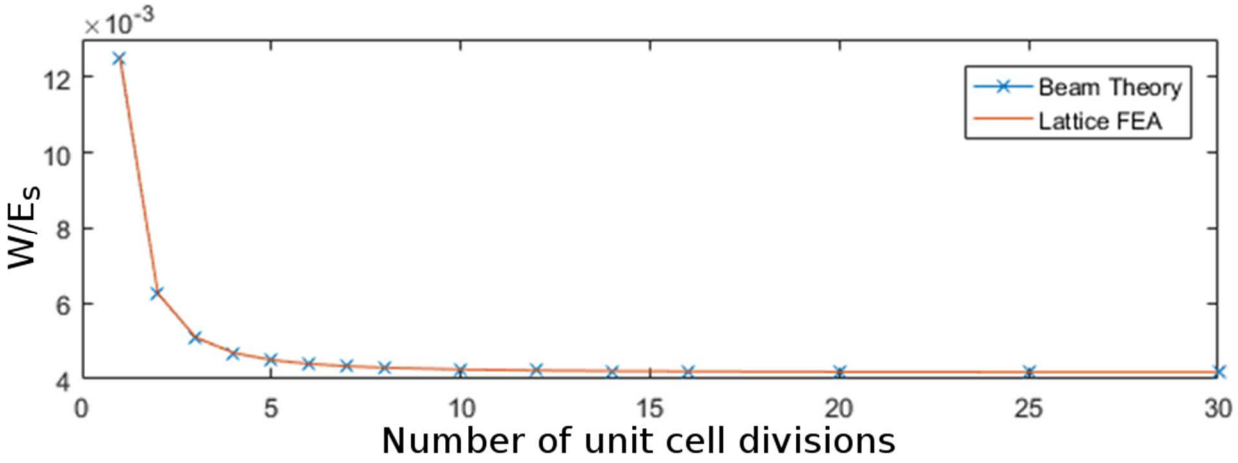

Figure 19: Comparison of two predictions of bending in a square lattice structured beam: beam theory vs. lattice FEA.

This shows that this specific size effect was created by redistributing material within a structure. This will be referred to as a material distribution effect. The square lattice in bending was examined because it was simple enough to be amenable to simple analytical calculations. Future work will examine material distribution effects in other situations, such as shear loading.

2.3.9 Comparison with Literature

(Liu & Su, 2009a) derives material properties for a variety of cellular materials based on couple stress theory, including square and mixed triangle A lattice topologies that match the ones used in this work. Couple stress elasticity is a simplification of micropolar elasticity. The micro-rotation tensor is constrained to be equal to the macro-rotation tensor instead of being independent as in micropolar elasticity. Liu and Su derived their material properties based on assumed strain and curvature fields for a unit cell and applied these material properties to a couple-stress model of a beam made of a lattice material. The couple-stress beam model was tested in pure bending and the prediction of the micropolar size effect between their couple-stress beam model and the discrete lattice match nearly exactly. For the square and mixed

triangle A topology studied, the pure bending problem only activates size effects in the bending deformation of beams with but does not include edge size effects. In general, size effects include the resultant actions of both the edge effects and the micropolar beam bending effects (Anderson and Lakes, 1994).

Table 7 compares the material properties reported in Liu and Su for coupled stress theory the equivalent micropolar properties used from Kumar and McDowell which are consistent with other derivations in the literature as discussed earlier and implemented in this paper. Although the properties relating stresses to strains, D_{11}, D_{22}, D_{12}, and $D_{33C} = D_{33} + D_{34}$, are the same for both papers the properties relating couple stress to curvature, D_{55} and D_{66}, are different by an order of magnitude. The values for D_{55} reported by Liu and Su are 50 and 13 times larger for the square and mixed triangle A lattices respectively. Liu and Su note a mismatch between their D_{55} properties and those derived for couple stress theory (Adachi, Tomita, & Tanaka, 1998; Banks & Sokolowski, 1968). In Table 7, the material properties reported for micropolar elasticity were recalculated to match the 20% relative density reported by Liu and Su. The properties reported from (Liu & Su, 2009a) are reported to two significant figures because they had to be read off of graphs.

Table 7: Material Properties from Liu and Su (Couple Stress) vs Kumar and McDowell (Micropolar).

	Square		Mixed Triangle A	
	Couple Stress	Micropolar	Couple Stress	Micropolar
D_{11}/E_s	0.10		0.071	
D_{12}/E_s	0		0.029	
D_{33C}/E_s	1.0E-3		0.029	
$D_{55}/(E_s*t^2)$	1.7	0.033	0.55	0.0414

Table 7 shows that the material properties D_{55} in Liu and Su are dramatically larger than those in Kumar and McDowell, while the other material properties are identical. Using the D_{55} of Liu and Su, the micropolar size effects for a coupled-stress beam model matched the discrete lattice size effect. As shown earlier, using the Kumar and McDowell properties for the same pure bending problem, the micropolar size effects shown were smaller than the discrete lattice size effects. The properties developed by Liu and Su, while matching size effects in pure bending, to our knowledge, have not been tested in a continuum model for general loading cases in order to determine whether the D_{55} they derived is accurate under general conditions. The material properties taken from the literature and used in this work are designed for general loading conditions within a micropolar continuum model, and have not been tailored for any particular loading.

2.4 Discussion

The results show that the primary boundary conditions create global behaviors which are modeled well by micropolar elasticity when many cells are used. They also create size effects, which are modeled less well. When there are many unit cells, size effects are negligible and the micropolar elastic model produces total strain energy results similar to the lattice model.

This paper documents three explanations for why size effects arise in the lattice mode. The three types of size effects are:

1. Stiffening size effects due to local beam bending effects,
2. Surface softening effects due to softer surface layers, commonly related to zig-zagging model edge arrangement,

3. Stiffening or softening effects due to the arrangement of material within the material domain,

This section will reexamine all of the results presented in this work and examine how they may relate to each of these three causes of size effects. More than one of these causes may be present in any given load case. Only the first of these three causes is included in the micropolar elastic model.

Micropolar elasticity attempts to model size effects in lattice structures by including microrotation variables with effective stress-strain material models, including couple stresses related to local curvature to capture the beam section rotation of thin-walled lattice structures. Micropolar material properties derived by (Kumar & McDowell, 2004; Stronge & Wang X.L., 1999) and others are based on the assumption that the beam nature of the lattice material can be modeled by relating micropolar rotation to joint rotation at the vertices of periodic lattice structures. This implies that the size effects modeled by micropolar elasticity arise because of the beam nature of lattice materials. The results of this work show that using these material properties help predict size effects trends compared to classical elasticity in most cases, but severely under predict the total size effect.

Several authors (Diebels & Scharding, 2011b; Tekoğlu, 2007) describe how constrained beam rotation near the fixed boundaries can produce a size effect that can be modeled by micropolar elasticity. Gauthier (Gauthier, 1974) explains how beam rotation can make a lattice-structured beam in pure bending stiffer than the classical properties would suggest. These authors developed analytical solutions for micropolar elasticity that predict size effects. The micropolar FEA code used in this paper was validated against those analytical solutions (shown in Appendix A1) and is consistent with their quantitative size effect predictions.

As discussed earlier, several authors (Diebels & Scharding, 2011b; Tekoğlu, 2007) study how a softer layer on the free surface can create a softening effect. Section 2.3.3 shows that these softer layers are more common when the transverse edges of the model are arranged in a zig-zagging pattern. Section 2.3.8 showed that a size effect can be created by rearranging material within the material domain.

2.4.1 Examination of Causes of Size Effects in Primary BCs.

The primary set of boundary conditions show mixed stiffening and softening size effects, which can be explained using all three causes of size effects. The BCTs with softening effects are much more likely to have zig-zagging transverse edges, which are connected to surface softening effects. Softening size effects were also more likely to be seen at high aspect ratios, where the transverse edges are long and the fixed edges are short. Conversely, the stretching and transverse boundary conditions uniformly showed a stiffening size effect at low aspect ratios. The transverse boundary conditions at low aspect ratios are dominated by shearing. Many authors, (Diebels & Scharding, 2011b; Tekoğlu, 2007) examined shearing in detail and showed how beam bending size effects create stiffer layers within one or two unit cells of the fixed edges. This suggests that for the primary boundary conditions there are stiffening beam bending effects associated with the fixed edges and softening effects associated with the transverse edges.

2.4.2 Examination of Causes of Size Effects in Other BCs

The halfspace boundary conditions create large strains in a small area, and smaller strains in a large area. Both the lattice and micropolar model show larger size effects than for the primary boundary conditions. The lattice model always shows stiffening size effects. The lack

of softening effects can be partly explained by the fact that the halfspace boundary condition contains only one free edge, and the load is directed away from this edge. By contrast, the primary boundary conditions have two free edges and the cells adjacent to these edges carry as much or more stress than those on the interior. The large stiffening size effect is consistent with beam bending effects being very important and surface layer effects being negligible.

The entire behavior of the local rotation boundary condition is a size effect. These size effects are always stiffening. The strain energy is concentrated next to the prescribed displacement edge. The rest of the material domain, including the free edges is relatively unstressed. These size effects are relatively well modeled by micropolar elasticity. The size effects in local rotation are the epitome of a beam bending size effect.

2.4.3 Size Effects in the Micropolar Model

The micropolar size effects for the primary boundary conditions and halfspace boundary conditions are far smaller than those observed in the lattice model. This pattern is consistent for all of the primary boundary conditions and the half space boundary conditions but is not seen in the local rotation boundary condition. The lattice and micropolar size effects are often highly correlated for a given boundary condition and topology. The two size effects may rely on underlying variables, such as macro-aspect ratio, in a similar way.

2.4.4 Future Work

This work attributes causes to size effects by examining global stiffness behavior without examining any local variables, such as local beam forces, or stress and strain in the micropolar model. Future work will distinguish between the different sources of size effects by examining local variables.

A material distribution effect was shown for square lattices in pure bending. This topology and boundary condition are simple enough to be amenable to analytical calculations. Future work will try to distinguish between material distribution effects and other types of size effects in a variety of other topologies and global behaviors.

Micropolar elasticity is meant to predict local lattice beam bending effects, which can often have a relatively small contribution to global stiffness compared to the contribution from translational displacements. The conclusions made in this paper focus on global behavior and do not quantify the ability of micropolar elasticity to predict local effects, such as local stiffness behavior or the reduced stress concentrations observed by (Mora & Waas, 2000; Nakamura & Lakes, 1988).

2.5 Conclusions

A tool was created to compare results of a micropolar elastic model with results of the equivalent thin-walled, periodic lattice structure modeled with exact beam elements and also compare to a classic elasticity model. As expected, it was shown that the models match well when there are many unit cells. It was also shown that the size effects predicted by micropolar elasticity follow similar trends as the discrete lattice model but are far smaller than the size effects predicted by the lattice model. For square structures undergoing pure bending, evidence was provided that suggests that the size effects in the lattice model are mostly caused by differences in material distribution in the transverse direction for lattices with only a few cells in this direction, not by the beam rotation effects modeled by micropolar elasticity.

2.6 Appendices to Chapter 2

A1. Micropolar FEA Code Verification

The micropolar FEA code was compared to an analytical solution for an infinitely wide patch in shear (Diebels & Steeb, 2002). A micropolar FEA problem in Transverse Y boundary conditions was run using the material properties for hexagonal lattices. The problem is 1000 cells wide by 2 tall, with a macro-aspect ratio of 1/289. To ensure accuracy, there were 500 quadratic micropolar finite elements in the y direction, and 20 in the x direction. The displacements and micro-rotations were taken from a vertical line of nodes on the centerline of the material domain. These displacements were processed to calculate the strains and curvatures at the integration points using standard FEA procedures.

Figure 20a and b compare the strain results of the simulations. They appear identical. Figure 20c shows the analytical results compared directly to the FEA results. In all cases the results match to better than 0.013%. Therefore, the micropolar FEA shows the correct behavior.

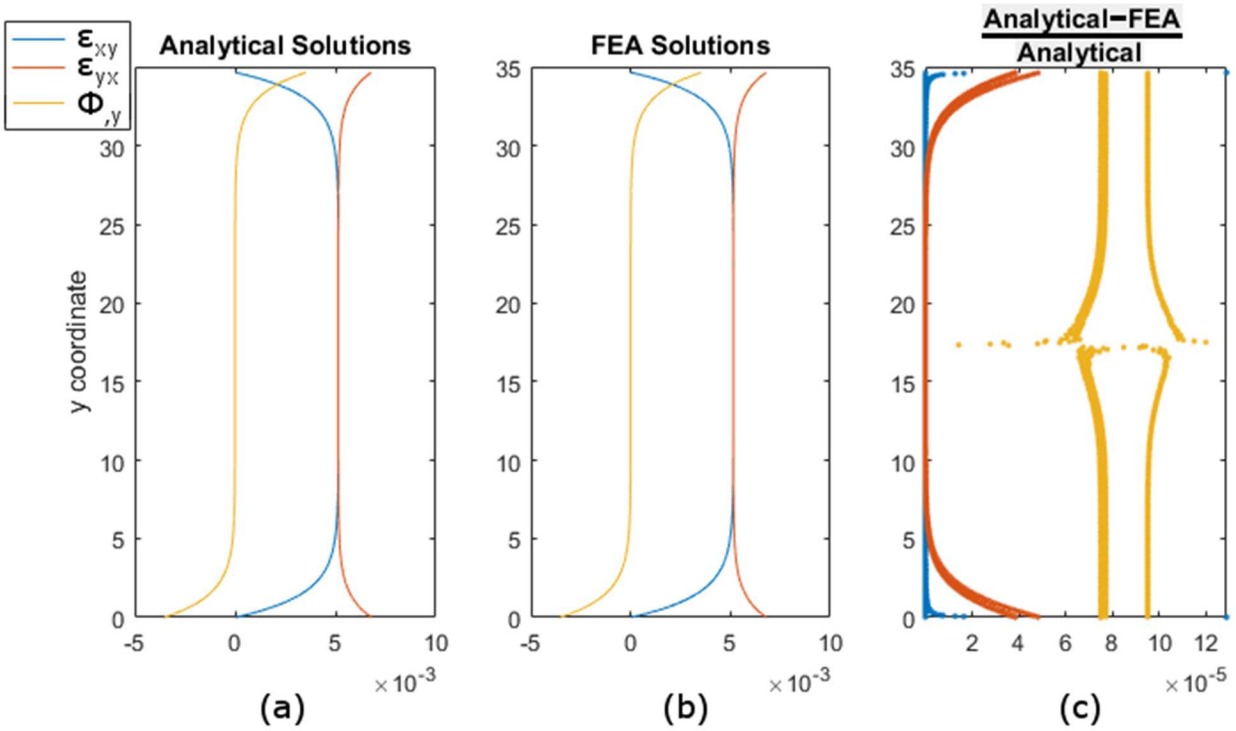

Figure 20: Comparison of analytical solution to FEA solution.

A2. Micropolar FEA Code Convergence Study

A convergence study was run using the micropolar FEA. The problem parameters used in the convergence study are shown in Table 8. The problem domain was divided into a rectangular grid with 4 finite elements in the x direction and 4 in the y. The global strain energy was calculated using Equation 1. The problem was then rerun with twice as many elements in each direction. This process was repeated until there were 256 elements in each direction, 65536 elements total.

Table 8: Problem parameters for Convergence Study.

Lattice Type	Triangle
Ligament Thickness	1
Cell Width	10
Macro dimensions	120 wide by 69.2 tall (12 unit cells by 4 unit cells)
Boundary Conditions	Transverse Y

The solution for strain energy at this last mesh fineness, F_C, was assumed to represent the converged solution. Although no solution can ever be completely converged, this solution is assumed to have negligible convergence error. The convergence error of every other solution, $Error_i$, was calculated using Equation 9, where W_i is the global strain energy for the i-th solution. Figure 21 shows the error plotted against simulation run time for every solution except the converged one.

$$Error_i = \frac{W_i - W_C}{W_i} \qquad 9$$

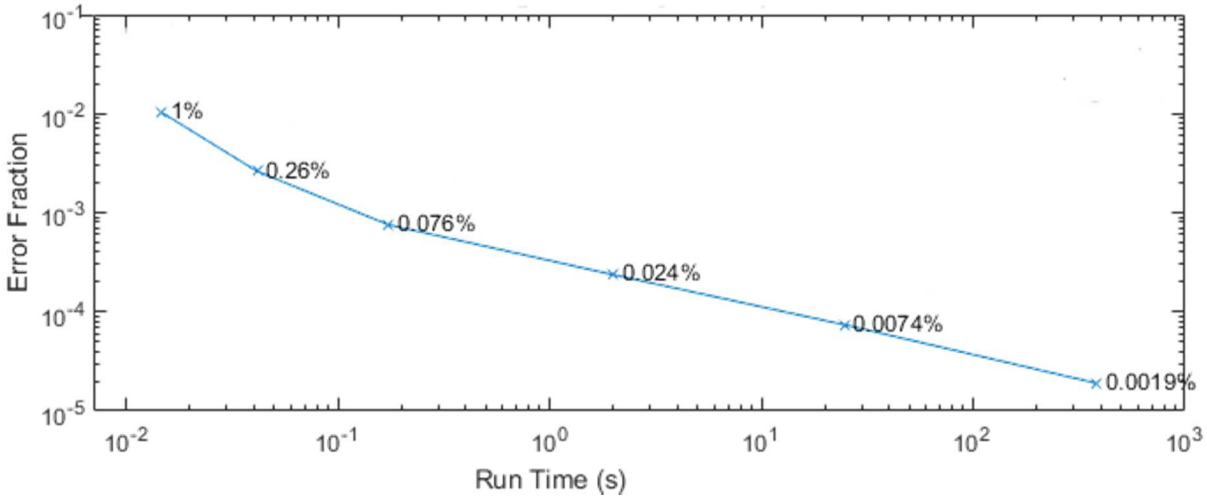

Figure 21: Results of Convergence Study of Strain Energy.

Figure 21 shows that the micropolar exhibits stable convergence behavior. The default meshes fineness used in this paper is 35 elements in each direction. This fineness has a

convergence error similar to 0.024%. Therefore convergence errors are assumed to be negligible.

A3. Corrected Material Property Formulas from (Kumar & McDowell, 2004)

(Kumar & McDowell, 2004) presented a generalized method for deriving the micropolar material properties for a periodic lattice material with unit cells that have indistinguishable node points. The material property formulas for mixed triangle and diamond lattices had an error in the algebra. A Matlab code in the supplementary materials (see appendix A4) reworks this method to derive the correct material properties. The code and the method in the paper follow the following steps:

1. Describe the unit cell. The unit cell has a single node at the origin, x=0 and y=0, and nodes at the end of ligament. Calculate the area of the unit cell.
2. Apply a symbolic Taylor series displacement field to these nodes. The displacement and rotation field is a function of the x,y position of the nodes and of strain variables. The material properties are correct when the strain energy of a continuum with this displacement field is equal to the strain energy of a lattice unit cell with the same displacement field.
3. Calculate the strain energy of the ligaments based on the displacement field, using a standard Euler-Bernoulli stiffness matrix and a nodal displacement vector calculated from the displacement field. The result of this calculation is strain energy as a function of the strain and curvature variables.
4. The material properties are derivatives of the strain energy with respect to the strains.

The original paper had an algebra mistake in Step 3. The stiffness matrix should depend on the length of each ligament. However, the original paper used the same stiffness matrix for all of the ligaments in the unit cell. This is correct for equilateral triangles and square lattices, which have all of the ligaments the same length. However, this was not correct in the original paper for mixed triangle, and diamond lattices, which have different length ligaments. The Matlab code provided in the supplementary material uses the correct length for all ligaments. Table 9 shows the material property formulas for the lattices that have revised material properties. L is the length of the horizontal and vertical ligaments. t is the thickness of the ligaments.

Table 9: New material property formulas for Mixed Triangle and Diamond lattices.

	Mixed Triangle A	Mixed Triangle B	Diamond
D_{11}/E_s	$\frac{t}{L^3}\left(\left(1+\frac{\sqrt{2}}{2}\right)L^2+t^2\right)$	$\frac{t}{4\,L^3}\left(\left(4+\sqrt{2}\right)L^2+t^2\right)$	$\frac{t}{2\,L^3}\left(\left(1+\sqrt{2}\right)L^2+t^2\right)$
D_{22}/E_s	$\frac{t}{L^3}\left(\left(1+\frac{\sqrt{2}}{2}\right)L^2+t^2\right)$	$\frac{t}{4\,L^3}\left(\left(4+\sqrt{2}\right)L^2+t^2\right)$	$\frac{t}{2\,L^3}(L^2+t^2)$
D_{12}/E_s	$\frac{t}{L^3}(\frac{\sqrt{2}}{2}L^2-t^2)$	$\frac{-t}{4\,L^3}(t^2-\sqrt{2}\,L^2)$	$\frac{t}{2\,L^3}(L^2-t^2)$
D_{33}/E_s	$\frac{t}{L^3}(\frac{\sqrt{2}}{2}L^2+2\,t^2)$	$\frac{t}{4\,L^3}(\sqrt{2}L^2+5\,t^2)$	$\frac{t}{2\,L^3}(L^2+2\,t^2)$
D_{34}/E_s	$\frac{t}{L^3}(\frac{\sqrt{2}}{2}L^2-t^2)$	$\frac{-t}{4\,L^3}(t^2-\sqrt{2}\,L^2)$	$\frac{t}{2\,L^3}(L^2-t^2)$
D_{55}/E_s	$\frac{2\,t^3}{3\,L}$	$\frac{2\,t^3}{3\,L}$	$\frac{2\,t^3}{3\,L}$
D_{66}/E_s	$\frac{2\,t^3}{3\,L}$	$\frac{2\,t^3}{3\,L}$	$\frac{t^3}{3\,L}$

A4. Instructions for Supplementary Materials

This chapter was originally submitted as a paper to the *International Journal of Solids and Structures*, entitled “Size effects in lattice structures and a comparison to micropolar elasticity.” The supplementary materials are available on their site.

https://doi.org/10.1016/j.ijsolstr.2018.03.013

3. Edge Softening Effects

3.1 Introduction

This chapter will examine two explanations of why size effects occur:

1. Models for cellular materials have a rotational degree of freedom in addition to translation. This gives rise to couple stresses in a continuum model and contributes an additional stiffness that is most important when there are few unit cells in the finite size periodic lattice structure.
2. A layer of damaged or poorly connected cells near the free surfaces of the material contributes less to the stiffness than cells in the bulk of the material.

3.1.1 Literature Examining Beam Bending Effects

Lattices composed of truss elements with pin connections and loads at end points can be homogenized into a classical (Cauchy) elastic continuum (Tollenaere & Caillerie, 1998), because the deformation of truss elements can be completely described by translation and extension behavior. In contrast, a lattice of beam elements can be homogenized using a generalized continuum theory, one common choice is a micropolar elastic continuum (Dos Reis & Ganghoffer, 2012). Both micropolar elastic continuum and beam element models contain a rotational degree of freedom that classical elasticity and truss structures lack. The micropolar elastic rotation gives rise to couple-stresses, which are analogous to the internal couples of individual beams in a thin-walled lattice, and contribute additional stiffness particularly when the cell size is comparable to the size of the whole structure.

Chapter 2 found that the size effects present in a micropolar model were much smaller than the size effects in a discrete lattice beam model. That work used material properties

derived on the assumption that the micropolar continuum arises from the rotational degrees of freedom of the beam lattice and effects of the boundaries are negligible. Based on these studies, this work assumes that the beam behavior of lattice materials is one cause of size effects.

3.1.2 Literature Examining Edge Softening Effects

Several papers have concluded that the free edges of a cellular material contribute less to stiffness than the interior, and attribute a global softening effect to this. All of these papers attribute this to damaged or incomplete cells near the surface of the material. Figure 22 shows an example of a simulated stochastic foam with incomplete surface cells.

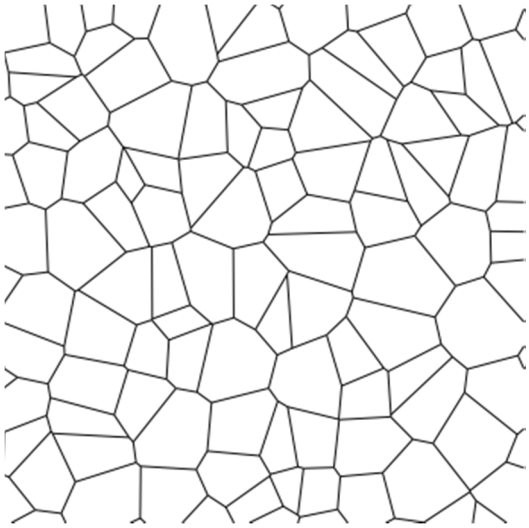

Figure 22: Virtual sample of 2D stochastic foam with open cells on the surfaces.

(Brezny & Green, 1990) observed softening size effects in experimental specimens of reticulated vitreous carbon, a stochastic foam, loaded in bending and torsion. They attributed the softening effect to a surface layer where “the cells are poorly connected” or have been damaged by a machining operation. The experimental data was compared to a mathematical

model of a beam with the surface made of a softer material. The best fit between the model and data occurred when the softer surface material had close to zero stiffness, indicating that “This layer of poorly connected cells is included in the total sample volume but contributes very little to the mechanical properties.”

(Anderson & Lakes, 1994) experimentally examined size effects in a closed cell foam. A stiffening size effect was seen when the specimens were machined while taking great care not to damage the surface, but a softening size effect was observed when specimens were “lathe-cut with no particular care to avoid damage.” They observed damaged and incomplete cells near the surface of the material. These specimens were in bending and torsion, which put the most stress on the surface of the material and maximized the softening effect of this surface layer.

(Tekoğlu, 2007) used simulations to examine size effects in 2D stochastic foams, and concluded that there is a softening layer near the free surfaces caused by incomplete unit cells. The results clearly show cell walls hanging in space and significant voids near the free surfaces of his simulated material.

(Liebenstein, Sandfeld, & Zaiser, 2018) examined simulated size effects in both an ordered hexagonal lattice, and a stochastic foam based on a perturbed honeycomb lattice. Their specimens were loaded in stretching and shear. They developed a method for mapping an effective stress and strain from the discrete model. For the ordered hexagons in stretching, they averaged their results over a variety of different lattice realizations, where some lattice realizations had incomplete cells on the free surfaces. They observed a global softening size effect, and a slight dip in stress near the free edges, but they attributed the global softening size effect to a decrease in stress in the whole lattice as the unit cells became coarser, rather than a softer surface layer due to incomplete cells near the surface.

It is important to note that not all stochastic foams show a net softening effect. Several papers from Lakes's group, (Anderson & Lakes, 1994; Lakes, 1983, 1991a; Rueger & Lakes, 2016) examined open and closed cell foams and showed stiffening size effects in bending or torsion. They all used the careful specimen preparation methods introduced in (Anderson & Lakes, 1994) to avoid surface damage. Tekoğlu (Tekoğlu, 2007) and Diebels and Steeb (Diebels & Steeb, 2002) separately found stiffening effects when simulating a 2D stochastic foam and periodic honeycombs in shear. Because periodic boundary conditions were used, there were no free edges, and no possibility of free surface effects.

Several authors have derived theoretical effective material properties for periodic lattice structured materials (Bažant & Christensen, 1972; Dos Reis & Ganghoffer, 2012; Gibson & Ashby, 1999; Kumar & McDowell, 2004). These works use an analysis of a single unit cell to construct effective properties for a lattice made of periodic repetitions of that unit cell. All of these works assume, implicitly or explicitly, that the cell is surrounded on all sides by neighboring identical cells, and thus are not truncated next to a boundary; Cells on the edge boundaries are not given any special consideration. The results of this work will show that this assumption is mostly correct for most lattice topologies, but needs amendment in certain situations.

3.1.3 Problem Statement

This paper helps explain and quantify the causes of size effects in periodic lattice structured cellular materials. In particular, this paper will examine how changes in the bending of beams in stretch dominated lattice contributes to size effects, and examine how a softer

constitutive relation near the free surface of a periodic cellular material contributes to softening size effects.

This work quantifies how much softer the free surface layers are than the bulk of the material, and connects that softer surface layer to a global softening size effects. The results demonstrate that although the presence or absence of edge softening layers is dependent mostly on lattice topology, macro-aspect ratio and boundary conditions can have an effect on the scale of this size effect.

Although much of the literature focuses on size effects in stochastic cellular materials, this work examines only periodic cellular materials. Because the mechanical behavior of stochastic cellular materials depends both on the number of cells and the random arrangement of cell walls, any examination of size effects in stochastic cellular materials must filter out this random noise to see the size effect signal. This work only examines periodic cellular materials in order to remove the effects of this randomness, and more directly examine the causes of size effects, especially near free boundaries. . Stochastic cellular materials are unlikely to have complete unit cells on their free surfaces. This work chooses to examine periodic cellular materials with surface cells as complete as possible.

3.2 Methods

The beam lattice model first introduced in Chapter 2 is used again here with small modifications. The total strain energy of the lattice is calculated using,

$$W_L = 1/2\ \vec{u}^T K \vec{u} \qquad 10$$

where $\vec{u}$ is the global displacement and rotation vector, and *K* is the global stiffness matrix.

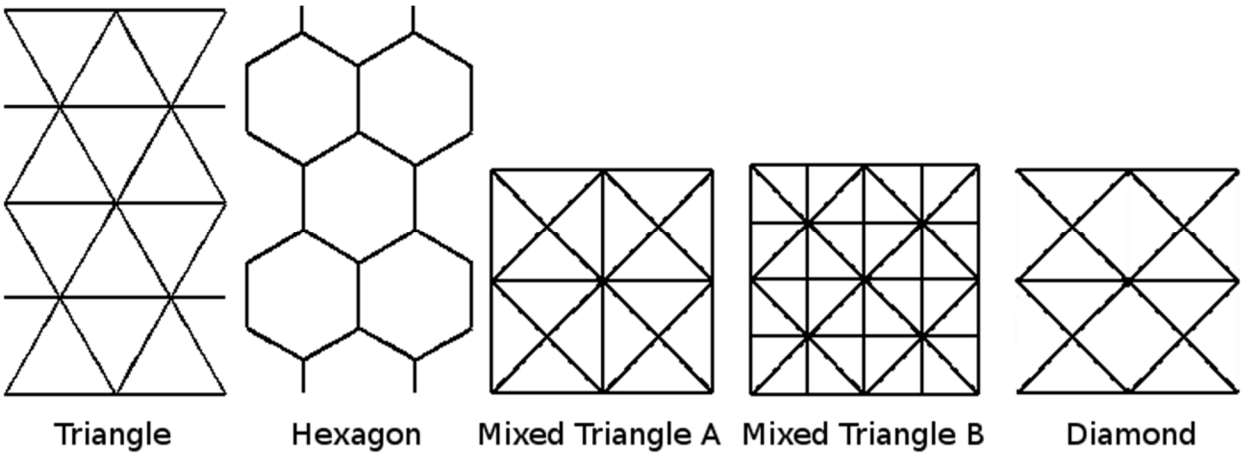

Figure 23: Two unit cells by two unit cells of each lattice topology.

Figure 23 shows the different lattices examined in this study. The square lattices examined in Chapter 2 are omitted here. Figure 24 shows a hexagon lattice using a different choice of unit cell that leaves open cells on the surfaces.

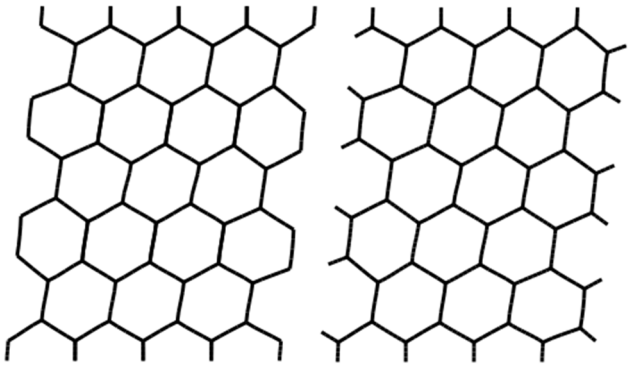

Figure 24: On the left, a hexagon lattice used in this work. On the right, an alternative not used which has open cells on the boundaries.

The literature on edge softening describes damaged and incomplete unit cells on the free edges. By contrast, the unit cells used in this work are chosen so that they are as complete as possible at the free edges; the number of stress free cell walls on the edges is minimized. The

reason for this is to show that, for certain topologies, significant edge effects occur when the edge connections are neither poor nor incomplete.

Figure 25 illustrates the X direction half of the boundary conditions applied to the lattice model. Only the Free Stretch boundary condition is new to this chapter.

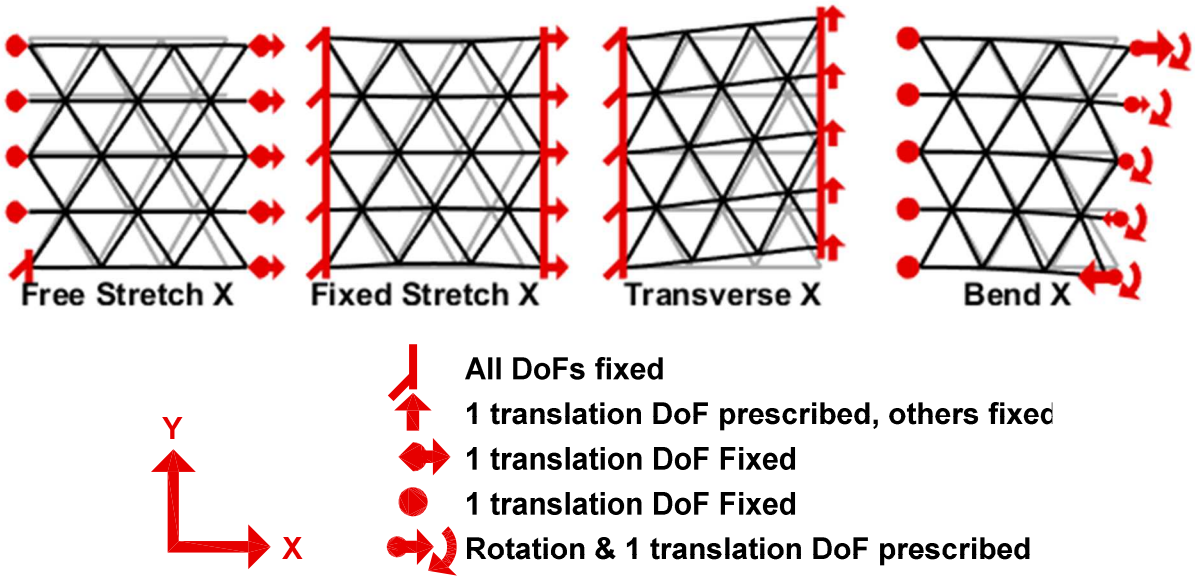

Figure 25: boundary conditions for the X direction.

In the bending-x boundary condition, the x displacement and micro-rotation DOFs are prescribed to produce a rotation of C radians as defined by,

$$u_x = C\,y \quad and \quad \phi_z = C \tag{11}$$

For boundary conditions other than transverse, the aspect ratio was either 1/3, 1, or 3. For the transverse boundary condition, lattices with a high aspect ratio will show a global bending behavior, while lattices with a low aspect ratio will have a global shearing behavior. Any lattices with an aspect ratio greater than 3 are referred to as transverse bending, less than 1/3 as transverse shearing, and lattices between those two cutoffs are defined as “transverse intermediate”. This is a narrower range of as than those used in Chapter 2.

To study size effects, series of simulations are run with the same boundary condition and topology but varying the fineness of the unit cells. The first lattice has either 5 or 6 unit cells in its smaller dimension; The number of starting cells is referred to as the number of base cells. The second has twice as many cells in each direction, and the cells are half the size, with ligaments half the length and thickness. This change keeps the overall dimensions and amount of material constant. The remaining lattices have 4,8,16, and 32 times as many cells respectively. Figure 26 illustrates this. The final three lattices are omitted from Figure 26 because the cells are too small to be seen clearly. The number of cells in each lattice is a slight change from the methods of Chapter 2.

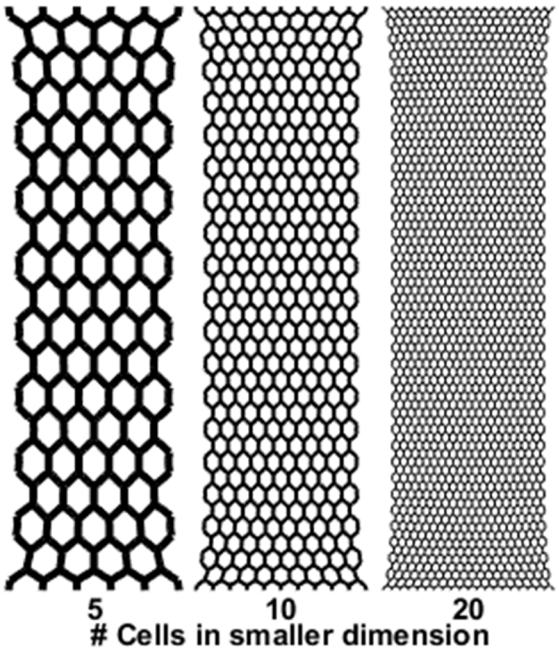

Figure 26: The first three lattices in a selected size effect series.

As the mesh is refined, the strain energy converges asymptotically to a constant value. The lattice size effect for each series is quantified by comparing the lattice strain energy in the finest lattice, W_{LF}, and the strain energy most different from that, W_{LC},

$$SE_L = \frac{W_{LC}}{W_{LF}} - 1 \qquad 12$$

For most series, W_{LC} is the strain energy of the coarsest lattice. Sometimes the lattice strain energy has a non-monotonic size effect; It has a maximum or minimum in the second or third mesh refinement. In these cases,

$$W_{LC} = sign(W_L - W_{LF}) \max(|W_L - W_{LF}|) \qquad 13$$

3.2.1 Bending Energy Size Effects

3.2.1.1 *Calculation of local beam bending strain energy*

The stiffness matrix of a beam element, K_{el}, has an axial component, K_A, and a transverse component, K_B. Equations 14 and 15 show the stiffness matrix written as the sum of two components along with the associated degrees of freedom.

$$K_A\overrightarrow{u_A} = \frac{EA}{L}\begin{bmatrix} 1 & -1 \\ -1 & 1 \end{bmatrix}\begin{bmatrix} u_{a1} \\ u_{a2} \end{bmatrix} \qquad 14$$

$$K_B\overrightarrow{u_B} = \frac{EI}{L^3}\begin{bmatrix} 12 & 6L & -12L & 6L \\ & 4L^2 & -6L & 2L^2 \\ & & 12 & -6L \\ sym & & & 4L^2 \end{bmatrix}\begin{bmatrix} u_{t1} \\ \theta_1 \\ u_{t2} \\ \theta_2 \end{bmatrix} \qquad 15$$

where $\overrightarrow{u_A}$ and $\overrightarrow{u_B}$ are displacement vectors for the axial and transverse dofs, u_a, u_t are the axial and transverse components of displacement, θ, is the beam rotation, the subscripts 1 and 2 denote the two nodes, and L is the length of the beam element. The strain energy of an element can similarly be broken into bending and axial components (w_B and w_A) as,

$$w_{el} = \frac{1}{2}\vec{u}^T K_{el}\vec{u} = \frac{1}{2}\overrightarrow{u_B}^T K_B\overrightarrow{u_B} + \frac{1}{2}\overrightarrow{u_A}^T K_A\overrightarrow{u_A} = w_B + w_A \qquad 16$$

The total bending strain energy of the lattice is the sum of the element strain energies,

$$W_B = \sum w_{el} \qquad 17$$

3.2.1.2 *Local beam bending strain energy size effect*

Much like the lattice size effect, as the mesh fineness increases the bending strain energy converges asymptotically to a constant value. The bending size effect, SE_B, is quantified using,

$$SE_B = \frac{W_{BC} - W_{BF}}{W_{LF}} \qquad 18$$

where W_{BF} is the bending strain energy of the finest lattice, and W_{BC} is the bending strain energy most different from that (similar to Equation 13).

Because the local beam bending size effect is normalized by the total lattice energy, the bending size effect can be compared to the lattice size effect; when the lattice size effect and bending size effect are almost equal ($SE_B \approx SE_L$), it can be concluded that the lattice size effect is caused by the changes in beam bending energy.

Calculation of a bending size effect is used to examine size effects only in stretch dominated lattices. In a bending dominated lattice, the bending energy is approximately equal to the total energy, the bending size effect is approximately equal to the total size effect, and examining bending strain energy does not help explain the causes of size effects. Hexagons are the only bending dominated lattice used in this work.

3.2.1.3 *Motivation for examining local beam bending size effects*

The motivation for examining bending strain energy comes from micropolar elasticity, which models the behavior of cellular materials using equivalent continuum strains. The micropolar elastic model homogenizes a lattice into a continuum with a rotation degree of freedom in addition to the displacement degree of freedom in classical elasticity. For lattice

materials, micropolar rotation is analogous to beam rotation in a beam lattice model. Micropolar elasticity defines curvature as a gradient of rotation, and predicts size effects arising from resistance to curvature.

Consider a single unit cell of a triangular lattice, a type of stretch dominated lattice (Gibson & Ashby, 1999). Assume that the cell wall thickness is one tenth of the length, but the length is left as a variable. Following the methods of (Kumar & McDowell, 2004) the center of this cell is at the origin (x=y=0). A displacement is applied to the nodes using a linear Taylor series. Figure 27 illustrates the unit cell when the displacement and rotation of the i-th node is given by

$$\begin{aligned} u_{xi} &= \varepsilon_{xx} x_i + (\varepsilon_{yx} - \theta_i)\, y_i \\ u_{yi} &= (\varepsilon_{xy} + \theta_i)\, x_i + \varepsilon_{yy} y_i \\ \theta_i &= \kappa_x x_i + \kappa_y y_i \end{aligned} \qquad 19$$

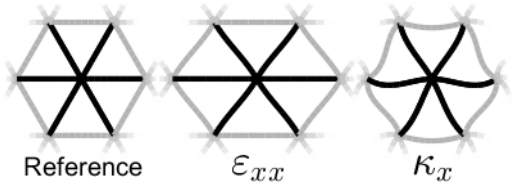

Figure 27: Illustration of the strain displacement relationship in Equation 19. For each case, the strain components other than the indicated strain are 0.

The strain energy and bending strain energy of each ligament are calculated using Equation 16. Table 10 shows strain energy density in the unit cell when one component of the strain is non-zero, and what percentage of that energy is contributed by bending. The energy for normal and shear strains are not dependent on the cell size, and a very small percentage of their strain energy comes from bending. By contrast, the strain energy for curvature is proportional to the cell wall length squared, L^2, and all of the strain energy is due to bending behavior. Because

the bending strain energy is constant with respect to the strains included in classical elasticity and variable with respect to curvature, it is reasonable to expect the bending strain energy for a stretch dominated lattice to converge asymptotically. As the lattice refines the resistance to curvature approaches zero but the normal and shear strains remain relatively constant.

Table 10: Strain energy density in the unit cell for different equivalent continuum strains.

Strain component ≠ 0	W/A	W_B/W
ε_{xx} or ε_{yy}	0.0652	0.33%
ε_{yx} or ε_{xy}	0.0223	2.9%
κ_x	2.89E-4 L^2	100%

Although the methods in this work cannot estimate bending size effects in a bending dominated lattice, this cause of size effects is not necessarily absent. Micropolar elasticity predicts that all beam lattices should have some resistance to curvature and this should cause a size effect.

3.2.2 Edge Softening Size Effect: Constitutive Law Energy Prediction

Previous literature has examined softening size effects due to the free edges of the material being softer than the rest of the lattice. The methods described in this section will quantify how much softer the edge cells are and connect that to a global size effect.

Although Chapter 2 has shown that the micropolar model does not accurately capture size effects for the cases examined in this work, this model provides a useful framework in which to examine size effects. In a micropolar continuum model stress and couple stress, $\vec{\sigma}$, and strain and curvature, $\vec{\varepsilon}$, are related by the constitutive law, $\vec{\sigma} = D\vec{\varepsilon}$, where D is a matrix containing the effective material properties of the lattice. This work will show that, for certain

lattices, the constitutive relation is softer near the edges than in the center; certain elements of the D matrix are smaller near the free edges of certain lattices.

The strain mapping procedure begins after the displacement solution, $\vec{u}$, has been solved. The first step is to map out the effective strains $\varepsilon_{xx}, \varepsilon_{yy}, \varepsilon_{xy}, \varepsilon_{yx}$ and curvatures, κ_x, κ_y for each unit cell. This is done by fitting a 2d linear regression model between the nodal positions and displacements in each unit cell, and using the coefficients of that regression as the derivatives of displacement and curvature. Next, the expected strain energy for each unit cell is calculated using the micropolar constitutive matrix, $w = \frac{1}{2}\vec{\varepsilon}D\vec{\varepsilon}$ and then compared to the actual strain energy of the ligaments in that unit cell. In most cases, the two match to within 1%, but for certain lattices and boundary conditions the actual strain energy is smaller than the expected strain energy on the free edges. This edge softening effect is then used to estimate a global softening effect due to edge softening.

3.2.2.1 *Strain mapping procedure*

The strain mapping procedure is applied individually to each unit cell in the lattice. The nodal coordinates in this unit cell are denoted, x_i and y_i. The displacements and nodal rotations are u_{xi}, u_{yi}, θ. On the edges of the lattice, there are some half-length ligaments where a full length ligament would extend beyond the material boundaries; Any node that is only part of a half-length element is excluded from this analysis. Three two-dimensional weighted linear regressions are used to create a best fit plane relating the nodal coordinates and each component of displacement and rotation using the following equations

$$u_x(x,y) = A + u_{x,x}x + u_{x,y}y \quad (20)$$

$$u_y(x,y) = B + u_{y,x}x + u_{y,y}y \quad (21)$$

$$\theta(x,y) = C + \theta_{,x}x + \theta_{,y}y \quad (22)$$

The six variables from derivatives of displacement and rotation, $u_{x,x}$, $u_{x,y}$, $u_{y,x}$, $u_{y,y}$, $\theta_{,x}$, $\theta_{,y}$, are fit coefficents in the regression. A subscript comma denotes a partial derivative. The constants A, B, and C are also fit coefficients, giving a total of 9 regression coefficients. The regression equation gives nodes on the edges and corners of the cell half and one quarter weight respectively, because those nodes are shared between two and four unit cells.

For the hexagon, mixed triangle, and diamond lattices there are two distinct types of node points and are known as Distinguishable Node Point (DNP) lattices (Perano, 1983). The displacement of these two distinguishable node types do not fit well into a simple linear pattern. Instead they exhibit a stair step displacement. To address this, an additional term, $+D\ w$, is added to the end of Equations 20-22. Where D is another fit coefficient and w is a classifying parameter for the different types of nodes in a DNP lattice; defined as $w_i = 1$ if the i-th node is of the first type and -1 for the second. This modification to a standard plane regression allows the regression to smooth out the two types of node point behavior. Appendix A5 provides a visual guide that illustrates this behavior. Because this behavior is particularly pronounced in hexagon lattices, nodes from neighboring unit cells are included in the regression, but given only ¼ of the weight of nodes completely in the unit cell.

The effective strains are related to the derivatives of displacement and rotation using the micropolar definition of strain:

$$\vec{\varepsilon} = \begin{bmatrix} \varepsilon_{xx} \\ \varepsilon_{yy} \\ \varepsilon_{xy} \\ \varepsilon_{yx} \\ \kappa_x \\ \kappa_y \end{bmatrix} = \begin{bmatrix} u_{x,x} \\ u_{y,y} \\ u_{y,x} - \theta_c \\ u_{x,y} + \theta_c \\ \theta_{,x} \\ \theta_{,y} \end{bmatrix} \qquad 23$$

where θ_c is $\theta(x, y)$ evaluated at the center of the unit cell.

Examination of the resulting strain maps showed that the effective Poisson's ratio sometimes changes near the free edges. The adjusted strain vector, shown in Equation 24, replaces the transverse strain with the expected transverse strain, the axial strain times the Poisson's ratio. This is allows an estimate of what the strain energy would be if the lattice followed the same constitutive law in the center and on the free edges.

$$\varepsilon_{yy} = \varepsilon_{xx}\,\nu \quad \text{for x axial direction} \qquad 24$$
$$\varepsilon_{xx} = \varepsilon_{yy}\,\nu \quad \text{for y axial direction}$$

3.2.2.2 *Constitutive law energy and actual unit cell energy*

The micropolar elastic constitutive law is used to compute expected strain energy from the effective strains. The law relates micropolar continuum stresses and couple stresses to strains and curvatures as,

$$\vec{\sigma} = D\vec{\varepsilon} \qquad 25$$

where D is a matrix of the effective material moduli properties. Several authors (Kumar & McDowell, 2004; Mora & Waas, 2007) have derived formulas for calculating these material properties, based on complete, interior unit cell dimensions and ligament thickness. These formulas were used in Chapter 2 to examine the ability of micropolar elasticity to predict size effects.

These properties are used to test the assumption that the entire material follows the same constitutive effective stress/effective strain relation. The constitutive law energy of a unit cell is given by the micropolar formula for energy density times the unit cell volume, V_{UC},

$$w_C = \frac{1}{2}\overrightarrow{\varepsilon_a}^T D\,\overrightarrow{\varepsilon_a}\,V_{UC} \qquad 26$$

This expected unit cell energy is compared to the actual unit cell energy, which is the sum of the individual ligament strain energies in that unit cell. Each ligament has strain energy, w_{el}, given by

$$w_{el} = \frac{1}{2} {u_{el}}^T K_{el} u_{el} \quad (27)$$

where K_{el} is the element stiffness matrix and and u_{el} is the nodal displacement matrix in global coordinates. The total strain energy in a unit cell is given by

$$w_{UC} = \sum_i \{w_{el}\}_i \, f_i \quad (28)$$

where f_i is the fraction of the i-th element that is inside the unit cell.

The example results presented in Section 3.2.2.4 compare the expected and actual energies using the ratio

$$r = \frac{w_{UC}}{w_C} - 1 \quad (29)$$

When r=0, the expected energy and the actual energy are equal. When r<0 the lattice is less stiff than the micropolar constitutive law predicts.

3.2.2.3 *Connection to a global size effect*

For certain lattice topologies and boundary conditions, most unit cells within two unit cells of a free edge have less actual energy, w_{UC}, than expected energy, w_C. This set of cells is denoted, E, and the cells not in this set $\neg E$. The total constitutive law energy of this set is denoted, $\sum_E w_C$ and total actual energy of all cells not in this set is denoted, $\sum_{\neg E} w_{UC}$. If the edge cells followed the same constitutive law as the rest of the lattice, the total strain energy of the lattice would be approximately equal to $\sum_E w_C + \sum_{\neg E} w_{UC}$. Equation 30 calculates the size effect due to edge softening as:

$$SE_E = \frac{W_L}{\sum_E w_C + \sum_{\neg E} w_{UC}} \quad 30$$

Edge softening is seen only in triangles and hexagons with a Y axial direction boundary condition, and Mixed Triangle B with either axial direction. Edge softening size effects are assumed to be non-existent for other cases.

The edge softening size effect is then added with the bending size effect to find a total size effect. This total size effect gives an estimate of how the two causes of size effects combine to explain the size effect observed in the lattice model.

$$SE_T = SE_E + SE_B \quad 31$$

As discussed previously, SE_B, cannot be calculated for hexagon lattices. Although it is assumed to be 0 in these cases, this is done for lack of a better alternative, not because of any theoretical consideration. SE_E is assumed to be zero for the lattices and boundary conditions that do not have a clear edge softening layer.

3.2.2.4 *Examination of selected results in detail*

This work covers a variety of boundary conditions, aspect ratios and starting number of unit cells. The plots shown in this section are selected because they illustrate broader trends. Triangles in Fixed Stretching with an aspect ratio of 0.96 are selected for illustration because

they clearly show edge softening effects with a minimum of extraneous details.

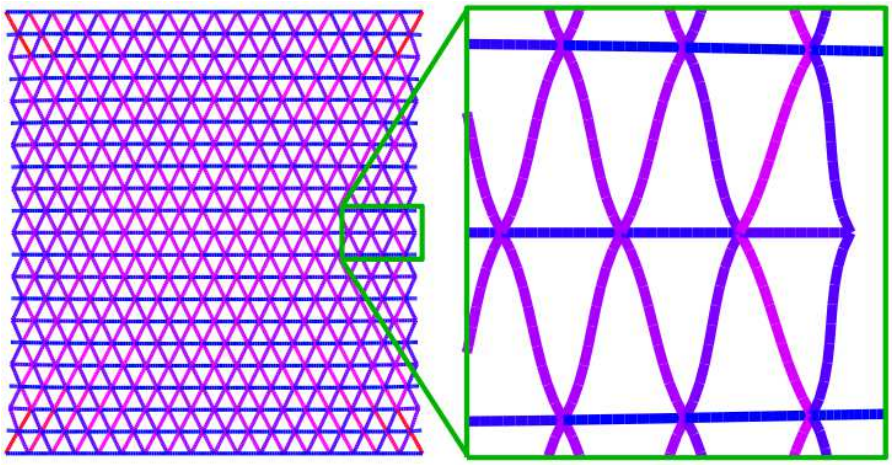

Figure 28 shows the displacement of the second coarsest lattice in the series, along with a magnified portion near the free edges. The deformation of the magnified portion is scaled up 5 times to visualize that cell walls adjacent to the edge deform differently compared to the cell walls just two unit cells in. This suggests that the lattices do not have the same constitutive relation on the edges as in the center. The interior cell walls are surrounded by other walls on all sides. The repeating pattern of cell walls gives rise to a pattern of internal forces. At the free edges, the pattern of cell walls is truncated and the pattern of forces must adjust to that truncation.

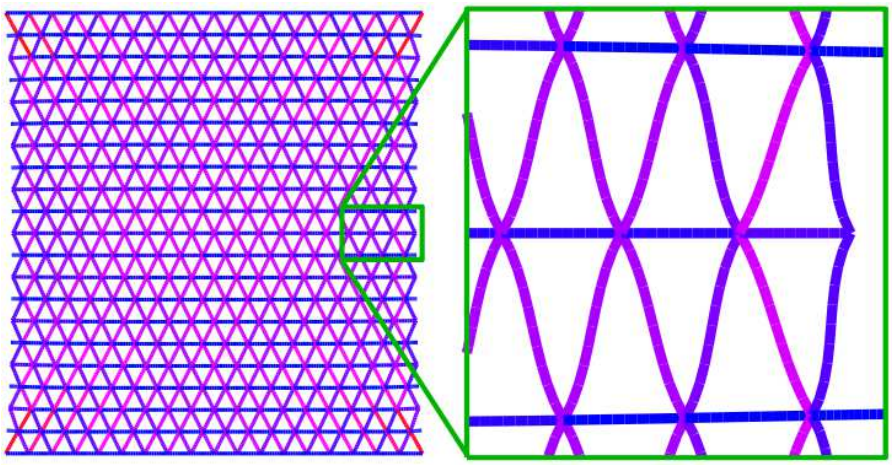

Figure 28: Triangles show a different deformation pattern near the free edges. Cell walls are colored according to element strain energy, with red elements having the most.

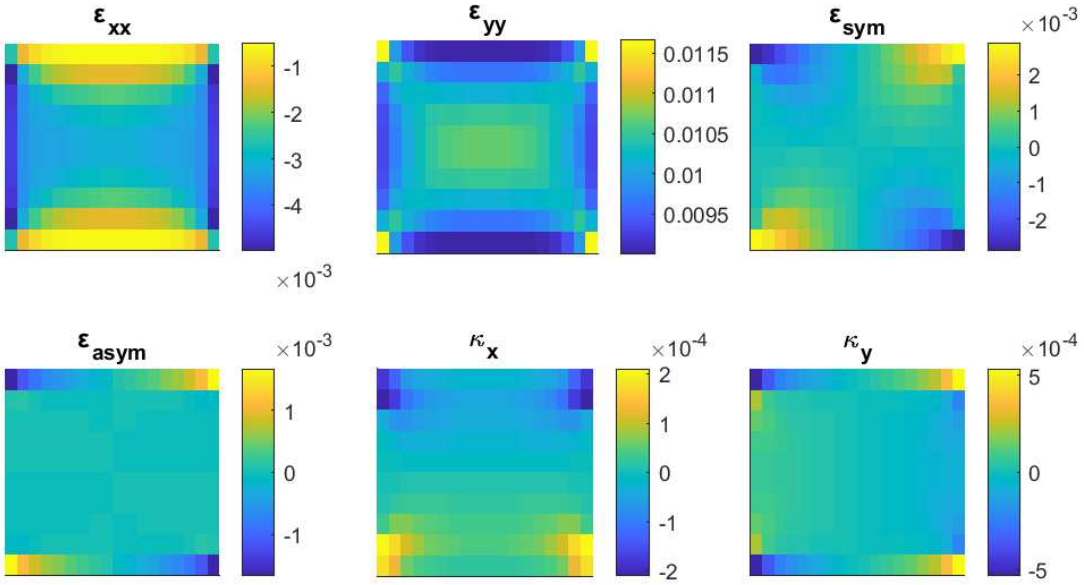

Figure 29: Strain map of example lattice.

Figure 29 shows the strain/curvature map for this lattice. The strain map matches qualitative expectations for this boundary condition. The axial normal strain, ε_{yy}, is positive, with an average value that matches the prescribed strain from the boundary conditions. The

transverse normal strain has the opposite sign and a smaller magnitude than the axial strain. There is significant shear strain near the corners, but little away from them.

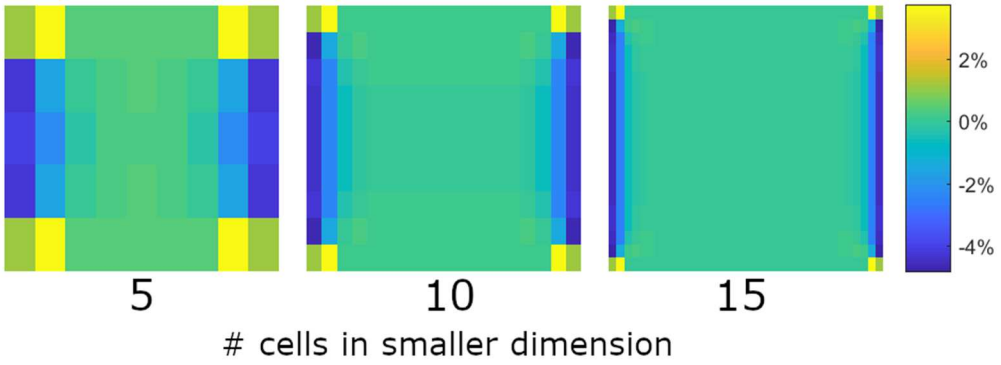

Figure 30: Comparison of constitutive law strain energy vs actual in a series using Equation 29.

Figure 30 shows a comparison of the constitutive law strain energy and the actual strain energy for the coarsest three lattices in the example series. The finer lattices show the same pattern but are omitted to save space. Away from the free edges, the constitutive law unit cell strain energy, w_C, matches the actual unit cell strain energy, w_{UC}, to within 0.5% for the coarsest lattice, and 0.03% for the finest lattice shown. In most of the unit cells adjacent to the free edges w_{UC} is roughly 4% less than w_C. One and two unit cells towards the center, the effect diminishes to 2% and 0.6% respectively. This edge-softening layer is always two unit cells thick regardless of the size of those unit cells. The methods assume that the third unit cell of this edge softening effect can be excluded from any calculation of global size effects. As the mesh becomes finer, the area affected by edge softening becomes smaller and less important relative to the whole. This creates a softening size effect that decays as the mesh refines.

Unlike the edge softening examined in (Anderson & Lakes, 1994; Brezny & Green, 1990; Liebenstein et al., 2018; Tekoğlu & ONCK, 2008) , these unit cells are neither damaged nor incomplete.

3.2.2.5 *Other topologies and boundary conditions*

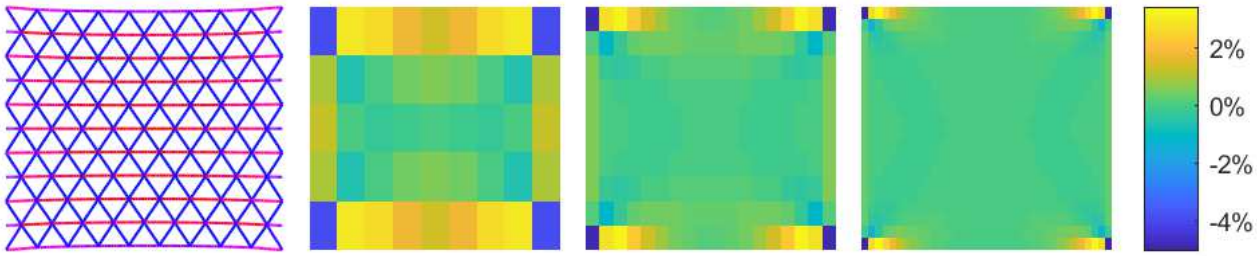

Figure 31: The example with stretching in X instead of Y has no edge-softening layer.

Figure 31 shows the strain energy comparison for the example lattice stretched in the X direction instead of the Y direction. There is no edge-softening layer. Although there is a pattern near the corners on the free edges where w_C and w_{UC} differ by a few percent, examination of any effect this might have on size effects is outside the scope of this work.

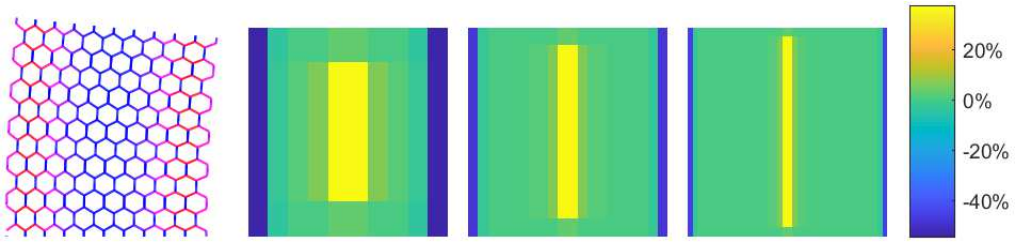

Figure 32: Edge softening effects for hexagons in pure bending.

Figure 32 shows plots of edge softening effects for hexagons in pure bending. These edge softening effects are much larger than those seen for triangles, roughly 50% as opposed to roughly 4%. This plot shows a vertical stripe in the center of the lattice, where the actual strain

energy is 30% greater than the constitutive law energy. This stripe is present in most series in pure bending, where there is very little strain energy near the center and a small absolute error causes a large relative error. Along with the patterns near the corners in Figure 31, this illustrates that the strain mapping/constitutive law energy process is only approximate. The results will show that despite these limitations, it is useful for connecting edge-softening layers with a global size effect.

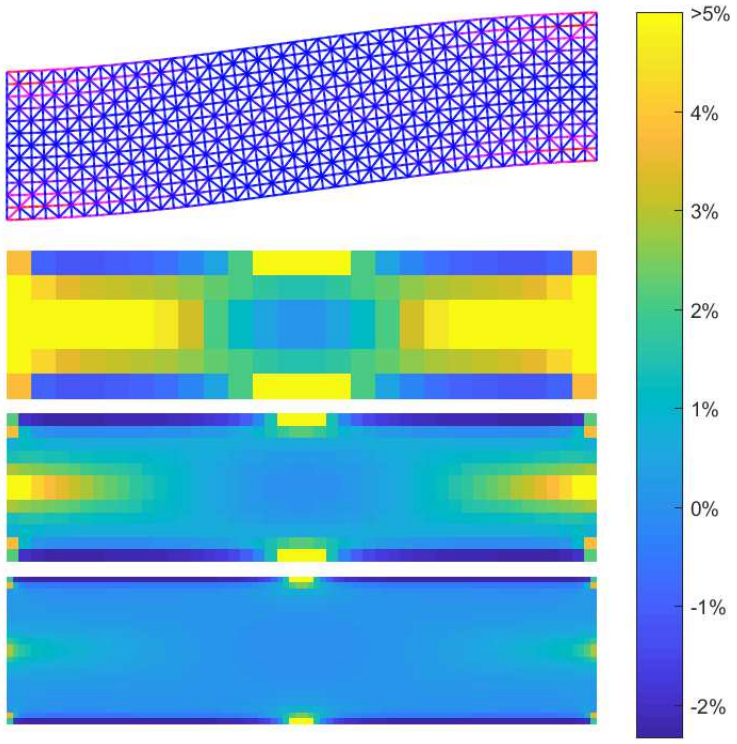

Figure 33: Edge softening effects in Mixed Triangle B in Transverse Bending.

Figure 33 shows that edge softening effect in mixed Triangle B are smaller than the other two boundary conditions, roughly 2%. It also shows that there is an interruption in the edge softening layer in the center of the free edge for transverse bending. At this point there is very little normal strain and shear strains are dominant. The actual energy is larger than the

constitutive law energy. This suggests that the edge softening effect may be associated with normal strains, not shear strains. This hypothesis is difficult to test in detail because shear strains are small on the free edges for all of the boundary conditions used in this work. Further examination is out of the scope of this work.

3.2.2.6 *Recap of Example results*

The results reviewed in this section show that hexagons and triangles have edge softening effects when the free edges are stretched in the Y direction. Mixed Triangle B shows edge softening effects in both directions. Hexagons showed the largest edge softening effect, followed by triangles and then Mixed Triangle B. For these combinations of topology and axial directions, edge-softening effects are present in all of the boundary conditions examined in this work.

3.3 Application to Free Stretching Boundary Condition

This section will examine edge softening size effects in the free stretching boundary condition, which has a simpler displacement behavior than the others. A classical (non-cellular) material in this boundary condition has a simple displacement solution, which is given for the y-axial direction by

$$u_y = C\ y$$
$$u_x = -C\ x\ \nu \qquad 32$$

where ν is the Poisson's ratio of the material, and C the prescribed strain. The classical solution has no shearing or rotation, only normal stresses and strains. Lattices in free stretching have a similar, but not identical, behavior. They have large relatively constant normal strains, and small shear strains and curvatures.

This simple behavior means that many potential causes of size effects are eliminated. Any cause that depends on shear strains, rotations, non-linear deformation, or distribution of material should be minimal in free stretching. Future work will explore causes of size effects due to these behaviors in other boundary conditions.

All of the size effects in free stretching are softening. They can be divided into two categories, those with and without edge softening effects. As shown in Figure 34, the ones without edge softening effects are very small, less than 0.11%. Local beam bending is the only cause of size effects ($SE_T = SE_B$), and it almost exactly matches the actual lattice size effect. The difference is always less than 2.4% when it is calculated as,

$$e = \left|\frac{SE_T}{SE_L} - 1\right| \qquad 33$$

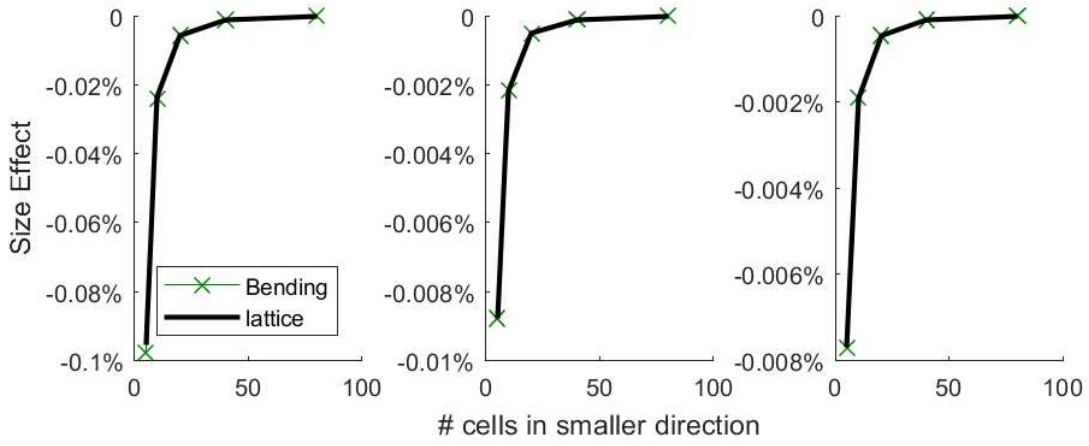

Figure 34: Selected size effects without edge softening in free stretching. From left to right Diamond lattice with an X axial direction, an aspect ratio of 1, and 5 starting cells. Mixed Triangle A lattice with an aspect ratio of 1/3 and 5 starting cells. Triangle with an X axial direction, an aspect ratio of 1 and 5 starting cells.

The size effects caused by edge softening are larger than those local bending; ranging from 0.24% to 12.7%. When the edge softening effect is present, the total size effect predicts

the size effect magnitude well, but is less precise than the size effects due to bending only. The errors as calculated by Equation *33* range from 2.9% to 60%.

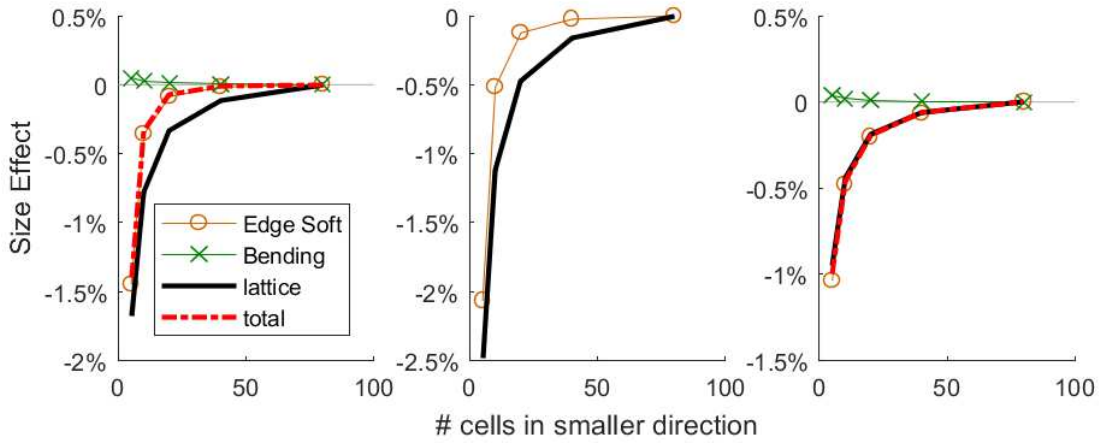

Figure 35: Selected size effects with edge softening in free stretching. From left to right: Triangle with a Y axial direction, an aspect ratio of 0.96 and 5 starting cells, Hexagons with a Y axial direction, an aspect ratio of 0.33 and 5 starting cells, Mixed Triangle B with an aspect ratio of 1 and 5 starting cells.

Figure 36 shows the magnitude of the actual lattices size effect versus the total predicted size effect for all of the series in free stretching. The dashed green line indicates where the actual size effect is exactly equal to the total predicted size effect, $SE_L = SE_T$. When a series lies close to this line, the two causes of size effects explain the causes of the lattice size effects. Hexagons in Free Stretch X are omitted from this figure because there is neither an edge softening size effect or a beam bending size effect.

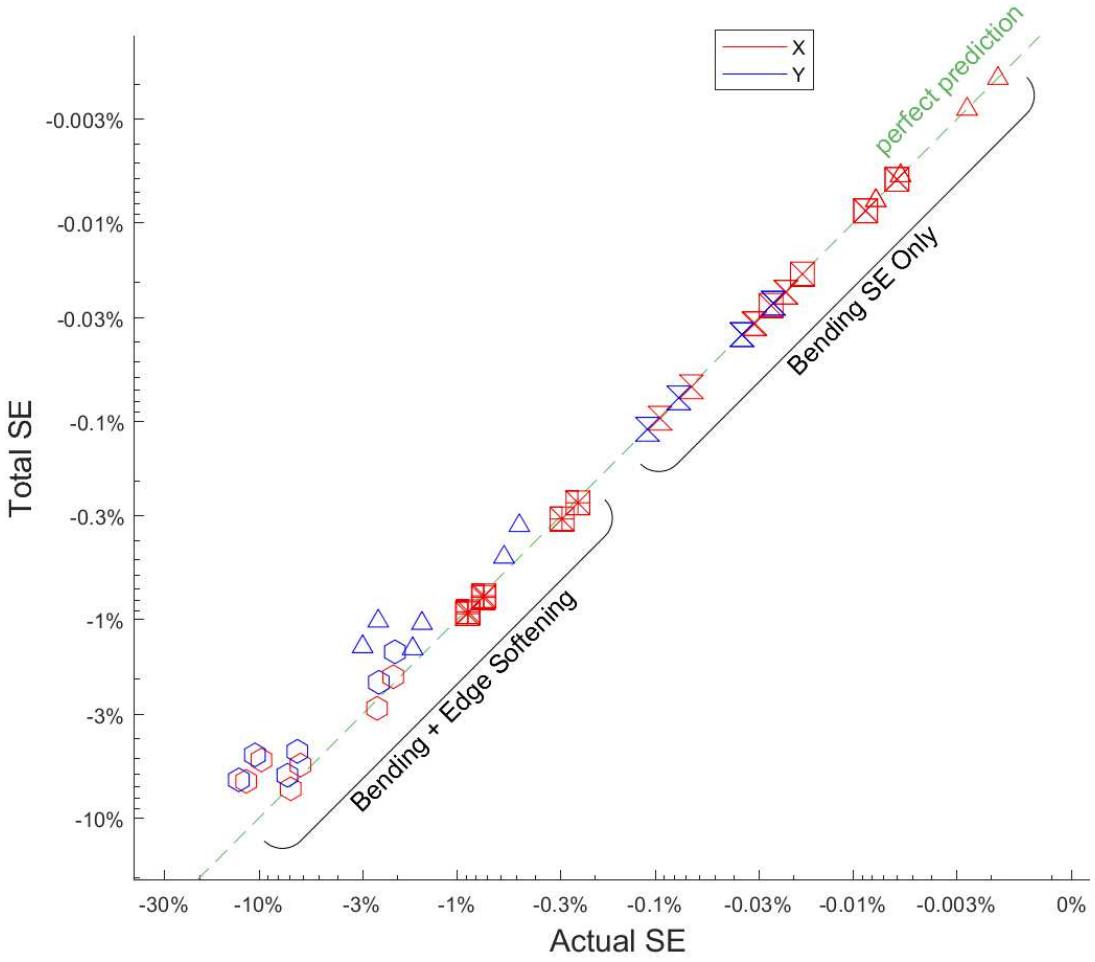

Figure 36: Size effects for every series in free stretching. Lattice topology is indicated by the shapes of the markers.

The strong correlation between total and actual size effects shown in Figure 36 suggests that local beam bending and edge softening are the two dominant causes of size effects in the free stretching boundary condition. The relatively simple displacement behavior in free stretching excludes other possible causes of size effects.

The quality of prediction is not perfect, particularly for the series with edge softening, and accuracy is somewhat exaggerated by the log scale of the graph. The predictions of the

scale of an edge softening effect help explain the total size effect, but are less than perfect. On average, their predictions differ from the actual size effect by 20%.

Figure 36 shows that the scale of edge softening effects depends on topology, aspect ratio, and starting number of cells. The data in the figure is the Mixed Triangle B lattices have the smallest effects, and hexagons the largest. Triangle lattices fall in between the two, but the largest size effects for Mixed Triangle B are larger than the smallest triangle size effects. Figure 37 examines the edge-softening ratio (ESR), defined as the difference between the actual and constitutive law energy in the edge region, calculated as:

$$ESR = 1 - \frac{\sum_E w_{UC}}{\sum_E w_C} \qquad 34$$

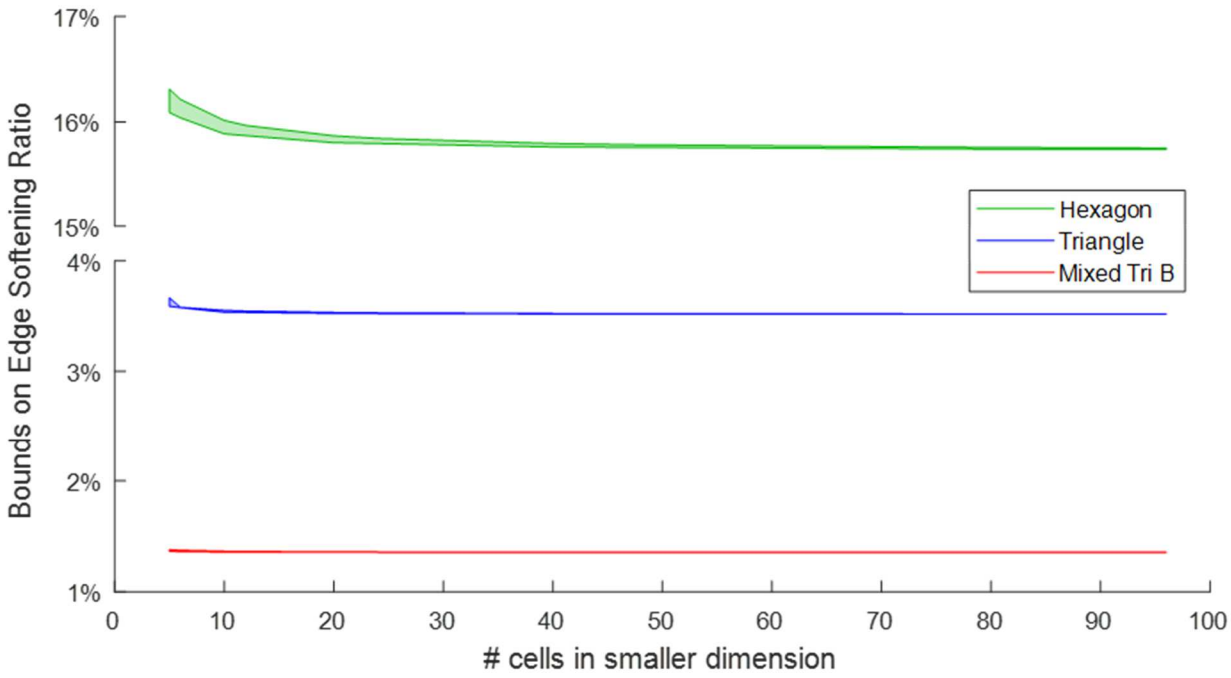

Figure 37: Difference between actual and constitutive law energy in edge softening as a function of lattice refinement.

Figure 37 shows that ESR in free stretching depends almost entirely on lattice type and not on aspect ratio or number of unit cells. The figure shows the upper and lower bounds for ESR for all of the series examined in this section. ESR for each lattice type in free stretching is almost constant as the lattice refines. This means that the softening effect decays as the lattice refines because the edge region becomes smaller, not because the percent softening changes. Series with a higher aspect ratio and a lower starting number of cells have a larger size effect, because the edge region is a larger fraction of the whole.

3.4 Edge Softening Effects in a Variety of Boundary Conditions

The results presented in the previous sections showed that 3 topologies have pronounced edge softening effects when loaded in free stretching, and that these edge softening size effects provide a good explanation of the total size effect. This section will apply the same methods to lattices with the same topologies but other boundary conditions.

Figure 37 showed that for free stretching, the ESR remains constant as the lattice refines, and does not strongly depend on aspect ratio or starting number of cells. By contrast, Figure 38 shows that, for other boundary conditions, the ESR can change as the lattice refines. The ESR follows the same pattern of relative scale in the various boundary conditions as in free stretching; Hexagons have larger ESR than triangles, which are larger than Mixed Triangle B.

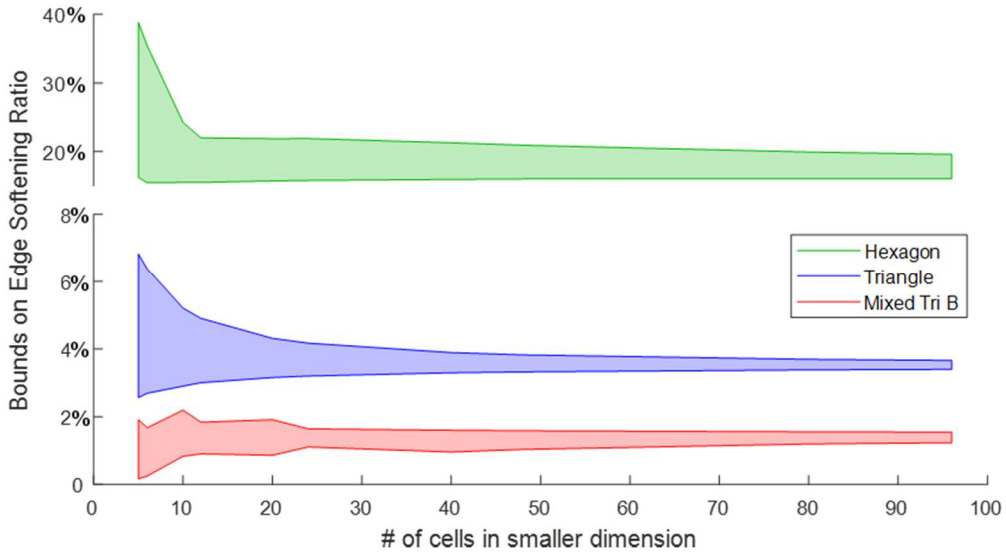

Figure 38: Bounds on Edge Softening Ratio (ESR) for the various boundary conditions.

Figure 39 shows results from a series where the edge-softening ratio changes non-monotonically. Figure 39a shows that the ESR changes significantly as the mesh refines, and that there is also a non-monotonic size effect in the lattice. Figure 39b shows that this happens because the edge-softening region is not seen near the lattice corners or in the center of the free edges. For the coarsest lattice, the majority of free edge is within a few cells of the corners or center, and the edge softening layer is not as pronounced as in the more refined lattices.

In Fixed Stretching and Transverse boundary conditions edge softening does not occur near the corners. In the transverse boundary condition, it is also absent near the center of the free edge. All of these have significant amounts of shear in addition to stretching. Figure 39 illustrates this. Although this suggests that the edge softening effect is tied to stretching in the absence of shear, a detailed examination of this is out of scope of this work. This interaction between shear and edge softening explains why the edge softening size ratios for all boundary conditions (Figure 38) are more chaotic than those for just free stretching (Figure 37).

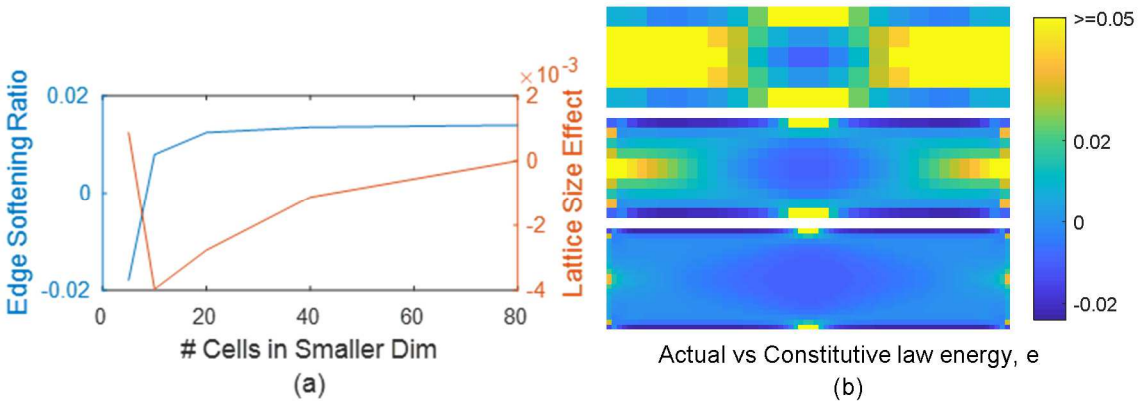

Figure 39: Corners and center can limit the edge softening region and produce a non-monotonic size effect.

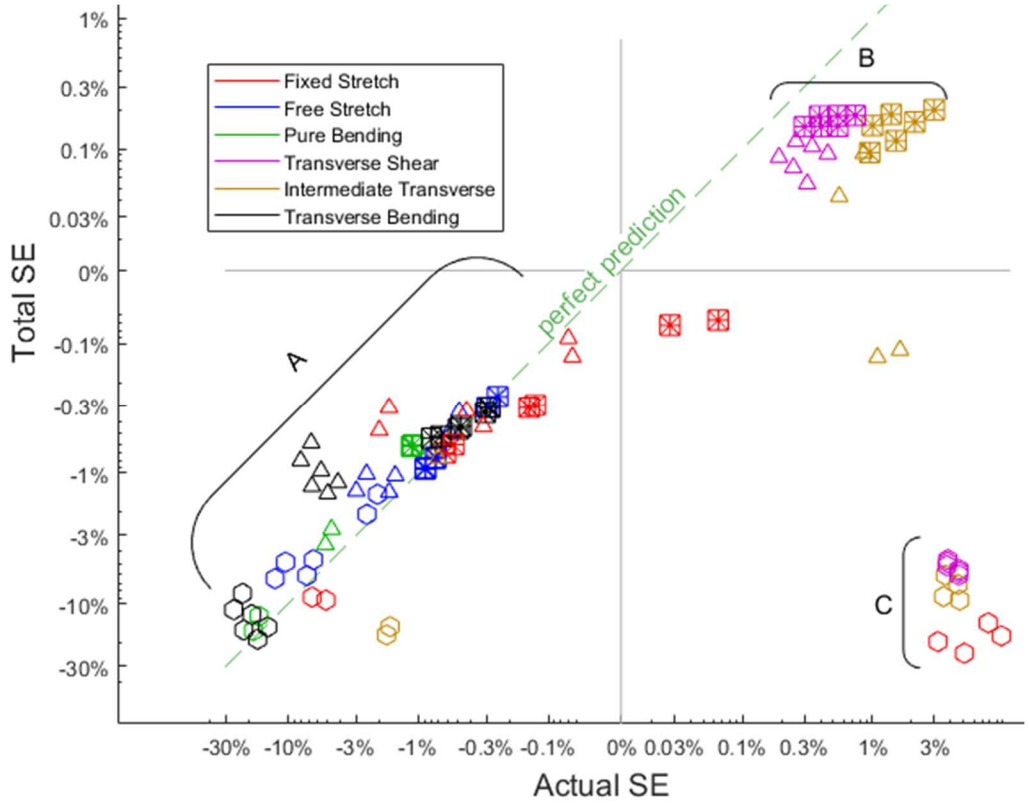

Figure 40: Actual vs Predicted size effects for all series with edge softening effects.

Figure 40 shows actual and predicted size effects for all of the series with edge softening including free stretching. The predicted size effects are correlated to the actual effects seen, but the correlation is imperfect. These results show several regions of interest worthy of closer inspection.

Group A shows an actual and predicted softening size effect. The predicted results show a clear connection with the actual, but the accuracy of the prediction varies greatly. The series in group A are in boundary conditions dominated by normal stresses, Free and Fixed Stretching, Pure Bending, and Transverse Bending. This is because the edge softening size effects are strongest when shear has the least influence.

Unlike free stretching, these boundary conditions have complicated deformation patterns which allow other possible causes of size effects that are not accounted for in this work. Future work will examine these series to see if edge softening is interacting with causes of size effects other than local beam bending.

The series in Group B have stiffening local bending size effects that are larger than their edge softening effects. They are shear dominated because they have relatively low aspect ratios; less than 3 for Mixed Triangle B, and less than 0.5 for triangle. Figure 39 illustrated a pattern where the corners and center of a transverse boundary condition interfere with the edge softening effect. This same pattern is present in these series. Because they have a low aspect ratio and therefore short free edges, everywhere on the free edges is within a few unit cells of the corners or center and the edge softening effect is small.

Various authors have examined size effects in shearing (Diebels & Scharding, 2011b; Tekoğlu, 2007), and concluded that there is a stiffening size effect associated with the restricted rotations near the fixed edges (Diebels & Steeb, 2003; Tekoğlu, 2007). Section 3.2.1.3 examined

how changes in rotation are connected to a change in beam bending energy. Because these series have a low aspect ratio, the region close to the fixed edge is large relative to the whole, and the stiffening size effect due to local beam bending can be relatively large.

Lattices in a transverse boundary condition have an edge softening size effect that grows with increasing aspect ratio, and a local beam bending size effect that shrinks with increasing aspect ratio. These two combine to create a bending size effect that dominates over the edge softening size effect at a low aspect ratio. The series in Group C are hexagon lattices with an actual stiffening effect, but a predicted softening effect. Some of these lattices ought to fit in with group B; they have a low aspect ratio and are in a transverse boundary condition. However, bending size effects cannot be calculated for hexagon lattices because they are bending dominated. Therefore, the edge softening size effect, however small, is the only cause of size effects that can be considered.

Group C also includes a few series of hexagons in fixed stretching. Because hexagons have a high Poisson's ratio, close to 1 (Gibson & Ashby, 1999), there are relatively large effective shear strains near the corners. Therefore, all of the series in group C have significant shear strain.

The series with large shear strains examined in this work have a stiffening size effect. For the stretch dominated lattices, this is linked to a beam bending size effect. The results for honeycomb lattices suggest that there is also a beam bending size effect that cannot be quantified using the methods of this work. The results in Groups B and C suggest a strong link between stiffening effects due to shear, and local beam bending size effects.

3.5 Conclusions

In the first part of the paper, a method was developed for quantifying the amount of strain energy due to local beam bending versus local beam stretching in periodic lattices. The results showed that a change in bending strain energy accurately explains the size effects in free stretching of a lattice structure. Stiffening size effects in shear loading are also strongly linked to changes in local beam bending energy.

In the second part, a separate method was introduced to quantify the effective strains in every unit cell of a lattice, and then to calculate an expected strain energy according to the micropolar constitutive law. The material properties for this constitutive law were derived under the assumption that the unit cell is surrounded by other cells on all sides. When this assumption is true, this constitutive law energy agrees with the actual unit cell energy well, usually to within one percent. For most lattices, this assumption is still true when the assumption is broken on the free edges. For Hexagon and Triangle lattices with a Y axial direction loading, and Mixed Triangle B lattices with loading any perpendicular axial direction the free edges are significantly softer than the constitutive law would predict. Cells on the free edges of these lattices have a softer stress strain relationship than those in the center.

As discussed in the Introduction, previous literature has examined edge-softening effects in stochastic foams with incomplete surface cells (Tekoğlu, 2007) or in experimental samples with surface damage due to less than “great care during machining” (Anderson & Lakes, 1994) or in periodic lattices where the boundaries are chosen in a way that allows open cells on the free boundaries (Liebenstein et al., 2018). In contrast the lattices in this paper have an edge softening effect but their cells are neither damaged nor incomplete. However, since they are adjacent to boundary edges, they are not surrounded on all sides.

This local softening effect was used to calculate an expected global size effect due to edge softening, and this expected edge softening effect is able to explain size effects well in free stretching. The combined bending and edge softening size effects were applied to a set of boundary conditions that were expected to have edge softening effects. These combined causes of size effects were shown to have useful but limited predictive capability to explain size effects in these cases. The results from these studies suggest that there are other causes of size effects that are active, and examination of these other causes is needed to fully explain size effects in all cases.

A5. Chapter 3 Appendix: Demonstration of stair step displacement and fitting equation

Node displacements in lattices with distinguishable node points cannot be approximated well by a linear Taylor series. To demonstrate this, consider the hexagon lattice in Free Stretch Y shown in Figure 41a. Figure 41b labels the two types of nodes in a hexagon lattice. Figure 42 shows that u_y shows a stair step pattern; the vertical ligaments stretch very little, and almost all of the deformation is concentrated in the diagonal ligaments. The regression equation has a linear component, which captures the slope of this stair step, and an alternating component, *+D mw,* where D quantifies the size of the stair steps. Without this additional term, the stair step behavior is noise that makes the linear regression less accurate.

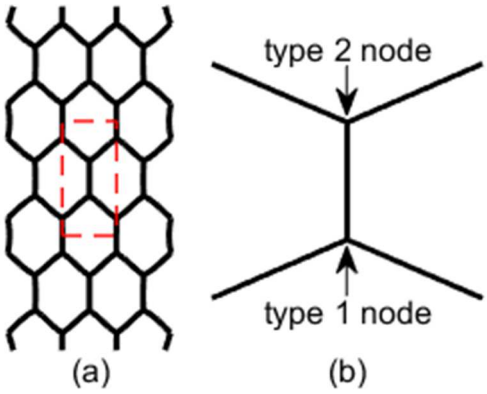

Figure 41: (a) Lattice for illustration of stair step displacement. The unit cell being considered is outlined in red. (b) a single unit cell with the two types of nodes labeled.

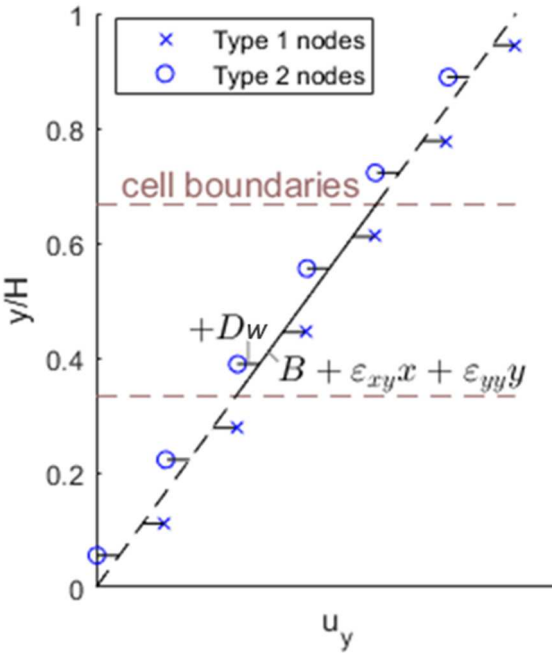

Figure 42: u_y for the highlighted unit cell and cells above and below. Also shown is the linear regression and the additional alternating component +D w.

4. Material Distribution Effects

4.1 Continuum theories for size effects in bending.

Cellular materials such as foams and thin-wall lattice structures display size dependent behaviors. When modeled as a continuum, the apparent moduli of cellular materials relating stress and strain measures depend on sample size. When the apparent moduli increase when there are fewer cells in the sample, this is a stiffening size effect. The reverse is a softening size effect. This phenomenon has also been demonstrated in natural cellular materials such as bone (Goda, Assidi, & Ganghoffer, 2014; Goda & Ganghoffer, 2015; Lakes et al., 1990), artificial stochastic cellular materials such as metal or polymer foams (Andrews et al., 2001b; Lakes, 1991b), as well as periodic lattice structured materials such as honeycombs (Bažant & Christensen, 1972; Diebels & Steeb, 2002; Wheel et al., 2015; Yoder, Thompson, & Summers, 2018). This work presents a novel explanation of a mechanism that causes size effects in periodic cellular materials for structures in bending. This mechanism is not present in other boundary conditions such as pure shear or in stochastic cellular materials. This mechanism for bending of periodic cellular structures will be called a material distribution size effect.

4.1.1 Continuum theories to model size effects

Micropolar elasticity has been used extensively to model size dependent behaviors in cellular materials. This generalized continuum theory extends classical elasticity, by introducing micro-rotation as an additional independent variable. Derivatives of micro-rotation define curvature components in the same way that derivatives of displacement define strain components. Couple-stress arises in response to curvature in the same way that stress arises in response to strain. The introduction of an independent rotation removes the requirement that

the shear strains be symmetric, in other words $\sigma_{ij} \neq \sigma_{ji}$. The difference between the shear stress components, $\sigma_{asym} = ½(\sigma_{ij} - \sigma_{ji})$, is referred to as asymmetric shear stress. Asymmetric shear strain is defined similarly, $\varepsilon_{asym} = ½(\varepsilon_{ij} - \varepsilon_{ji})$. For an isotropic two dimensional micropolar model, there are two additional material properties not present in classical elasticity. γ defines the relationship between curvature and couple stress, and κ defines the relationship between asymmetric shear strain and stress. The in-plane constitutive law for a transverse isotropic material and definition of strain can be written,

$$\begin{bmatrix} \sigma_{xx} \\ \sigma_{yy} \\ \sigma_{sym} \\ \sigma_{asym} \\ m_x \\ m_y \end{bmatrix} = \begin{bmatrix} \frac{E}{1-\nu^2} & \frac{E\,\nu}{1-\nu^2} & 0 & 0 & 0 & 0 \\ & \frac{E}{1-\nu^2} & 0 & 0 & 0 & 0 \\ & & \mu & 0 & 0 & 0 \\ & & & \kappa & 0 & 0 \\ & sym. & & & \gamma & 0 \\ & & & & & \gamma \end{bmatrix} \begin{bmatrix} \varepsilon_{xx} \\ \varepsilon_{yy} \\ \varepsilon_{sym} \\ \varepsilon_{asym} \\ \phi_{z,x} \\ \phi_{z,y} \end{bmatrix} \quad 35$$

where σ and ε are stress and strain. Subscripts x and y are coordinate directions. E, ν, and μ, are Young's modulus, Poisson's ratio, and shear modulus.

The couple stress model is a simplification of the micropolar model where the asymmetric shear strain has been removed by constraining the micro-rotation to be equal to the macro-rotation, $½(u_{j,i} - u_{i,j})$. The micropolar model converges to the couple stress model as κ approaches infinity.

The additional material properties make the micropolar and couple stress models stiffer than the classical elastic model; therefore, they can only model stiffening size effects.

4.1.2 Descriptive literature on size effects focusing on bending

A number of papers have done experimental or simulation studies of size effects in cellular materials. Many of these have used micropolar elasticity or couple stress elasticity to

model these size effects. Although many of these works studied a variety of situations, this literature review will focus on the results relevant to bending.

The literature reviewed here examines both periodic and stochastic cellular materials. A periodic cellular material is made of a strictly repeating pattern, such as a honeycomb made from perfect hexagons. A stochastic cellular material has a random component, such as a foam. Many papers discuss size effects in both types (Liebenstein, Sandfeld, & Zaiser, 2016; Liebenstein et al., 2018; Tekoğlu, 2007). Although it is reasonable to assume that the two types will share some causes for size effects, there may be some size dependent behaviors present in periodic cellular materials that are not present in stochastic, and vice versa. This work focuses on periodic cellular materials with thin walls.

(Tekoğlu & ONCK, 2008) examined size effects in a simulated stochastic foam and a simulated honeycomb lattice in shear and bending. They found stiffening effects in shear and softening effects in bending and concluded that the softening in bending comes from “free edge effects” that are not be captured in a micropolar model.

A number of papers from Lakes and his collaborators, (Anderson & Lakes, 1994; Lakes, n.d., 1991b; Rueger & Lakes, 2016), experimentally use bending and torsion to find micropolar material properties of samples of metal and polymer stochastic foams. They find that these foams show stiffening effects when they are prepared carefully in order to prevent surface damage that would cause free edge softening (Anderson & Lakes, 1994).

These free edge softening effects have also been observed in a variety of other stochastic foams (Andrews et al., 2001b, 2001a; Brezny & Green, 1990). They are commonly attributed to a layer of damaged or poorly connected cells on the free surface that contribute less to stiffness than the cells in the interior.

Chapter 3 examined size effects in a variety of periodic cellular materials modeled as a network of beam elements, and showed that in certain cases edge softening size effects can occur in a lattice material that is neither damaged nor poorly connected. The edge cells have a softer constitutive relationship than interior cells, because they are not surrounded on all sides by other cells.

A series of papers examined size effects in a model material in pure bending. The meta-material was a solid material perforated with a repeating pattern of holes. The first three papers (Beveridge et al., 2012; McGregor & Wheel, 2014; Waseem et al., 2013) found a stiffening size effect, and interpreted this as being consistent with micro polar elasticity theory, and quantified micropolar material properties for the model material.

A fourth paper by Wheel (Wheel et al., 2015), examined size effects in two different types of material. The first was similar to the model material from the first three papers, but with two variations, where the perforations either do or do not intersect the surface of the material. They found that when the voids intersect the surface, there is a softening size effect and a stiffening size effect otherwise. The second type of material was a laminate made of alternating layers of stiff and soft material. When the soft layers were on the outer surfaces, there was a softening size effect and a stiffening size effect otherwise.

Wheel's results show that remarkably similar materials can have both stiffening and softening size effects. This suggests that in certain situations stiffening and softening size effects can come from the same mechanism. If both directions of effect can come from the same mechanism, it seems inappropriate to model this mechanism using micro polar elasticity, which only models stiffening effects.

(Dunn & Wheel, 2016) used a beam element finite element analysis (FEA) to build on Wheel's previous work. This analysis showed that for a square thin walled lattice structure, there was a stiffening size effect when the cell walls were coincident with the boundaries of the beam, and a softening size effect when they were not. He estimated a characteristic length based on this stiffening size effect, and showed that it was inconsistent with the theoretical characteristic length derived from the literature (Bažant & Christensen, 1972). Figure 43 illustrates the beams studied by Wheel and Dunn.

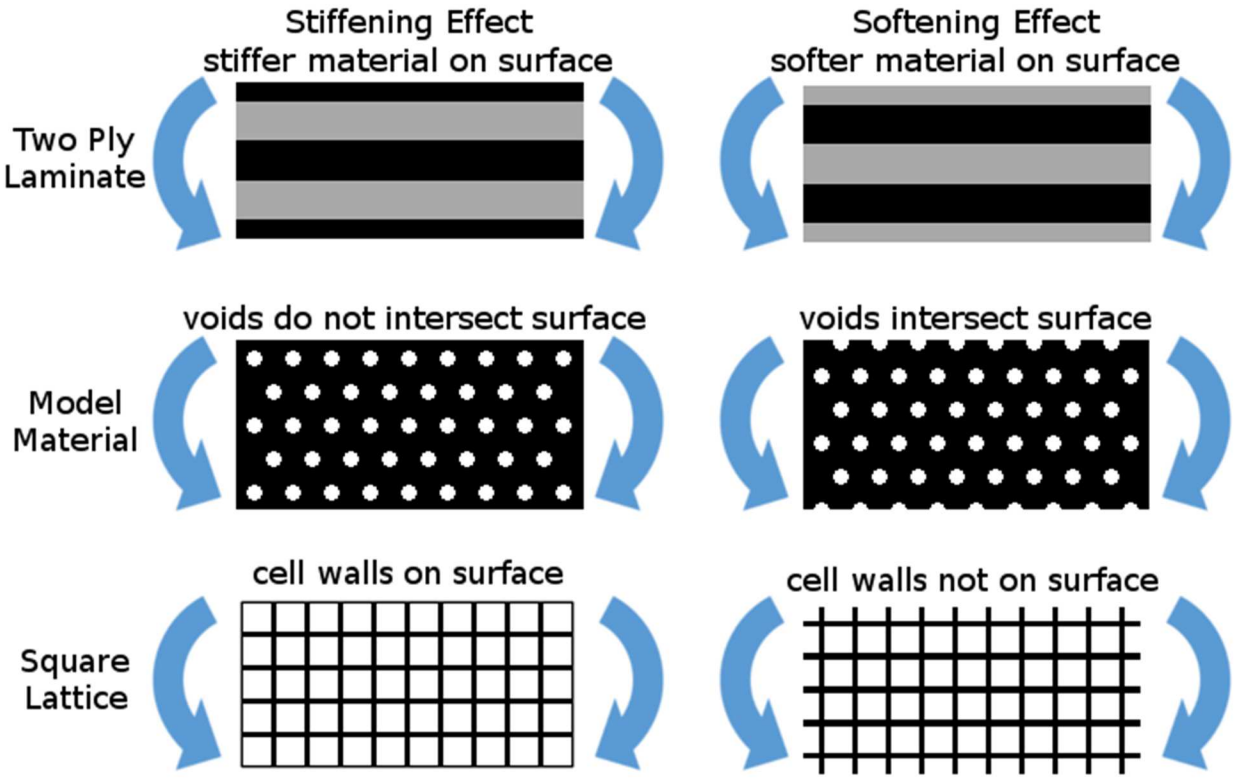

Figure 43: Three different types of beams with both stiffening and softening size effects.

Astute readers may wonder if the softening size effects observed in (Wheel et al., 2015) are a result of edge softening effects. In an edge softening effect there is a layer of cells on the free edges that contribute less to stiffness than is expected; They have a softer effective

constitutive relationship than cells in the interior. For Wheel's laminate material, the constitutive relationship was prescribed, which would eliminate any chance of a different constitutive relationship. For the model material, an edge softening effect cannot be ruled out. However, the current work will provide an alternative explanation.

The current work is divided into two parts. The first part will investigate the ability of two sets of micropolar material properties to predict size effects in both shear and bending. This analysis will show that there is no set of material properties capable of accurately predicting size effects in both load cases.

The second part will derive a theoretical resistance to bending for a single unit cell and show that in bending, this predicts either a stiffening or a softening size effect. This analysis will then show that this formula is capable of accurately predicting size effects for a variety of lattices for both pure bending and transverse bending.

4.2 Comparison of two material models with different definitions of couple stress and curvature

4.2.1.1 *Kumar and McDowell's material properties*

As discussed in Chapter 2, (Kumar & McDowell, 2004) derived effective micropolar properties for a variety of lattice topologies, including square and mixed triangle A. They began with the assumption that the micropolar properties are correct when the lattice structure and an equivalent micropolar continuum have the same strain energy and the same displacement. They then specify the lattice displacement of a single unit cell in terms of the micropolar strains. The relationship between prescribed strains and prescribed displacements is derived from the micropolar model, assuming that micropolar translation and rotation are equal to the beam translation and rotation at the ends. The cell walls are modeled as Euler-Bernoulli beam

elements, and the strain energy is calculated as a function of the prescribed strains. The material properties are the derivatives of this strain energy with respect to the prescribed strains.

4.2.1.2 *Liu and Su's material properties*

(Liu & Su, 2009a) derived effective couple stress properties for square and mixed triangle lattices. For each lattice, they modeled a single unit cell using Euler-Bernoulli beam elements and then applied a variety of boundary conditions to that single unit cell. Each boundary condition was specified to activate a single material property, and the strain energy for that unit cell with the specified boundary conditions is then used to calculate that material property.

For the boundary conditions used to derive properties specific to bending, the nodes on the unit cell boundaries have a prescribed displacement as if they were attached to a rigid plate that is rotating. However, the beam rotation DoFs are left free, and obtained by solving the unit cell problem with these boundary conditions.

4.2.1.3 *Micropolar properties and choice of unit cell*

Both of these works found matching classical elastic material properties, the properties relating stress to strain. However, the two papers found different values for γ, the material property relating couple stress to curvature. Liu and Su found values for γ far larger than those found by Kumar and McDowell; 50 times larger for square lattices, and 13 times larger for mixed triangle A lattices. One goal of the present paper is to explain the discrepancy in the predicted apparent material property, γ, relating local curvature to couple stress.

4.2.1.4 *Micropolar elasticity and Couple stress elasticity*

Although the two papers derive material properties for different but related models, the differences in these models disappear when a pure bending problem is considered. The biggest difference in the two models the presence of asymmetric shear stress, but for a beam in pure bending, shear stress does not appear. Therefore, the properties derived by both papers are directly comparable when examining size effects in pure bending.

4.2.2 Lattice Model Description

The beam lattice FEA solver introduced in Chapter 2 is used to further investigate the size effects in bending. In this part of this chapter, it will be compared to continuum models that use the two sets of material properties, and will test their ability to predict size effects in bending and shear. In the next part of the paper, it will be used to derive and demonstrate material distribution effects. The total strain energy of the lattice is calculated using,

$$W_L = 1/2\ \vec{u}^T K \vec{u} \qquad 36$$

where $\vec{u}$ is the global displacement and rotation vector, and *K* is the global assembled stiffness matrix. Figure 44 shows the different lattices examined in this chapter.

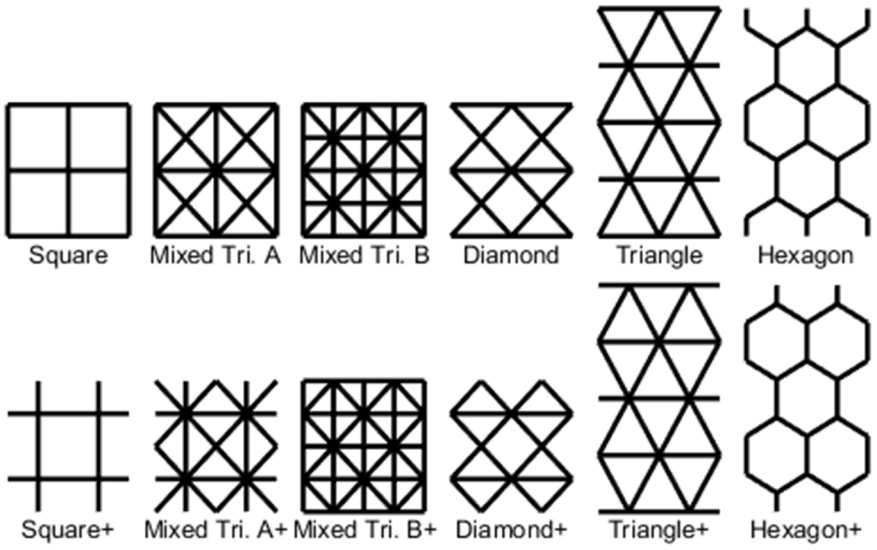

Figure 44: Two unit cells by two unit cells of each lattice type.

The bottom row of lattices types in Figure 44Figure 3 are alternate versions of the cells directly above them. When tiled infinitely, both will produce lattices with the same topology. When tiled a finite number of times, the resulting lattices will be truncated differently at the borders. The specific location of cell walls in the interior of the lattice is also subtly different. The results of this paper will show that the choice of unit cell has an impact on the magnitude and direction of size effects in bending.

Of the lattice types shown in Figure 44, only the squares, mixed triangle A and their + variants are used in the first part of this work. All of them are used in the later part.

Figure 45 illustrates the X direction half of the boundary conditions applied to the lattice model. The results of the simulations will be discussed in terms of the macro-aspect ratio which is defined as the ratio of the axial dimension, L, to the transverse dimension, T.

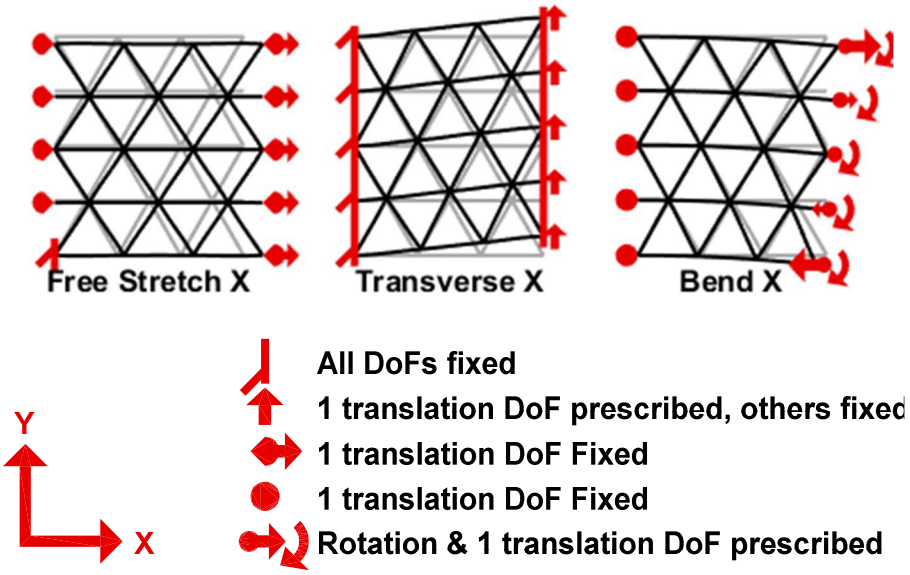

Figure 45: boundary conditions for the X direction.

In the bending-x boundary condition, the x displacement and micro-rotation DOFs are prescribed to produce a rotation of C radians as defined by,

$$u_x = C\,y \;\; and \;\; \phi_z = C \qquad 37$$

To study size effects, series of simulations are run with the same boundary condition and type but varying the fineness of the unit cells. The lattice refinement methods used in Chapter 3 are used again here. Figure 46 illustrates this. The final two lattices are omitted from Figure 46 because the cells are too small to be seen clearly.

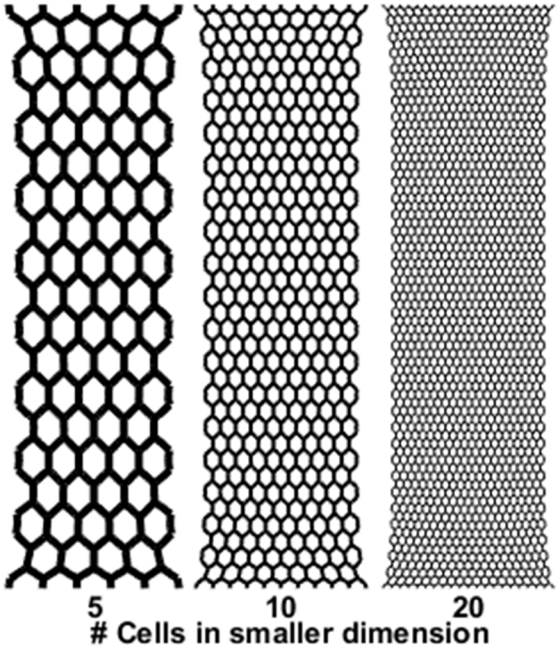

Figure 46: The first three lattices in a selected size effect series.

As the mesh is refined, the strain energy converges asymptotically to a constant value. The lattice size effect for each series is quantified by comparing the lattice strain energy in the finest lattice, W_{LF}, and the strain energy most different from that, W_{LC},

$$SE_L = \frac{W_{LC}}{W_{LF}} - 1 \qquad 38$$

For most series, W_{LC} is the strain energy of the coarsest lattice considered. Sometimes the lattice strain energy has a non-monotonic size effect; It has a maximum or minimum in the second or third mesh refinement. In these cases,

$$U_{LC} = sign(W_L - W_{LF}) \max(|W_L - W_{LF}|) \qquad 39$$

4.2.3 Strain Mapping and Edge Softening Effects

In Chapter 2, a slightly different version of this code was used to show that unit cells near the free edges of the lattice can behave more softly than cells in the interior. This effect is

only present for certain lattice types and boundary conditions. This was done by creating a map of the effective strain in the lattice, and then using the micropolar constitutive law to predict the strain energy in those edge cells. If the actual energy is significantly smaller than the predicted energy, the edge cells have a softening effect. This process can identify the situations where edge-softening effects occur and make quantitative predictions of the magnitude of this softening effect. The code to do this is run for every lattice examined in this paper.

4.2.4 Continuum Model Description

The size effects in the lattice model are compared to size effects in the micropolar model first introduced in Chapter 2 and couple stress model. The micropolar model uses the material properties for Squares and Mixed Triangle A originally derived by (Kumar & McDowell, 2004), and later corrected in Chapter 2. The couple stress model uses the material properties derived by (Liu & Su, 2009b). It runs using the same code as the micropolar model, but κ is set to be 100 times μ. Remember that the micropolar model converges to the couple stress model as κ approaches infinity. Higher values of κ led to numerical instability in the code. These formulas give micropolar and couple stress material properties that depend on cell size and cell wall thickness.

The continuum model is assumed to not distinguish between the details of how a unit cell is tiled. Therefore, one continuum model is run for both square and square+ lattices, and one for both Mixed Triangle A and Mixed Triangle A+ lattices.

4.2.5 Problem Set

In order to study the ability of the two continuum models to predict size effects, 4 series of lattices are run in bending and 4 series in shear. The four series each use a different lattice

type, square, square+, mixed triangle A, and mixed triangle A+. Each series has a base of 5 unit cells. For the bending series, the lattice has an aspect ratio of 1. For the shear series, the aspect ratio is 1/10.

Each case in each series is run three times, once with the lattice model, once with the micropolar model, and once with the couple stress model. The size effects are calculated using Equation 38, and

$$SE_M = \frac{W_{MC}}{W_{MF}} - 1 \, , SE_C = \frac{W_{CC}}{W_{CF}} - 1 \qquad 40$$

where the subscripts M and C stand for micropolar and couple stress respectively.

4.2.6 Results

Figure 47 shows the results of both continuum models compared to the results of the lattice model with both lattice types. For the shear boundary condition, the regular and + lattices produce similar size effects, but not the same size effects. For both topologies, Kumar and McDowell's material properties predict a size effect that is close to one or both of the lattice size effects. Kumar and McDowell's prediction is nearly a perfect match for the regular squares. Their prediction for mixed triangle A falls between the regular and + types. However, Liu and Su's material properties predict size effects roughly 50 times larger than the lattice size effects. They are too large to be comfortably shown on the same graph.

For the bending boundary condition, the regular lattice type shows a stiffening size effect, and the + configuration shows a softening size effect. L&S's properties provide a reasonable fit to the stiffening size effect. Kumar and McDowell's properties are far smaller than the lattice size effect, roughly 1/50th and 1/30th of the stiffening effect.

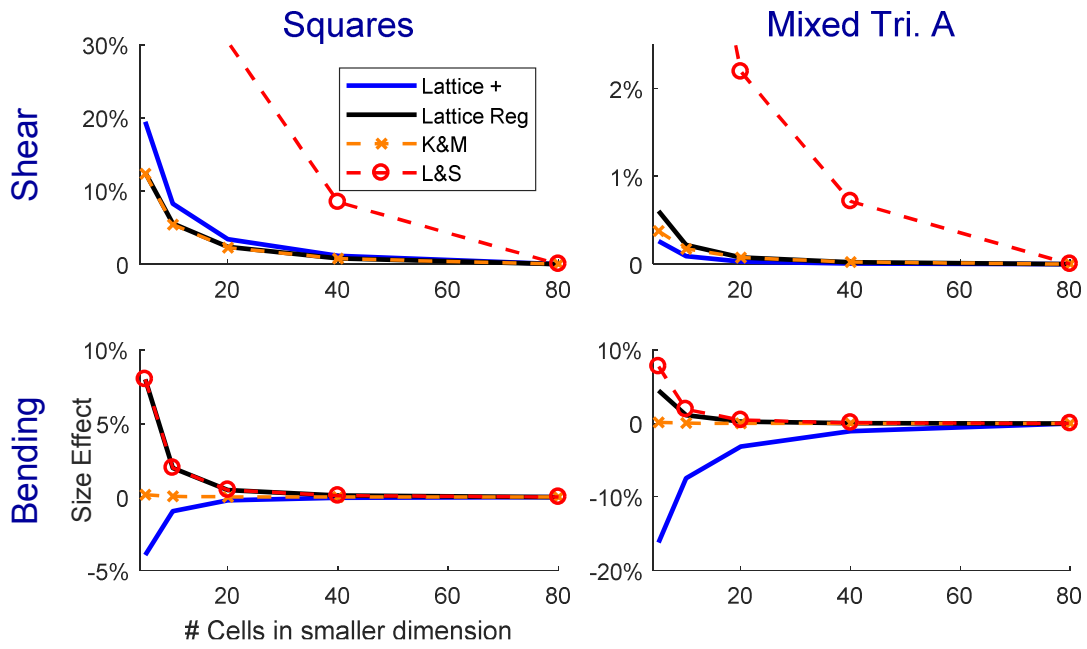

Figure 47: Continuum predictions of size effects vs actual lattice size effect.

In bending, the + lattices have a softening size effect, which the micropolar and couple stress models cannot predict. The strain mapping/constitutive law procedure was run on the + lattices to look for edge softening effects, that could be causing this softening size effect. The mixed triangle A + lattice shows edge softening effects, but the square + lattice does not.

4.2.7 Discussion

These results show that size effects in bending can be either stiffening or softening, and that edge softening effects are not responsible for all softening effects.

Each set of properties fits one boundary condition well, and the other poorly. L&S's properties are accurate in bending for the regular lattice type, but wildly overestimate size effects in shear. Kumar and McDowell's properties are accurate for shear, but wildly underestimate size effects in bending. When a material property only provides an accurate

model of size effects for certain boundary conditions, then this apparent property cannot be used for arbitrary general loading in all load cases.

Both sets of material properties were derived based on the assumption that size effects are caused by resistance to gradients of rotation, and can therefore be described well by the micropolar and couple stress models. This paper proposes that this mechanism is the dominant cause of size effects in shear, but only a minor contributor in bending. The material properties do not accurately represent size effects in both boundary conditions, because there is a mechanism causing size effects in bending that is not present in shearing.

4.3 Size Effect Due to Material Distribution

This section will show that for periodic cellular materials in bending, size effects can arise because material is unevenly distributed within a unit cell. Cells with material far from their centerlines have a resistance to bending that does not fit in the two extended continuum models examined here.

4.3.1 Qualitative Explanation of Second Moment of Area

Figure 48 compares cross sections of a square and square+ lattice in pure bending. The outermost horizontal cell wall of the square lattice is two cell heights away from the neutral axis, but the same outermost cell walls in the square+ lattice is only one and a half cell heights away. The second outermost cell wall for the square lattice is also half a cell wall farther from the axis than the equivalent in the square+ lattice. This pattern, where the cell walls in a square lattice are all farther from the neutral axis than their counterparts in the square+ lattice, continues as the number of unit cells in the lattice increases.

Because the contribution to stiffness of a cell wall is proportional to its distance from the neutral axis squared, and squares have cell walls farther from the neutral axis than square+, the square configuration is stiffer than the square+.

On the other hand, the outermost cell wall in the square lattice has only half thickness, but the outermost cell wall in the square+ lattice has full thickness. This is not enough to reverse the extra stiffness of the extra distance in the cell walls.

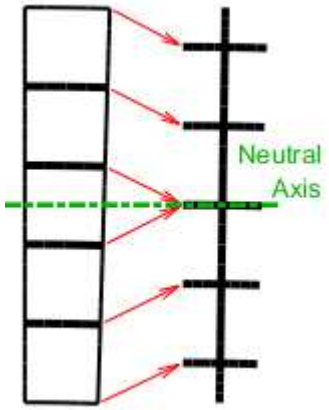

Figure 48: A cross section of a square lattice has cell walls that are farther from the neutral axis than the square+ lattice. This makes the square lattice stiffer.

This explains why a square lattice is stiffer than a square+ lattice, but does not explain why the stiffness converges to a constant value as the lattices are refined. Figure 49 shows a series of square lattices with different numbers of unit cells. When there is 1 unit cell, all of the material is at the extreme far edges of the structure. As the number of cells increases, more material moves closer and closer to the neutral axis. For the square+ lattice, the pattern is reversed; material moves away from the neutral axis as the number of cells increases. Because

the size effect is caused by moving material towards or away from the centerline, these are called material distribution size effects.

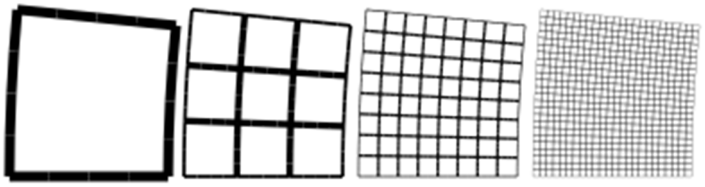

Figure 49: A series of square lattices in bending with between 1 and 24 unit cells.

4.3.2 Derivation of Second Moment of Area

For lattice topologies other than squares, there are diagonal cell walls, which do not have a constant distance from the centerline. This section will derive a relationship between the arrangement of a unit cell and the material distribution size effect.

Consider a beam in pure bending made from a periodic material with N unit cells in each direction, horizontal and vertical. The beam has an axial dimension, L, transverse dimension, T, and unit depth. Each unit cell of the beam has axial dimension $l = L/N$ and transverse dimension $t = T/N$. The y axis is defined as the neutral axis of the beam; y=0 at the horizontal centerline. On the left face of this beam the x displacement (u_x) and rotation (θ) are fixed. On the right face, u_x = y/C and θ = C. This applies a rotation of C radians to the right face of the beam. Figure 50 shows an example of this type of beam with a mixed triangle A lattice, and N=5.

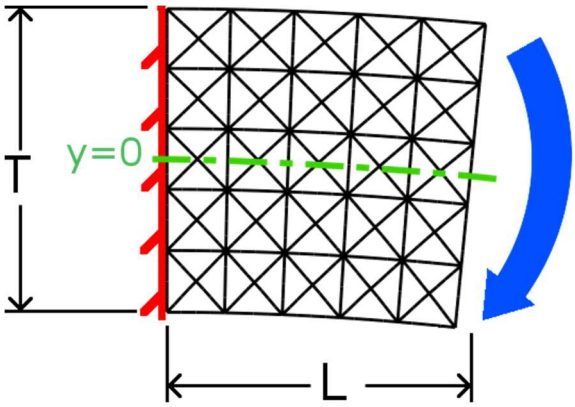

Figure 50: Example beam in bending.

Using Euler-Bernoulli beam theory, the strain energy in this beam is,

$$W = \frac{C^2 E\, I}{2\, L} \qquad 41$$

For a beam made of a homogenous material, second moment of area, I, is calculated from the cross section geometry, and used to model the flexural stiffness of the beam. For a beam made of a lattice material, there is no straightforward way to calculate I based on cross section geometry, but it can still be used to describe the beam's flexural stiffness. Because this is slightly different than the traditional definition, I is an effective second moment of area. We can solve Equation *41* for I as,

$$I = \frac{2\, L\, W}{C^2 E} \qquad 42$$

In this work, U and E will come from simulations using the lattice solver described in Section 4.2.2. The results of these simulations will show that there is a size effect in I; I depends on the number of unit cells in the lattice. However, there is no size effect in Young's modulus, E. Both of these findings are consistent with findings of other papers (Gibson & Ashby, 1999; Kumar & McDowell, 2004; Liu & Su, 2009a).

For a beam made from a single unit cell (N=1) the second moment of area of the beam is also the second moment of area of a single unit cell, I_{UC}. Because this second moment of area is proportional to the transverse dimension of the unit cell cubed, we can define a non-dimensional property of the unit cell as

$$I_{UC} = I_d t^3 \tag{43}$$

For a beam with many unit cells (N>1) the parallel axis theorem can be used to relate I_d to I. If the i-th unit cell has a center point at y_{ci}, its contribution to I is

$$I_i = I_d t^3 + t\, {y_{ci}}^2 \tag{44}$$

The center point of the i-th unit cell is located at

$$y_{ci} = \frac{T}{2}\left(\frac{2i-1}{N} - 1\right) \tag{45}$$

The total I of the beam is equal to the sum of the individual contributions,

$$I = \sum_i I_i = \sum_i (I_d t^3 + h\, {y_{ci}}^2) \tag{46}$$

After substitution and simplification this can be expressed as,

$$I = \frac{T^3}{12}\left(1 + \frac{12\, I_d - 1}{N^2}\right) \tag{47}$$

This formula will show a stiffening size effect if $I_d > 1/12$ and a softening size effect otherwise. The equation can be solved for I_d in terms of *I*, and *N*, *T* as

$$I_d = \frac{1 - N^2}{12} + \frac{I\, N^2}{T^3} \tag{48}$$

This allows I_d to be calculated as a function of the number of unit cells in the lattice and I. Because Equation 48 has one constant term and one inversely proportional to the number of unit cells squared, it will asymptotically converge to a constant value as the number of cells

increases. For a series with N_C cells in the coarsest lattice, and N_F cells in the finest, the size effect due to this material distribution will be,

$$SE_M = \frac{1 + \frac{12\, I_d - 1}{{N_C}^2}}{1 + \frac{12\, I_d - 1}{{N_F}^2}} - 1 \qquad 49$$

4.3.3 Numerical Calculations of I_d

This section describes how the lattice solver described in Section 4.2.2 is used to find the effective I, and I_d. The next section will use that data to make and test predictions of size effects in bending.

The lattice solver is used to simulate a series of lattices for each combination of type and axial direction. Each series consists of 7 cases, with N ranging from 1 to 7. Each case has N unit cells in the axial direction, and N+6 cells in the transverse direction. The central N x N unit cells are called the active region, and this is where all of the relevant results are taken from. The additional cells are a buffer region. The active region works similarly to the size effect series discussed in Section 4.2.2. Because cell size and cell wall thickness are inversely proportional to N, the overall dimensions and amount of material in the active region remain constant. The cells outside the active region have the same size and wall thickness as those inside the active region, but the overall size and amount of material in the buffer region do not remain constant. Figure 51 illustrates this.

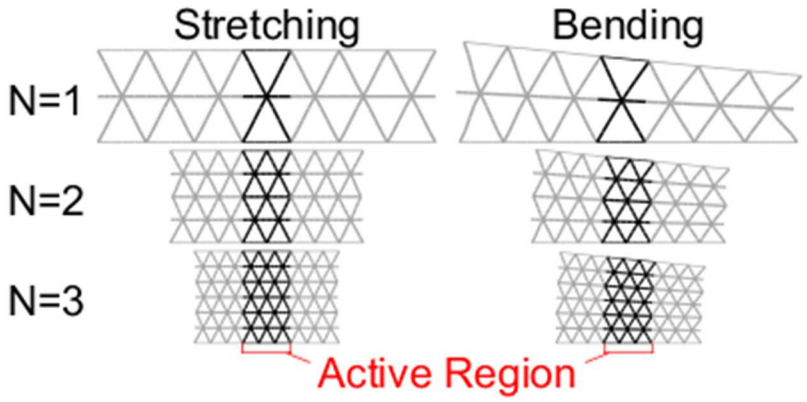

Figure 51: Series used for calculating I_d.

The only purpose of the 3 cells on either side of the active region is to insulate the active region from edge softening effects at the free edges; Chapter 2 showed that for certain lattice types, unit cells on or near the free edges contribute less to stiffness than cells in the center of the lattice. This effect is strongest on the cells immediately adjacent to the free edges and decays towards the center, becoming completely negligible in the fourth cell away from the free edges. It would be possible to include this buffer region only for lattice types that have an edge softening effect, however for the sake of consistency it is done for all types.

In order to find the effective Young's modulus of the lattice, a free stretching boundary condition is applied, and the strain energy in the active region, W_s, is found using

$$W_s = 1/2\ \vec{u}^T K_A \vec{u} \qquad 50$$

where K_A is a stiffness matrix assembled just from the elements in the active region. E is found using,

$$E = \frac{2\ W_s\ L}{\delta^2\ T} \qquad 51$$

where δ is the prescribed displacement in stretching. For the hexagon lattice types, this process produced a Young's modulus that varied with the number of unit cells; as a result, for this case, the Young's modulus is determined instead by values calculated using formulas taken from the literature (Stronge & Wang X.L., 1999).

A pure bending boundary condition is then applied to the lattice and the strain energy in the active region, W_b, is found using Equation 50. The effective I is found using Equation 47, and I_d is found using Equation 48. Because I_d is found separately for each case, the N-th I_d is denoted I_{dN}. Because this process is repeated for each axial direction, it produces two separate results, denoted I_{dx} and I_{dy}.

4.3.3.1 *Results in I_d and E*

For each series, the effective Young's modulus, E, is almost perfectly constant. It varies by less than 0.3% in all of the cases examined, except hexagons as previously noted. This observation is consistent with various papers deriving effective material properties of lattice materials (Dos Reis & Ganghoffer, 2011; Gibson & Ashby, 1999; Kumar & McDowell, 2004; Liu & Su, 2009b).

I_{dN} is also almost constant in most cases, with a couple of notable exceptions. Triangle and Triangle+ in the Y axial direction are relatively constant, but have a maximum value at N=2 that is 5.7% higher than their minimum value, which occurs at N=7. Hexagons and Hexagons+ in the Y axial direction change by 13.8% between their maximum and minimum values. This may indicate that this derivation process applies less well to hexagons than other lattice types. The I_{dN} values for all of the other series were almost perfectly constant, varying by less than 0.1% as the number of unit cells changed. For further calculations, I_d is assumed to be the average value of the seven I_{dN} values in a series.

Figure 52 shows the I_d values obtained using the above procedures for the different series, rank ordered from highest to lowest. Triangles, hexagons, and diamonds, the axial direction is indicated after the name of the lattice type. The other lattice types are not sensitive to a 90 degree rotation, and I_d is the same in either direction. . The dashed red line is drawn at $I_d = 1/12$. Equation 49 indicates that values greater than this value predict a stiffening size effect, and values less have a softening size effect.

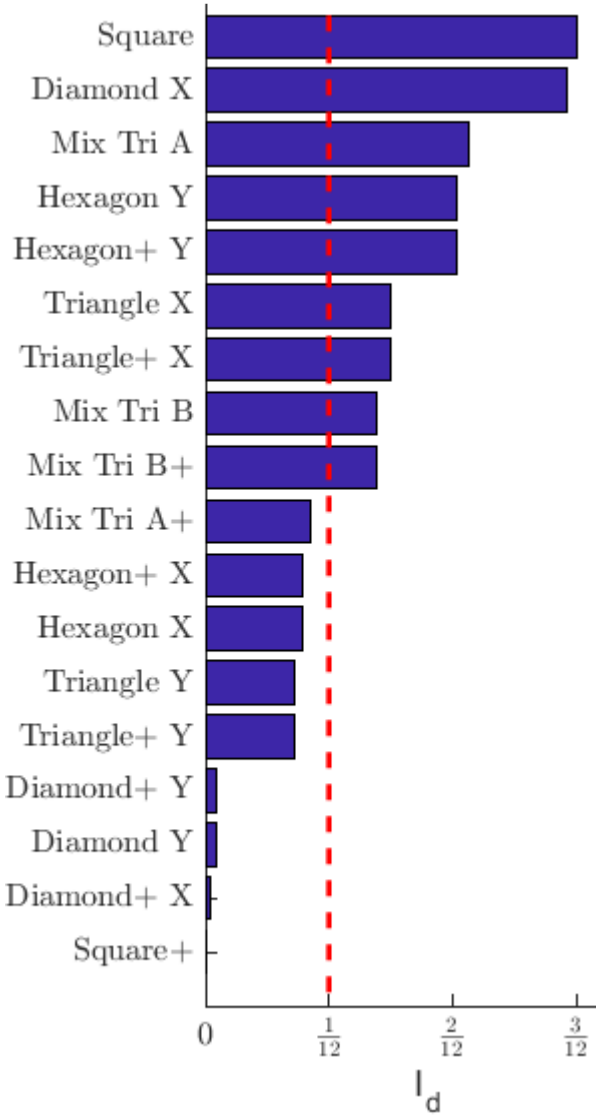

Figure 52: Rank ordered unit cell non-dimensional moments of area.

Unit cells with their material the farther from their axial centerlines have higher I_d. For the square cells, all of the material is at the extreme edges of the cell, and squares have the highest I_d, 0.25083. The square+ cells have all of their material at the centerline, and a I_d too small to show on the graph, 0.00083.

The I_d value in both cases ends in 0.00083, which comes from the flexural stiffness of the cell walls. In the square+ lattice with N=1, there is a single cell wall with full thickness, a length of T, and a regular (not effective) second moment of area $I = (\frac{T}{10})^3/12$. Using this *I* in Equation 48 gives $I_d = 0.00083$. This was quantified in Chapter 3 as bending strain energy, and is a few percent or less of the total stiffness. The flexural stiffness of cell walls can be considered as a separate cause of size effects, but the methods of this work do not separate it from material distribution effects. Based on the results Chapter 3 it should be negligible.

4.3.3.2 *Theoretical Maximum and Minimum Size Effects from Material Distribution*

I_d for square lattices is a theoretical maximum because it is not possible to move material any farther from the centerline. Similarly, the theoretical minimum of 0 is almost achieved in Square+ cells. Using Equation 49, this implies that the largest possible stiffening size effect and the largest softening size effect are approximately,

$$SE_{max} = \frac{2}{N^2} \quad SE_{min} = \frac{-1}{N^2} \tag{52}$$

This implies that the maximum size effects caused by material distribution for a lattice of 5 cells would be +8% and -4%. This is consistent with the results presented in the next section.

4.3.4 Prediction of Size Effect Magnitude

In order to test the ability of this method to predict size effects in bending, series of simulated lattices are created. The series cover every lattice type shown in Figure 44. Each series has a base number of either 5 or 6 unit cells, and refines from there. Each series has either a bending or transverse boundary condition. For the bending series, the aspect ratio is approximately 1. For the transverse series the aspect ratios are either 4, 6, or 10. For the transverse boundary conditions, cases with a high aspect ratio are strongly bending dominated. Cases with a low aspect ratio (<1), are shear dominated. The lowest aspect ratio in this range, 4, is expected to show a combination of bending and shearing behavior. The set of series covers every combination of lattice type, boundary condition, aspect ratio, and base number. After the series is run, the lattice size effect, SE_L, is quantified using Equation 38. This will be compared to the material distribution size effect calculated using Equation 49.

4.3.4.1 *Summary of Edge Softening Methods*

Many of these series are affected by the edge softening effects described in Chapter 3, and briefly summarized in Section 4.2.3 of this chapter. The presence or absence of an edge softening effect depends on lattice type and axial direction. The following lattices used in this work show an edge softening effect:

- All triangle and hexagon lattices (regular and +) with a Y axial direction,
- All Mixed Triangle B lattices (regular and +),
- Mixed Triangle A + lattices.

For these lattices, the techniques used in [cite previous paper] will be used to make a prediction of size effect, denoted SE_E. For these cases it is expected that the edge softening size

effect is present in addition to the material distribution effect. These two effects are added together to make a single prediction of the total effect for that lattice,

$$SE_T = SE_M + SE_E \quad 53$$

When it edge softening effects are not present, SE_E is assumed to be 0 and $SE_T = SE_M$. Simply adding the two effects together assumes that the two causes of size effects do not have any second order interactions. For a bending boundary condition, the free edges contribute more to the stiffness than the center, and the free edges are the only thing affected by the edge softening effect. Although it would make sense for the material distribution effect and the edge softening size effect to have a second order interaction, this work does not have any method for quantifying it.

4.3.5 Results

The results in this section are for either pure bending or transverse bending. Some combinations of lattice type and axial direction have edge softening effects, while others do not. The material distribution size effect was derived based on an assumption of pure bending, and no edge softening. The following results will show accurate predictions of size effects when these assumptions are true, and less accurate results when one or both assumptions are violated.

4.3.5.1 *Pure Bending Without Edge Softening*

Figure 53 shows a pair of selected size effect series in pure bending with no edge softening effects. As the number of cells increases, the size effect decays away. SE_M almost perfectly matches SE_L.

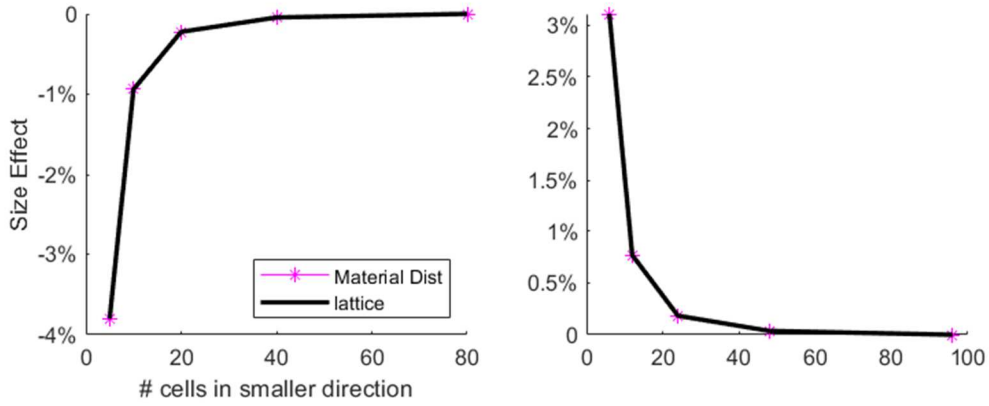

*Figure 53: Selected size effect series in pure bending **without** edge softening. Left Diamond+ with X axial direction and 5 base cells. Right Mixed Tri. A with 6 base cells.*

Figure 54 compares SE_M to SE_L for all series in pure bending without edge softening. The dashed green line indicates where the material distribution of size effects almost perfectly match the lattice model ($SE_M = SE_L$); All of the data falls within 0.1% of this line.

Figure 54 and several figures presented later on, have a log-log scale on both sides of the zero axis. This type of graph effectively presents positive and negative data that spans several orders of magnitude, but the log scale can visually exaggerate the accuracy of predictions.

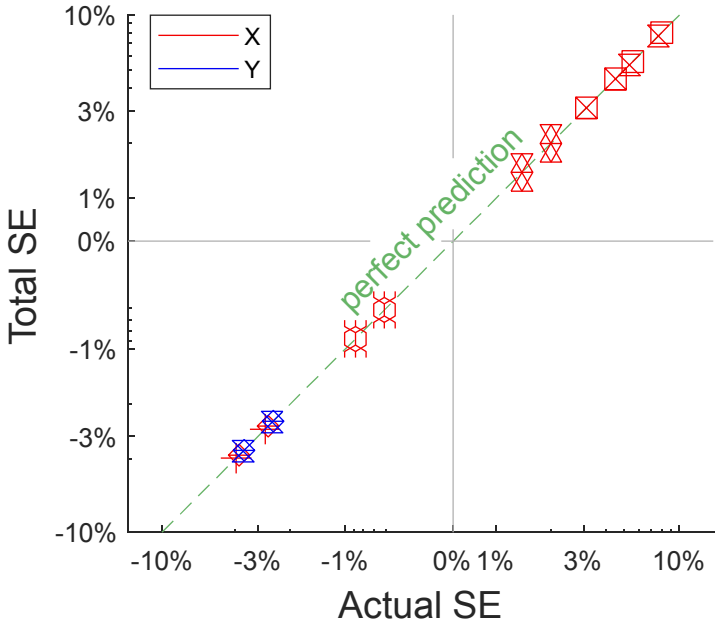

*Figure 54: Size effect predictions vs lattice model for pure bending **without** edge softening.*

4.3.5.2 *Transverse Bending Without Edge Softening*

Figure 55 shows the same two size effect series as Figure 53, but in the transverse boundary condition with aspect ratios of 10 and 4. When the aspect ratio is high, this boundary condition is bending dominated with a small shear component. As the aspect ratio decreases, the shear becomes progressively more important. The derivation of material distribution effects assumes pure bending, which has no shear. A beam in the transverse boundary condition is most similar to pure bending when the aspect ratio is very high.

The top two series in Figure 55 show that, for a high aspect ratio, the material distribution size effect is still fairly accurate, but less accurate than for pure bending. The bottom two series have a lower aspect ratio and the prediction is markedly less accurate. If the

aspect ratio is further decreased, it is expected that the size effect in the lattice model would continue to diverge from the material distribution prediction.

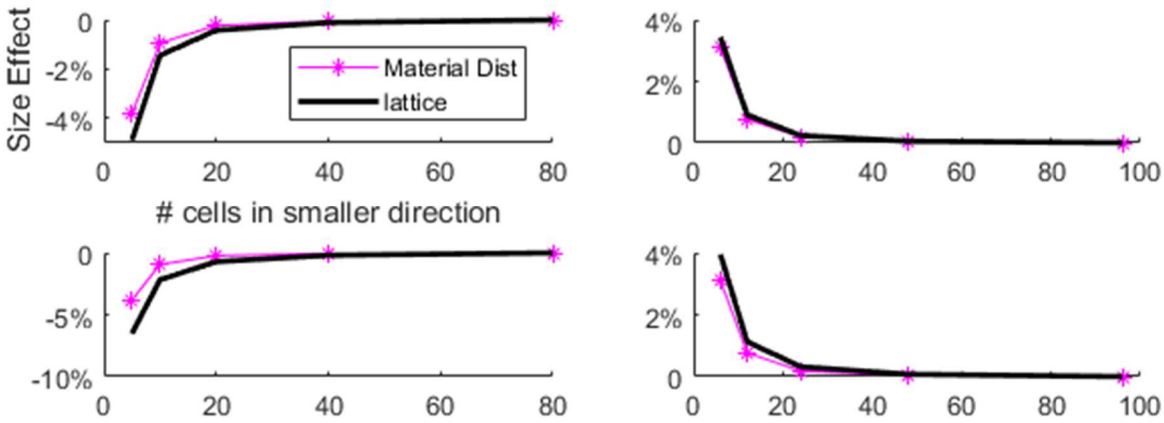

*Figure 55: Selected size effect series in transverse bending **without** edge softening. Left column: Diamond+ with X axial direction and 5 base cells. Right column: Mixed Tri. A with 6 base cells. Top row: aspect ratio of 10. Bottom row: aspect ratio of 4.*

Figure 56 compares SE_M to SE_L for all series in pure bending without edge softening. It shows that this trend of decreasing accuracy with aspect ratio holds for most lattice types. The accuracy is much better for lattices with a stiffening size effect and a large I_d. The scale of size effects in these lattices are also relatively insensitive to aspect ratio.

These observations show that material distribution is a cause of size effects in transverse bending, but it may not be the only cause.

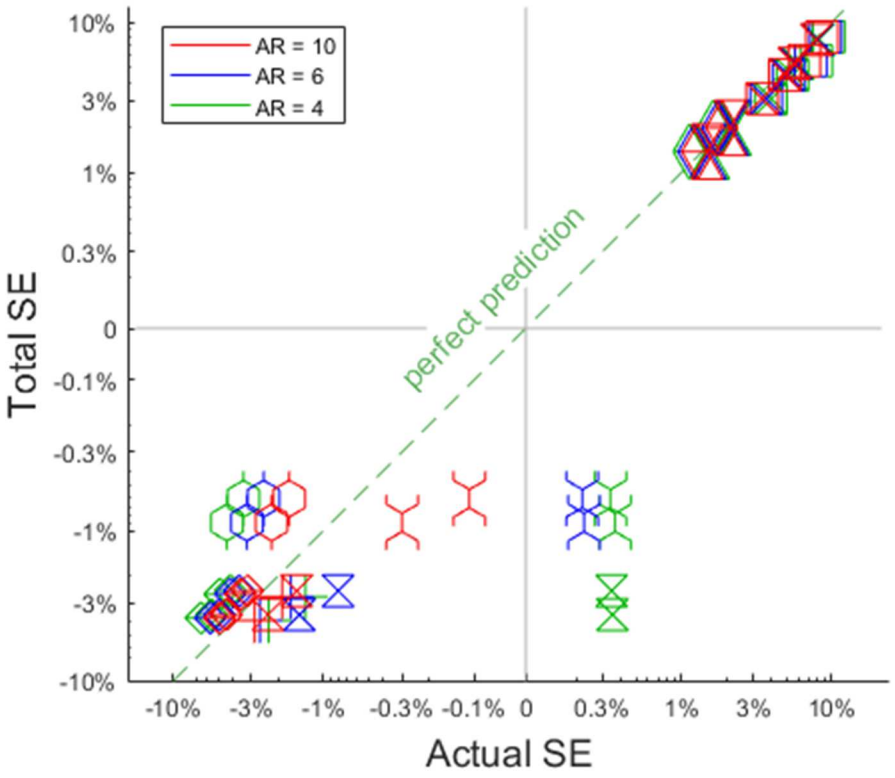

Figure 56: Size effect predictions vs lattice model for transverse bending ***without*** *edge softening.*

4.3.5.3 *Pure Bending With Edge Softening*

Because the data in the previous four figures excludes situations with edge softening, material distribution was the dominant source of size effects. By contrast, in the following data, material distribution and edge softening are both present and can combine to create a total size effect. Figure 57 and Figure 58 show data for cases of pure bending that also include edge softening. Figure 57 shows a typical pair of size effect series, and Figure 58 compares the size effect predictions for all of these cases.

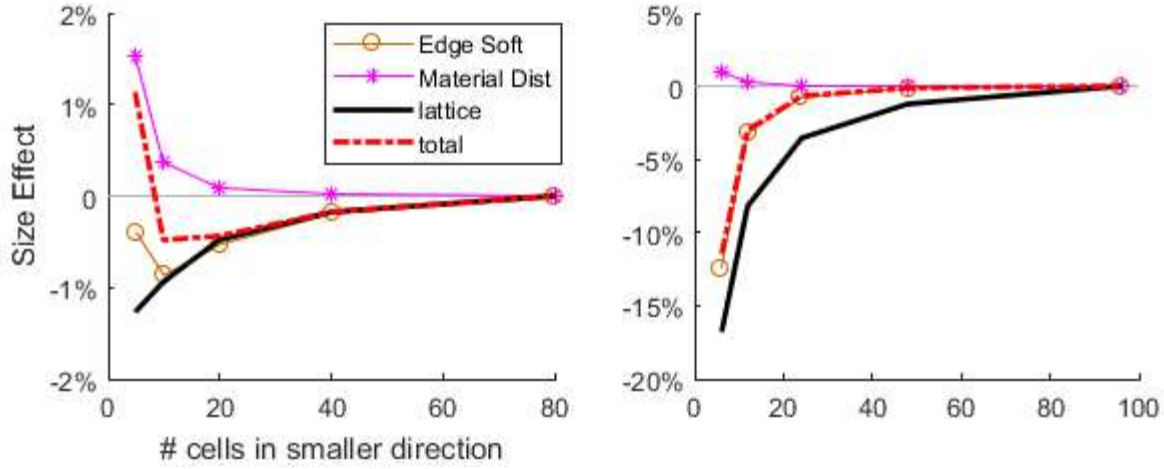

*Figure 57: Selected size effect series in pure bending **with** edge softening. Left: Mixed Triangle B with 5 base cells. Right Hexagon with Y axial direction and 6 base cells.*

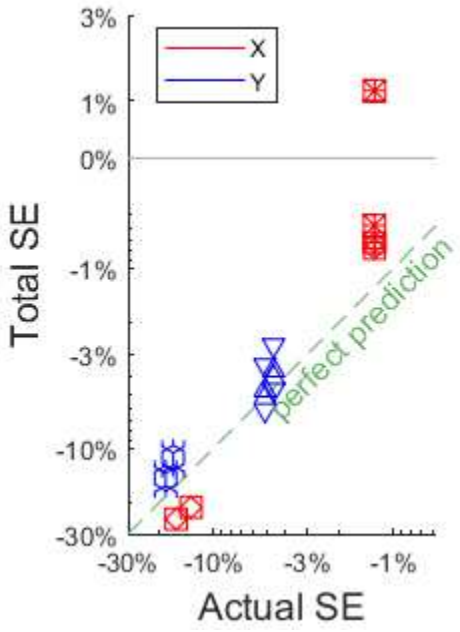

*Figure 58: Size effect predictions vs lattice model for pure bending **with** edge softening.*

Figure 58 shows that the predictions of total size effects are reasonably accurate, but considerably less accurate than when material distribution is the only cause of size effects. The right half of Figure 57 shows a fairly typical combination of size effect causes; edge softening is

considerably larger than material distribution, and the edge softening effect has the same trend as the total lattice size effect.

Equation 52 suggests that the largest softening size effects arising just from material distribution are -4%. The size effects from edge softening are up to -11%, significantly larger than the material distribution size effects.

In one case of Mixed Triangle B, the lattice model shows a softening size effect, but the total predicted size effect is stiffening. The left half of Figure 57 shows the two causes of size effects for this case; both are between 1% and 2%, but they are in opposite directions. The material distribution size effect has a peak on the second lattice refinement, indicating that there is a fairly complicated interaction between the fixed edges and the edge softening effect on the free edges. When the two are combined, the material distribution is slightly larger, for a total predicted 1% stiffening size effect. Although this prediction is incorrect, the absolute error is only 2%. In other very similar situations, the two causes of size effects have different relative scales and combine to make a slightly softening size effect.

4.3.5.4 *Transverse Bending With Edge Softening*

Figure 59 show data for transverse bending with edge softening. The total predicted size effect is clearly correlated with the actual lattice model size effect, but that correlation is not nearly as strong as in previous sets of data. Previously Figure 56 showed that prediction accuracy decreases as aspect ratio decreases and bending becomes less dominant. When edge softening is present, this same pattern is not apparent. The edge softening effect is interacting with the shearing component of bending; the combination of these two phenomena makes for a less reliable prediction of size effects.

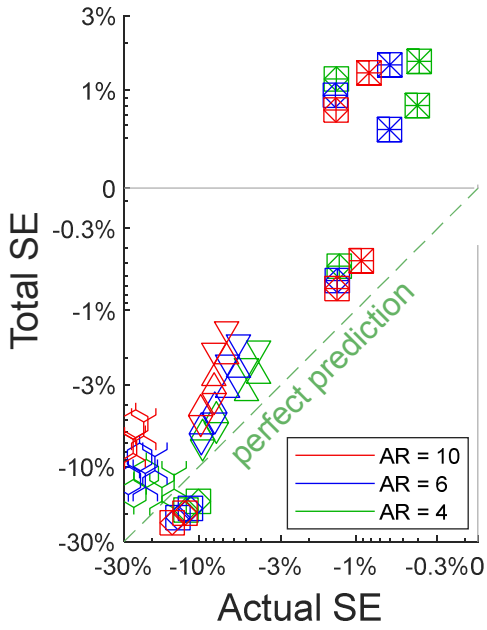

*Figure 59: Size effect predictions vs lattice model for transverse bending **with** edge softening.*

4.3.5.5 *Summary of Results for All Data Sets*

Figure 60 presents all of the previous data in a single graph. Taken as a whole, this data set shows that a formula derived from the effective bending resistance of a single unit cell gives a good prediction of size effects. Prediction accuracy is better for pure bending than transverse bending. It is also better when edge softening is not present. However, even when both of these assumptions are not present, the simplified prediction of size effects still captures the correct order of magnitude in all cases.

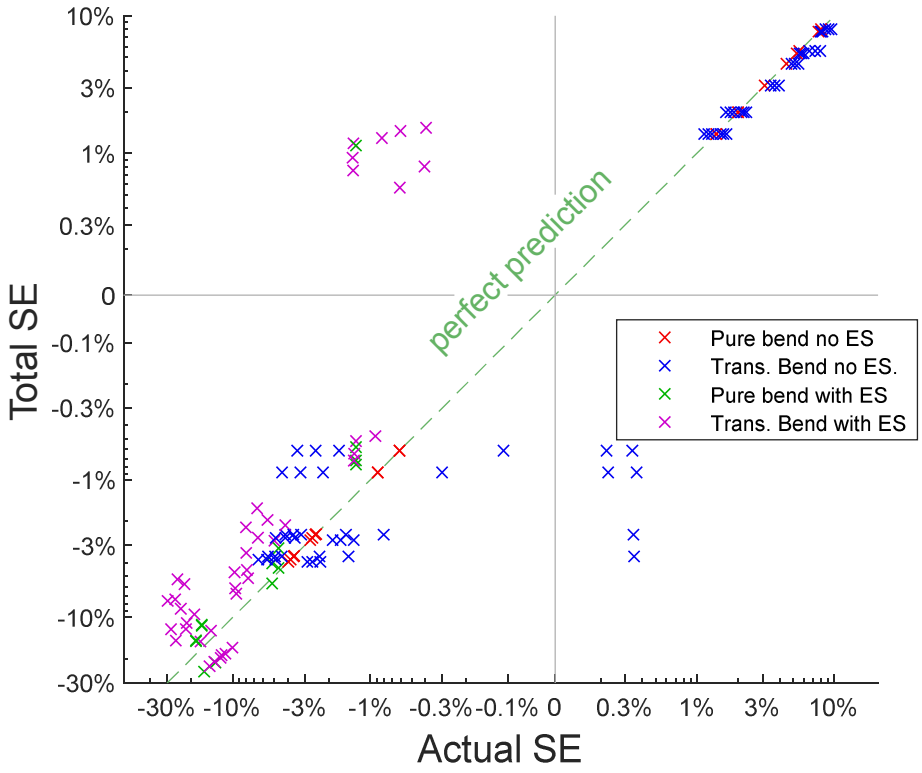

Figure 60: All results collected.

4.4 Discussion

These results show that material distribution explains both stiffening and softening size effects in bending of periodic cellular materials. The difference between a stiffening and a softening size effect depends on the specific choice of a unit cell. If a unit cell is chosen with most of the material close to the center of that cell, I_d will be small and there will be a softening size effect. If the material is far from the center of the cell, the reverse happens.

The results of this work are consistent with the results of previous work by other authors. (Wheel et al., 2015) found similar results when examining a model material, and a two ply laminate. The laminate was a beam made of alternating plies of stiff and soft material. A

stiffening size effect was observed when the plies were arranged so that the stiff material is on the outside, and a softening effect otherwise. The model material was made from a solid material with a regular pattern of holes. There was a softening effect when the holes intersected the surface, and a stiffening effect otherwise.

Results of this study confirm the results from (Dunn & Wheel, 2016), but the interpretation of the findings is different. Dunn examined the same square and square+ arrangement examined in this work, and observed size effects similar to those seen here, but attributed them to differences in the surface of the model. The resulting effects were attributed to differences in the surface of the model, concluding that the stiffening size effects were consistent with the micropolar model, and the softening effects are caused by surface softening.

In contrast, the results of this work show that both the stiffening and softening effects can result from the same mechanism. In certain lattice types, edge softening effects are present in addition to material distribution effects, but they are absent in the square+ lattices studied by Dunn. By focusing attention on the surface, differences in arrangement through the entire bulk where not considered. Figure 61 shows how the two configurations of model material used by (Wheel et al., 2015) can be created by choosing a different unit cell. When the unit cell is changed from centered holes to edge holes, every single hole moves farther from the centerline of the beam. This is very similar to what was shown in Figure 48. It shows that material distribution softening effects are not merely a surface effect t, they are distributed through the entire bulk.

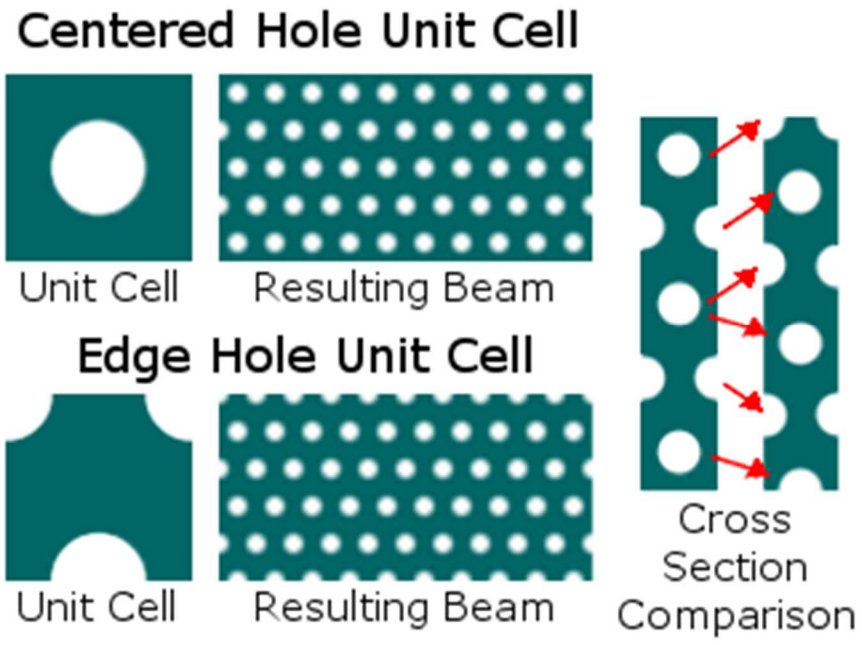

Figure 61: Comparison of model material with centered holes and edge holes. The edge hole model material has all of its holes farther from the centerline than the center hole material.

4.4.1 Inconsistency with Micropolar Model

Micropolar, couple stress, and other extended continuum models replace a discrete lattice with an equivalent continuum. Intentionally, the continuum model, as an approximation, does not contain all the information about the details of the lattice. The extended material properties of this extended continuum are meant to model relevant size dependent behaviors of the lattice, but how these material properties are derived affects which behaviors they will model.

These micropolar material properties predict that the stiffness of a micropolar beam structure is a constant plus a term with an inverse quadratic relationship to the number of unit cell divisions, $1/N^2$. This relationship was derived by (Gauthier, 1974) and has since appeared in other research (Dunn & Wheel, 2016; Lakes, 1986; Tekoğlu, 2007). Equation 54 highlights the

form of this relationship, with the actual material constants replaced by constants A and B. Equation *47* is reproduced here to facilitate direct comparison of the two.

$$K = A + \frac{B}{N^2} \qquad 54$$

$$I = \frac{T^3}{12}\left(1 + \frac{12\ I_d - 1}{N^2}\right) \qquad 55$$

Although the two have the same form, B is constrained to be greater than 0, and the micropolar model is constrained to stiffening effects. The equivalent term used in this work, $12\ I_d - 1$ is not, and as a result, can show both stiffening and softening effects.

Micropolar elasticity can be used to make a variety of predictions about the behavior of cellular materials. It can predict that cellular materials in bending (Rueger & Lakes, 2016) or shear (Diebels & Scharding, 2011a; Tekoğlu & ONCK, 2008) will be stiffer with larger unit cells, and the same volume of material. It also predicts size effects in stress concentrations (Nakamura & Lakes, 1988) and strain concentrations (Tekoğlu, 2007). If the mechanism that causes a stiffness size effect in bending is not consistent with the assumptions of micropolar elasticity, deriving a micropolar material property from observations of that stiffness size effect will produce spurious predictions of size effects in other situations.

The results of this work do not apply to stochastic cellular materials because I_d depends on how the unit cell is chosen. As a periodic lattice goes from coarse to fine, material systematically moves towards or away from the centerline. In a stochastic cellular material unit cells are not chosen; they are generated by a semi-random process, and a systematic movement of material is impossible.

4.5 Conclusion

The first part of this work examined size effects in square and mixed triangle A lattices, and looked at the ability of continuum models to predict those size effects. Two different versions of each lattice type were examined, one with closed cells and one with open cells. The open cell configuration was denoted +. In a shear boundary condition, both lattice types showed stiffening size effects. In a bending boundary condition, the + lattices showed softening size effects and the closed lattices showed stiffening effects.

The results of these lattices are then compared to a micropolar and a couple stress model using material properties derived by two different authors. The properties derived by (Liu & Su, 2009b) predicted size effects accurately in the closed cell lattice types in the bending boundary condition, but overestimated the size effects in shear by an order of magnitude. For the properties derived by (Kumar & McDowell, 2004) the situation is reversed; The prediction for shear was good, but the prediction for bending was an order of magnitude too small.

Both the micropolar and couple stress model exclusively predict stiffening size effects, which is inconsistent with the softening size effects observed in the + lattices. The results of the first part of the paper show that extended continuum material properties that work well in one boundary condition do not necessarily work well in another.

The second part of this work shows that the inconsistency seen in the first part happens because there is a mechanism causing size effects in bending that is absent in shear. This mechanism happens because as the lattice refines, there is a net movement of material either towards the neutral axis or away from it, depending on how the unit cell is chosen. This effect is termed a material distribution effect.

A formula is derived to characterize how the choice of unit cell affects material distribution effects. It centers on the effective resistance of a single unit cell to bending, I_d. The parameter I_d is large for closed cells, and small for open cells. The predictions of this formula are compared to size effects in the lattice model. In pure bending, the prediction quality is excellent. When bending is mixed with a transverse shear, the prediction quality is good, but shows some discrepancies. As the importance of shear deformation increases relative to bending, the prediction quality gets worse.

When edge softening effects are present, the methods used to quantify edge softening effects in Chapter 3 are combined with the current methods to make a single prediction. The two combined methods provide useful predictions, but are less accurate than predictions when only one or the other cause of size effect is present.

The results of the second part show that a single mechanism causes both stiffening and softening size effects for periodic cellular materials in bending. This is inconsistent with the micropolar and couple stress models which predict only stiffening size effects. If micropolar material properties are derived from observed size effects in a periodic cellular material in bending, those properties may not provide a useful prediction outside of the specific circumstance from which they were derived.

5. Conclusion and Future Work

5.1 Conclusion

The previous chapters presented methods that quantified different mechanisms that predict size effects for a broad variety of lattice types, boundary conditions, and aspect ratios. Figure 62 shows the predictions for the entire primary set of problems discussed in Chapter 2, as well as the corresponding + variants of those lattice types. Similar figures in Chapters 2 and 3 showed subsets of the data in Figure 62.

The total size effect is the sum of all of the applicable size effects. Local bending is applicable to all lattice types other than hexagons and squares in shear. Edge softening is applicable for the lattice types and axial directions for which it is present (see Chapter 2). Material distribution is applicable to pure bending and transverse boundary condition when the aspect ratio is greater than 3.5.

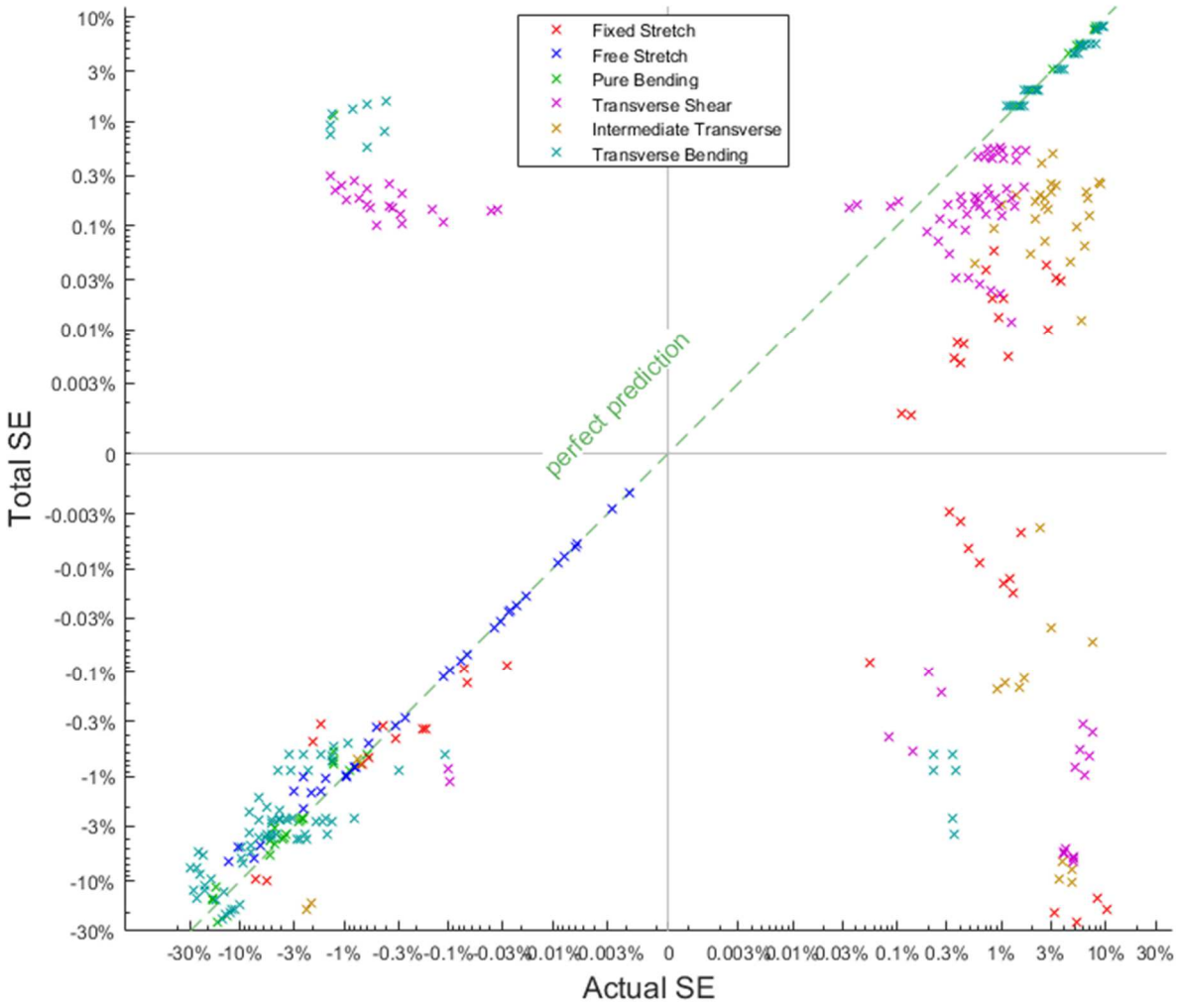

Figure 62: Predicted vs Actual size effects for all cases in the problem set.

Most of the cases cluster around the perfect prediction line; they have predicted size effects similar to their actual size effect. There are a few groups that are notably farther from this line.

In the upper left there is a group of series in transverse bending. These have an edge softening effect and a material distribution stiffening effect that are working against each other. Even though the visual distance between that group and the perfect prediction line is large, the absolute error is only about 2%. This group is also shown in Figure 17 of Chapter 2. Right below

that group, in the upper left there is a group of cases in shear with a slightly softening actual size effect, between -1% and -0.1%, and a slightly stiffening predicted size effect, between 0.3% and 0.03%. This absolute error is fairly small.

One the right half of the graph there are a large number of cases with actual size effects that are considerably stiffer than the predicted size effect. Some of these cases have a total softening size effect and a predicted stiffening effect, while others have a total stiffening effect that is smaller than the actual size effect. These cases are mostly transverse shear, transverse with an intermediate aspect ratio, or fixed stretching. Size effects for these groups are largely unexplained by the methods of chapters 3 and 4. They have a local bending size effect, but it is too small to match the actual size effect. This suggests that there is an as yet unexplained cause of size effects present in these cases.

This dissertation has presented methods for predicting size effects in periodic lattice structured materials in a broad variety of situations. The results shown in Figure 62 show that these methods are effective, but not yet complete.

5.2 Takeaways

This work explores three main causes of size effects, local bending, edge softening and material distribution. This work presents methods for quantifying local variables connected to those causes of size effect and then connecting those local variables to the global size effect in stiffness.

Local beam bending size effects are caused by the beam-like nature of cell walls in a lattice. This cause of size effects usually causes stiffening size effects and is smaller than the other two causes. It was only shown to be the dominant cause of size effects in shear.

Micropolar elasticity is an extension to classical elasticity that incorporates size dependent behavior. Some authors have derived micropolar material properties based on the assumption that size effects are caused by local beam bending. Size effects predicted by this model are an order of magnitude smaller than size effects in the lattice model, except in a shearing boundary condition, where they are approximately the right size. This work concludes that, except in shear, micropolar elasticity offers little additional benefit over classical elasticity.

Cells near the free edges of periodic lattice structured materials can have a softer constitutive relationship than interior cells. This creates a softening size effect. This cause of size effects only appears for certain lattice types and axial directions, but when it is present it can create a larger size effect than the other two causes.

Material distribution size effects only occur in bending. For lattices comprised of few unit cells, it is possible for material to be concentrated either at the edges of the lattice where it contributes the most to stiffness or in the center where it concentrates the least. As the lattice refines, the material is redistributed so that it is more evenly spread. These three causes explain size effects in a variety of cases, but there are remaining cases where size effects are left unexplained.

5.3 Future work: Size effects due to discretization

Future work will attempt to explain these cases, using the hypothesis that there is a mechanism that can cause size effects that is similar to convergence in a finite element model. When boundary conditions are applied to a linear elastic system, the solution will minimize the strain energy subject to those restrictions. In a linear elastic system, adding additional restrictions either increases the stiffness or leaves it the same. Removing restrictions, adding

freedom, either decreases the stiffness or leaves it the same. In a cellular material modeled as beam elements, only the beam nodes have independent displacements and rotations. When there are fewer cells, there are fewer nodes, and fewer degrees of freedom. This suggests that adding additional cells adds additional freedom to the system, and allows the lattice to find lower energy solutions. This may be a cause of stiffening size effects. Because it is related to a division of the material space into different numbers of discrete cells, it will be known as a discretization size effect.

To test this hypothesis, a classical elastic FEA was created using linear shape functions and run on a series of mixed triangle A lattices shown in Figure 63. The lattices have an aspect ratio of 1, and a transverse boundary condition. For each case in the series, the finite elements were squares the same size as a unit cell; as the unit cell size refined, the finite element mesh also refined. The two final refinements are left out of Figure 63 because the cells are too small to be shown.

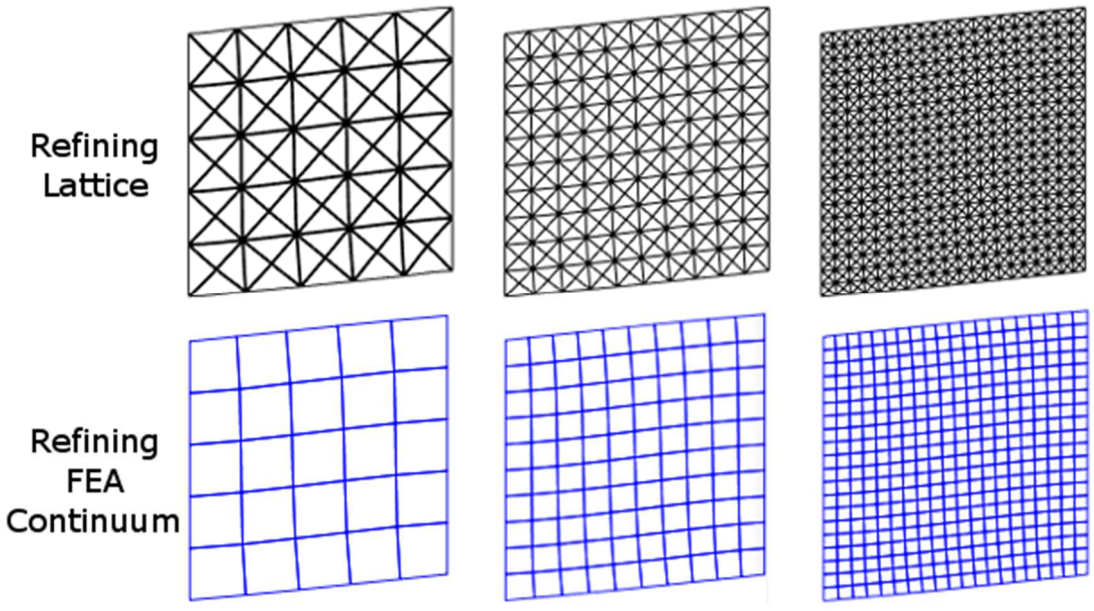

Figure 63: FEA mesh refinement mimics lattice refinement.

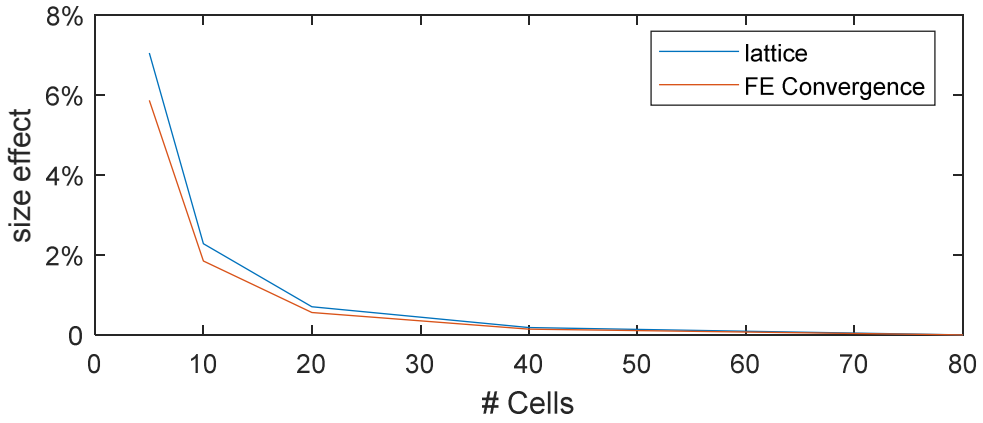

Figure 64: Lattice Size effect vs FE convergence.

Figure 64 shows that the global strain energy in the lattice and finite element models converge at approximately the same rate. The size effect in the continuum FEA is calculated by normalizing it by the refined result of the FEA model as,

$$SE_D = \frac{W_{DC}}{W_{DF}} - 1 \qquad 56$$

where W_{DC} and W_{DF} are the strain energy in the coarse and fine FEA models. Future work will test this as a potential cause for size effects, and hopefully show that it can explain the size effects left unexplained in this dissertation.

Bibliography

Adachi, T., Tomita, Y., & Tanaka, M. (1998). Computational simulation of deformation behavior of 2D-lattice continuum. *International Journal of Mechanical Sciences*, *40*(9), 857–866. http://doi.org/10.1016/S0020-7403(97)00127-6

Alderson, A., Alderson, K. L. L., Attard, D., Evans, K. E. E., Gatt, R., Grima, J. N. N., … Zied, K. (2010). Elastic constants of 3-, 4- and 6-connected chiral and anti-chiral honeycombs subject to uniaxial in-plane loading. *Composites Science and Technology*, *70*(7), 1042–1048. http://doi.org/10.1016/j.compscitech.2009.07.009

Anderson, W. B., & Lakes, R. S. (1994). Size effects due to Cosserat elasticity and surface damage in closed-cell polymethacrylimide foam. *Journal of Materials Science*, *29*(24), 6413–6419. http://doi.org/10.1007/BF00353997

Andrews, E. W., Gioux, G., Onck, P., & Gibson, L. J. (2001a). Size effects in ductile cellular solids. Part I : Modeling. *International Journal of Mechanical Sciences*, *43*, 0–1.

Andrews, E. W., Gioux, G., Onck, P., & Gibson, L. J. (2001b). Size effects in ductile cellular solids. Part II: Experimental results. *International Journal of Mechanical Sciences*, *43*(3), 0–1. http://doi.org/10.1016/S0020-7403(00)00043-6

Banks, C. B., & Sokolowski, M. (1968). On certain two-dimensional applications of the couple stress theory. *International Journal of Solids and Structures*, *4*(1), 15–29. http://doi.org/10.1016/0020-7683(68)90030-9

Bastawros, A.-F., Bart-Smith, H., & Evans, A. G. (2000). Experimental analysis of deformation mechanisms in a closed-cell aluminum alloy foam. *Journal of the Mechanics and Physics of Solids*, *48*(2), 301–322. http://doi.org/10.1016/S0022-5096(99)00035-6

Bažant, Z. P., & Christensen, M. (1972). Analogy between micropolar continuum and grid frameworks under initial stress. *International Journal of Solids and Structures*, *8*(3), 327–346. http://doi.org/10.1016/0020-7683(72)90093-5

Beveridge, A. J., Wheel, M. A., & Nash, D. H. (2012). The micropolar elastic behaviour of model macroscopically heterogeneous materials. *International Journal of Solids and Structures*, *50*(1), 246–255. http://doi.org/10.1016/j.ijsolstr.2012.09.023

Brezny, R., & Green, D. J. (1990). Characterization of edge effects in cellular materials. *Journal of Materials Science*, *25*(11), 4571–4578. http://doi.org/10.1007/BF01129908

Budynas, R., & Nisbett, K. (2006). *Shigley's Mechanical Engineering Design* (8th ed.).

Chen, Y., Liu, X., & Hu, G. (2014). Micropolar modeling of planar orthotropic rectangular chiral lattices. *Comptes Rendus - Mecanique*, *342*(5), 273–283. http://doi.org/10.1016/j.crme.2014.01.010

Chen, Y., Liu, X. N., Hu, G., Sun, Q. P., & Zheng, Q. S. (2014). Micropolar continuum modelling of bi-dimensional tetrachiral lattices. *Proceedings of the Royal Society A: Mathematical, Physical and Engineering Sciences*, *470*(2165), 20130734. http://doi.org/10.1098/rspa.2013.0734

Chung, J., & Waas, A. M. M. (2009). The micropolar elasticity constants of circular cell honeycombs. *Proceedings of the Royal Society A: Mathematical, Physical and Engineering Sciences*, *465*(2101), 25–39. http://doi.org/10.1098/rspa.2008.0225

Dai, G., & Zhang, W. (2009). Cell size effect analysis of the effective Young's modulus of sandwich core. *Computational Materials Science*, *46*(3), 744–748. http://doi.org/10.1016/j.commatsci.2009.04.033

Diebels, S., & Scharding, D. (2011a). From lattice models to extended continua. *Lecture Notes in Applied and Computational Mechanics*. http://doi.org/10.1007/978-3-642-22738-7_2

Diebels, S., & Scharding, D. (2011b). From Lattice Models to Extended Continua. *Advances in Extended and Multifield Theories for Continua*, 19–45.

Diebels, S., & Steeb, H. (2002). The Size Effect in Foams and Its Theoretical and Numerical Investigation. *Proceedings of the Royal Society A: Mathematical, Physical and Engineering Sciences*, *458*(2028), 2869–2883. http://doi.org/10.1098/rspa.2002.0991

Diebels, S., & Steeb, H. (2003). Stress and couple stress in foams. *Computational Materials Science*, *28*(3–4 SPEC. ISS.), 714–722. http://doi.org/10.1016/j.commatsci.2003.08.025

Dos Reis, F., & Ganghoffer, J. F. (2011). *Construction of Micropolar Continua from the Homogenization of Repetitive Planar Lattices*. (H. Altenbach, G. A. Maugin, & V. Erofeev, Eds.) (Vol. 7). Berlin, Heidelberg: Springer Berlin Heidelberg. http://doi.org/10.1007/978-3-642-19219-7

Dos Reis, F., & Ganghoffer, J. F. (2012). Construction of micropolar continua from the asymptotic homogenization of beam lattices. *Computers & Structures*, *112–113*, 354–363. http://doi.org/10.1016/j.compstruc.2012.08.006

Dunn, M. A., & Wheel, M. A. (2016). Computational Analysis of the Size Effects Displayed in Beams with Lattice Microstructures. In *Generalized Continua as Models for Materials* (Vol. 22, pp. 129–144). http://doi.org/10.1007/978-3-642-36394-8

Eringen, A. C. (1999). *Microcontinuum Field Theories, Vol. I: Foundations and Solids*. Springer, New York.

Fish, J., & Belytschko, T. (2007). *A First Course in Finite Element Analysis*. Chichester, West Sussex: Wiley.

Gauthier, R. D. (1974). *Analytical and Experimental Investigations in Linear Isotropic Micropolar*

Elasticity.

Gibson, L. J., & Ashby, M. F. (1999). *Cellular Materials: Structure and Properties* (2nd ed.). Cambridge University Press. Retrieved from http://books.google.com/books/about/Cellular_Solids.html?id=IySUr5sn4N8C&pgis=1

Goda, I., Assidi, M., & Ganghoffer, J. F. (2014). A 3D elastic micropolar model of vertebral trabecular bone from lattice homogenization of the bone microstructure. *Biomechanics and Modeling in Mechanobiology*, *13*(1), 53–83. http://doi.org/10.1007/s10237-013-0486-z

Goda, I., & Ganghoffer, J. F. (2015). Identification of couple-stress moduli of vertebral trabecular bone based on the 3D internal architectures. *Journal of the Mechanical Behavior of Biomedical Materials*, *51*, 99–118. http://doi.org/10.1016/j.jmbbm.2015.06.036

Hastie, T., Tibshirani, R., & Friedman, J. (2009). *The Elements of Statistical Learning: Data Mining, Inference, and Prediction* (2nd ed.). http://doi.org/10.1007/978-0-387-84858-7

Jeon, I., & Asahina, T. (2005). The effect of structural defects on the compressive behavior of closed-cell Al foam. *Acta Materialia*, *53*(12), 3415–3423. http://doi.org/10.1016/j.actamat.2005.04.010

Kumar, R. S., & McDowell, D. L. (2004). Generalized continuum modeling of 2-D periodic cellular solids. *International Journal of Solids and Structures*, *41*(26), 7399–7422. http://doi.org/10.1016/j.ijsolstr.2004.06.038

Lakes, R. S. (n.d.). Strongly Cosserat elastic lattice and foam materials for enhanced toughness. *Cellular Polymers*, *12*(1), 17–30. Retrieved from http://cat.inist.fr/?aModele=afficheN&cpsidt=4696175

Lakes, R. S. (1983). Size effects and micromechanics of a porous solid. *Journal of Materials Science*, *18*(9), 2752–2580.

Lakes, R. S. (1986). Experimental microelasticity of two porous solids. *International Journal of Solids and Structures*, *22*(1), 55–63. http://doi.org/10.1016/0020-7683(86)90103-4

Lakes, R. S. (1991a). Deformation mechanisms in negative Poisson's ratio materials: structural aspects. *Journal of Materials Science*, *26*(9), 2287–2292. http://doi.org/10.1007/BF01130170

Lakes, R. S. (1991b). Experimental micro mechanics methods for conventional and negative Poisson's ratio cellular solids as Cosserat continua. *Journal of Engineering Materials and Technology*, *113*(1), 148–155. http://doi.org/10.1115/1.2903371

Lakes, R. S., & Benedict, R. L. (1982). Noncentrosymmetry in micropolar elasticity. *International Journal of Engineering Science*, *20*(10), 1161–1167. http://doi.org/10.1016/0020-

7225(82)90096-9

Lakes, R. S., Nakamura, S., Behiri, J. C., & Bonfield, W. (1990). Fracture mechanics of bone with short cracks. *Journal of Biomechanics*, *23*(10), 967–975. http://doi.org/10.1016/0021-9290(90)90311-P

Liebenstein, S., Sandfeld, S., & Zaiser, M. (2016). Modelling Elasticity of Open Cellular Foams: Size Effects and Disorder. http://doi.org/10.1103/PhysRevB.94.144303

Liebenstein, S., Sandfeld, S., & Zaiser, M. (2018). Size and disorder effects in elasticity of cellular structures: From discrete models to continuum representations. *International Journal of Solids and Structures*, *146*, 97–116. http://doi.org/10.1016/j.ijsolstr.2018.03.023

Liu, S., & Su, W. (2009a). Effective couple-stress continuum model of cellular solids and size effects analysis. *International Journal of Solids and Structures*, *46*(14–15), 2787–2799. http://doi.org/10.1016/j.ijsolstr.2009.03.007

Liu, S., & Su, W. (2009b). Effective couple-stress continuum model of cellular solids and size effects analysis. *International Journal of Solids and Structures*, *46*(14–15), 2787–2799. http://doi.org/10.1016/j.ijsolstr.2009.03.007

McGregor, M., & Wheel, M. A. (2014). On the coupling number and characteristic length of micropolar media of differing topology. *Proceedings of the Royal Society A: Mathematical, Physical and Engineering Sciences*, *470*(2169), 20140150–20140150. http://doi.org/10.1098/rspa.2014.0150

Mora, R. J., & Waas, A. M. M. (2000). Measurement of the Cosserat constant of circular-cell polycarbonate honeycomb. *Philosophical Magazine A*, *80*(7), 1699–1713. http://doi.org/10.1080/01418610008212145

Mora, R. J., & Waas, A. M. M. (2007). Evaluation of the Micropolar elasticity constants for honeycombs. *Acta Mechanica*, *192*(1–4), 1–16. http://doi.org/10.1007/s00707-007-0446-8

Nakamura, S., & Lakes, R. S. (1988). Finite element analysis of stress concentration around a blunt crack in a cosserat elastic solid. *Computer Methods in Applied Mechanics and Engineering*, *66*(3), 257–266. http://doi.org/10.1016/0045-7825(88)90001-1

Perano, K. J. (1983). *Application of micropolar elasticity to the finite element continuum analysis of articulated structures*.

Pradel, F., & Sab, K. (1998). Cosserat modelling of elastic periodic lattice structures. *Comptes Rendus de l'Académie Des Sciences - Series IIB - Mechanics-Physics-Astronomy*, *326*(11), 699–704. http://doi.org/10.1016/S1251-8069(98)80002-X

Rueger, Z., & Lakes, R. S. (2016). Experimental Cosserat elasticity in open-cell polymer foam. *Philosophical Magazine*, *96*(2), 93–111. http://doi.org/10.1080/14786435.2015.1125541

Simulia. (n.d.). Abaqus CAE. Retrieved from http://abaqus.software.polimi.it/v6.14/index.html

Spadoni, A., & Ruzzene, M. (2012). Elasto-static micropolar behavior of a chiral auxetic lattice. *Journal of the Mechanics and Physics of Solids*, *60*(1), 156–171. http://doi.org/10.1016/j.jmps.2011.09.012

Stronge, W. J. J., & Wang X.L. (1999). Micropolar theory for two-dimensional stresses in elastic honeycomb. *Proceedings of the Royal Society A: Mathematical, Physical and Engineering Sciences*, *455*(January 1998), 2091–2116. http://doi.org/10.1098/rspa.1999.0394

Tekoğlu, C. (2007). *Size effects in cellular solids*. University of Groningen. Retrieved from http://www.narcis.nl/publication/RecordID/oai%3Aub.rug.nl%3Adbi%2F45a62baa835ee

Tekoğlu, C., Gibson, L. J., Pardoen, T., & Onck, P. R. (2011). Size effects in foams: Experiments and modeling. *Progress in Materials Science*, *56*(2), 109–138. http://doi.org/10.1016/j.pmatsci.2010.06.001

Tekoğlu, C., & ONCK, P. (2008). Size effects in two-dimensional Voronoi foams: A comparison between generalized continua and discrete models. *Journal of the Mechanics and Physics of Solids*, *56*(12), 3541–3564. http://doi.org/10.1016/j.jmps.2008.06.007

Tollenaere, H., & Caillerie, D. (1998). Continuous modeling of lattice structures by homogenization. *Advances in Engineering Software*, *29*(7–9), 699–705. http://doi.org/10.1016/S0965-9978(98)00034-9

Warren, W. E., & Byskov, E. (2008). A general solution to some plane problems of micropolar elasticity. *European Journal of Mechanics - A/Solids*, *27*(1), 18–27. http://doi.org/10.1016/j.euromechsol.2007.05.006

Waseem, A., Beveridge, A. J., Wheel, M. A., & Nash, D. H. (2013). The influence of void size on the micropolar constitutive properties of model heterogeneous materials. *European Journal of Mechanics, A/Solids*, *40*, 148–157. http://doi.org/10.1016/j.euromechsol.2013.01.002

Wheel, M. A., Frame, J. C., & Riches, P. E. (2015). Is smaller always stiffer? On size effects in supposedly generalised continua. *International Journal of Solids and Structures*, *67–68*, 84–92. http://doi.org/10.1016/j.ijsolstr.2015.03.026

Yoder, M., Thompson, L., & Summers, J. (2018). Size effects in lattice structures and a comparison to micropolar elasticity. *International Journal of Solids and Structures*, *143*, 245–261. http://doi.org/10.1016/j.ijsolstr.2018.03.013

Zhang, H., Wang, H., & Liu, G. (2005). Quadrilateral isoparametric finite elements for plane elastic Cosserat bodies. *Acta Mechanica Sinica*, *21*(4), 388–394. http://doi.org/10.1007/s10409-005-0041-y

Zheng, X., Lee, H., Weisgraber, T. H., Shusteff, M., DeOtte, J., Duoss, E. B., … Spadaccini, C. M. (2014). Ultralight, Ultrastiff Mechanical Metamaterials. *Science*, *344*(6190), 1373–1377. http://doi.org/10.1126/science.1252291